MULTIWAVELENGTH LASER SOURCES FOR BROADBAND OPTICAL ACCESS NETWORKS

A Dissertation
Presented to
The Academic Faculty

By

Jérôme Vasseur

In Partial Fulfillment
of the Requirements for the Degree
Doctor of Philosophy
in
Electrical and Computer Engineering

School of Electrical and Computer Engineering
Georgia Institute of Technology
August 2006

MULTIWAVELENGTH LASER SOURCES FOR BROADBAND OPTICAL ACCESS NETWORKS

Approved by:

Dr. Steve McLaughlin, Committee Chair
Professor, School of ECE
Georgia Institute of Technology

Dr. William Rhodes
Professor, School of ECE
Georgia Institute of Technology

Dr. Gee-Kung Chang, Advisor
Professor, School of ECE
Georgia Institute of Technology

Dr. Ali Adibi
Associate Professor, School of ECE
Georgia Institute of Technology

Dr. John Barry
Associate Professor, School of ECE
Georgia Institute of Technology

Dr. Rick Trebino
Professor, School of Physics
Georgia Institute of Technology

Date Approved: May 3, 2006

DEDICATION

To my parents.

ACKNOWLEDGMENTS

Now that I have reached the end of my Ph.D. studies, I would like to thank all the people who made this adventure possible. First, I would like to express my appreciation for the mentoring and support of my advisors Dr. Gee-Kung Chang and Dr. John Barry.

I would also like to thank my committee members Dr. Steve McLaughlin, Dr. William Rhodes, Dr. Ali Adibi, and Dr. Rick Trebino for their time, suggestions, and comments.

I would like to take this opportunity to thank all the people who were with me during this journey, on both sides of the Atlantic. Especially, I would like to thank my colleagues in Prof. Chang's group, the staff from Georgia Tech Lorraine, and all my friends from GTL-CNRS Telecom Laboratory. In particular, I would like to express my gratitude to Dr. Marc Hanna who has always been excellent and who was always present to help me. I also have a special thought for the "French Connection" and the "Belote players".

I would also like to thank Dr. François Malassenet, Director of GTL when I begun my studies, who spent long hours over the phone, late at night, to convince me to enroll in this new double doctoral degree program between France and the US. It was an incredible challenge and a sensational adventure.

Special thanks to Muriel for all her love. Last but not least, I thank my parents who were always here to encourage me in everything I wanted to accomplish.

TABLE OF CONTENTS

LIST OF TABLES

LIST OF FIGURES

SUMMARY

The objective of the proposed research is to develop multiwavelength lasers as cost-efficient sources for broadband optical access networks. Today's telecommunications networks have widely adopted optical fiber as the backbone transmission medium. Optical fiber systems are promising candidates for the broadband access networks to offer high-speed and future-proof services. To harness the available bandwidth in fiber and to meet the ever-growing bandwidth demand, wavelength division multiplexing (WDM) techniques have been investigated. There have been intense research activities for the creation of new low-cost laser sources for such emerging applications. In this context, multiwavelength fiber ring lasers have been significantly investigated as they present many advantages, including simple structure, low-cost, and selectable multiwavelength operation.

We propose a new laser system architecture that emits alternate multiwavelength picosecond pulses operating at room temperature. Optical signal generation is based on a single active component, an unbalanced Mach-Zehnder interferometer, inserted in an actively mode-locked erbium-doped fiber ring laser to provide both intensity modulation and wavelength-selective filtering. Time and frequency controls of the light emission are reached by inserting an additional modulator and a periodic filter in the cavity. This approach focuses on the application of multiwavelength lasers as sources for WDM passive optical networks.

CHAPTER 1

INTRODUCTION

Despite the collapse of the Internet bubble at the beginning of the 21st century, the demand for information technologies did not slow down. In the USA, the Internet penetration rate, nearly null 10 years ago, was about 68.1% in June 2005 [1] and 40.9 million American lines reach the Net via a broadband connection [2]. In a similar way, mobile phones represent a real social phenomenon, as they now rival landline phones in number. The value of global mobile business reached $414 billion in revenue in 2003, a tenfold increase in the decade since 1993, while over the same period the overall telecommunications sector grew by an average of 8.8% to reach $1.1 trillion. According to a recent study published by Infomedia Telecoms & Media, the number of cell phone subscribers globally reached over 2 billion by the end of 2005, about 30% of the world population, and is predicted to rise to 3.96 billion by 2011 [3].

Furthermore, the quantity of information exchanged keeps increasing drastically. Nowadays, multimedia systems transmit not only voice, but they also exchange numerical data, text, image, video... The multiplicity of communication means - such as videoconference, the Internet, videophony - has dramatically increased the volume of information exchanged worldwide.

The current growth of data transmission is facilitated by the advances of laser and fiber technologies. In the sixties, with the invention of the laser, the idea of using light as an information carrier emerged. The continuous developments of optical components, such as optical fibers and amplifiers, made light an efficient means of transmitting and delivering information for backbones and wide area networks. To be deployed in the access networks, technologies for high-speed, secure, and scalable networks must be amortized over a small number of customers. Currently, other technologies have been successfully implemented as optical access is too costly. However, with the arrival of lower cost mature technologies

and the positive experience on optical backbones, optical access networks, in particular passive optical networks, have shown great interest in the last few years.

To optimize the use of the bandwidth in optical fibers and to satisfy the bandwidth demand of future networks, multiplexing techniques that consist of merging several communications channels into one have been exploited. The wavelength division multiplexing (WDM) techniques have shown to unlock the available fiber capacity and to increase the performances of broadband optical access networks. One of the essential component is the creation of new low-cost laser sources. Candidates for such applications are multiwavelength fiber ring lasers as they have simple structure, are low cost, and have a multiwavelength operation.

The present research investigates such mutliwavelength fiber ring lasers. We present a new fiber laser source generating multiwavelength picosecond pulses at GHz repetition rates and the potential applications of multiwavelength sources in broadband optical access networks.

This document is organized as follows. After this brief introduction, a description of some relevant backgrounds and optical components is given in Chapter 2. The next chapter studies current advances in broadband access networks. Chapter 3 briefly summarizes the general techniques that have already been developed and discusses in detail passive optical networks. Then, a state of the art regarding existing laser sources that are used in such networks is presented. Chapter 4 introduces the principle of a new laser architecture emitting alternate multiwavelength picosecond pulses at room temperature at GHz repetition rates. This original pulse generation is based on a single active component, an unbalanced Mach-Zehnder interferometer, inserted in an actively mode-locked erbium-doped fiber ring laser to provide both intensity modulation and wavelength-selective filtering. The behavior of this laser is studied theoretically. We report how its mode of operation was numerically simulated and experimentally verified and evaluated. We present a detailed description of the design, the development, the building, and the testing of this original laser source. In

Chapter 5, we discuss ways to improve the laser design and its performances. Specifically, time and frequency controls of the light emission are tuned by inserting an additional conventional modulator and a periodic filter in the cavity. Stabilization of the pulsed laser source is also made possible by mixing two harmonics of the fundamental cavity frequency and driving a phase modulator with this signal. In Chapter 6, we introduce a different type of laser: a continuous-wave multiwavelength fiber ring laser based on semiconductor optical amplifier as gain medium. This laser is then used as a cost-effective light source for wavelength division multiplexed passive optical networks. The performances of the system for downstream signal are experimentally investigated. Finally, Chapter 7 concludes the current work and introduces possible future work, enhancements or avenues for applications.

CHAPTER 2

INTRODUCTION TO FIBER OPTICS COMMUNICATIONS

The idea to use guided light for data transmission appeared 40 years ago with the invention of the laser. Over the past few years, the field of fiber optics communications has experienced tremendous growth. This impressive development is due to the crucial breakthroughs that have been achieved in several key domains.

The objective of this chapter is to introduce the fundamentals of optical fibers that constitute the key element of today's optical networks. Then, we will focus on two specific technological advances: optical amplifiers and lasers. Finally, an overview of different optical pulse generation techniques is provided.

2.1 Fundamentals of optical fibers

Optical fibers transport and guide light. They provide huge bandwidth, low loss rate and cost-effectiveness. In this section, we will present the basic theory underlying the properties of optical fibers. We will focus on the optical transmission in this optical waveguide, as well as the different impairments of a signal when propagating through fiber, namely attenuation, dispersion, and non-linearities.

2.1.1 Light guide

An optical fiber is a dielectric cylindrical guide that transmits light, as shown in Figure 1. Fiber is generally made of silica. The fiber consists of a core surrounded by a cladding layer, whose refractive index is lower than that of the core. A protective layer, called coating and usually colored, is employed to protect the fiber mechanically and to prevent spurious light noise to enter into the fiber.

Considering the refractive indices of the core and the cladding, respectively equal to n_1 and n_2, we can distinguish two main categories of fibers [4, 5, 6]:

- step-index fiber: both refractive indices are constant with an abrupt change at the

core-cladding interface and with $n_1 > n_2$.

- graded-index fiber: n_1 decreases gradually inside the core. The refractive index n_1 is thus a decreasing continuous function of radial distance r.

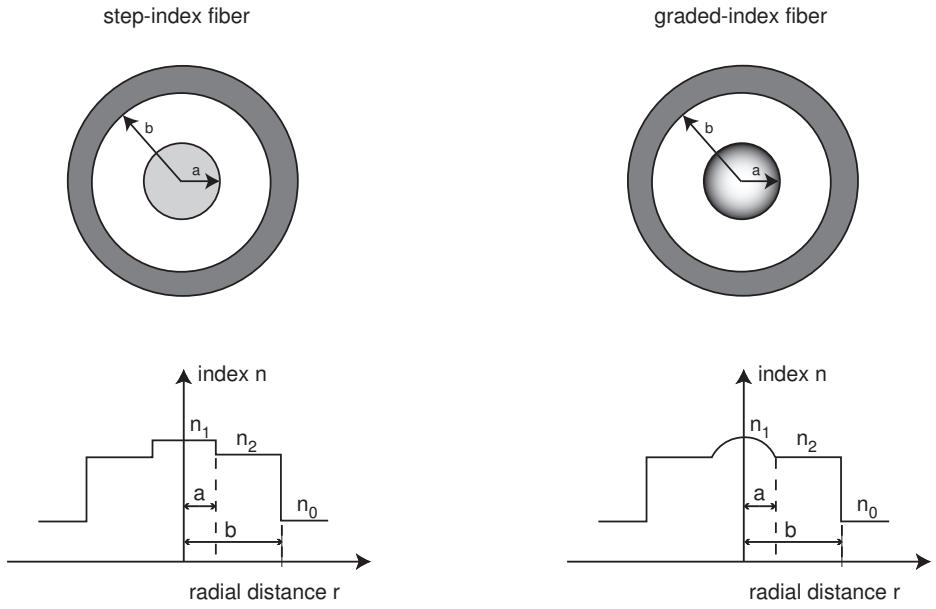

Figure 1: Cross-section and refractive index profile for step-index and graded-index fibers.

Light propagates by total internal reflections at the core-cladding interface. Total internal reflections are lossless. A wave may propagate through the fiber following many possible ways: each allowed way is called a mode. More formally, a mode corresponds to a solution of the wave equation derived from Maxwell's equations and subject to boundary conditions imposed by the optical waveguide. The number of modes actually allowed to propagate in the fiber is thus a function of the system geometry. In particular depending on the relative size of the core compared to the considered wavelength λ, there are two types of fiber:

- single-mode fiber (SMF): when the size of the core is sufficiently small, only one mode exists. In standard fibers, the core and the cladding have a diameter of 8-9 μm

and 125 μm, respectively.

- multi-mode fiber (MMF): the size of the core is larger (about 50-60 μm) and more than one mode may propagate through the fiber. The advantage of multi-mode fiber comes from the fact that injection of light into the fiber with low coupling loss can be done by using inexpensive, large-area light sources. However, its disadvantage is that it introduces the phenomenon of inter-modal dispersion. In such a fiber, each mode travels at a different velocity due to different angles of incidence at the core-cladding boundary. This effect results in a pulse which is spread out in the time domain.

The use of SMF when building a fiber ring laser contributes to its transverse single-mode functionality and thus to a part of its stability.

2.1.2 Attenuation

As light propagates along a fiber, its power, I, decreases exponentially with distance z, expressed in kilometers, due to fiber attenuation:

$$I(z) = I(0)\exp\left(-\frac{\ln 10}{10}\alpha_{dB}(\lambda)\,z\right), \tag{1}$$

where $\alpha_{dB}(\lambda)$ is the fiber attenuation coefficient, expressed in dB/km, at wavelength λ and $I(0)$ the optical power at the start of the fiber.

Many effects can lead to attenuation in a fiber: absorption, scattering, and radiative losses of the optical energy. Absorption losses are caused by impurities in glass material from residual foreign atomic substances, such as the hydroxyl ion OH^- or metallic ions (Cr^{3+}, Fe^{2+} or Cu^{2+}). Scattering losses, namely Rayleigh, Mie, Brillouin, and Raman scattering, arise from microscopic variations in the material density and from structural inhomogeneities. Radiation losses come from fiber bending. Intrinsic fiber characteristics can also cause loss of energy: changes in core diameter or difference in refractive indices, for instance.

Figure 2 represents the absorption profile of a standard optical fiber: attenuation is a function of the wavelength. Typically, three spectral regions are used for data transmission:

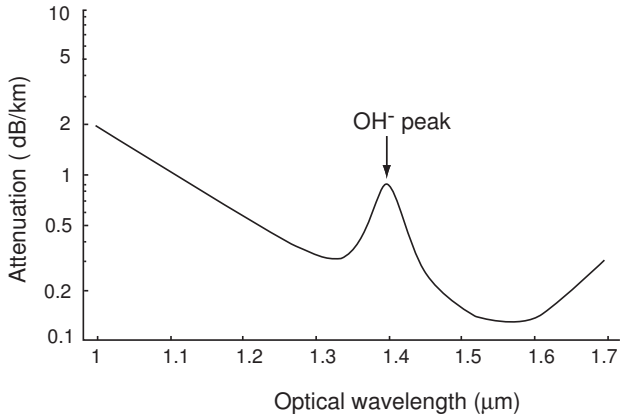

Figure 2: Absorption profile of a standard optical fiber.

at 850 nm (first telecommunications window), at 1300 nm (second window), and at 1550 nm (third window). The lowest attenuation occurs at the third window and is below 0.2 dB/km.

2.1.3 Dispersion

Dispersion is the broadening of a pulse duration while propagating through a fiber. If a pulse widens too much, it can interfere with neighboring pulses, leading to intersymbol interference. For this reason, dispersion is a critical parameter limiting the transmission data rate on a fiber-optic channel. Fiber dispersion can be classified into two basic categories: chromatic dispersion and polarization mode dispersion.

Chromatic dispersion Chromatic dispersion is the result of material dispersion and waveguide dispersion. The refractive index of the material is a function of the wavelength. As a result, if the transmitted signal consists of more than one wavelength, the different wavelengths will travel at different speeds.

This phenomenon can be modeled by expanding the wave propagation factor $\beta(\omega)$ in a Taylor series around the center frequency ω_0

$$\beta(\omega) = \beta_0 + \beta_1(\omega - \omega_0) + \frac{\beta_2}{2}(\omega - \omega_0)^2 + \frac{\beta_3}{6}(\omega - \omega_0)^3 + \ldots, \tag{2}$$

where $\beta_i = \left[\frac{\partial^i \beta}{\partial \omega^i}\right]_{\omega=\omega_0}$ for i=0,1,2...

The first term β_0 is related to the phase velocity of the wave, the second term β_1 is the inverse of its group velocity v_g, and the subsequent terms to group velocity dispersion of increasing order.

Chromatic dispersion is also the result of the waveguide characteristics, such as the indices and shapes of the fiber core and cladding.

Dispersion in fibers is usually quantified by the value of β_2, generally expressed in units of ps^2/km, or by the dispersion parameter D, which is related to β_2 by

$$D = -\frac{2\pi c_0}{\lambda^2}\beta_2, \tag{3}$$

where c_0 is the celerity of light in vacuum. D is most often expressed in ps/nm/km. Depending on the sign of the dispersion parameter, dispersion is said normal ($D < 0$) or anomalous ($D > 0$). In the normal case, the shorter wavelengths ("blue") are delayed more than the longer wavelengths ("red").

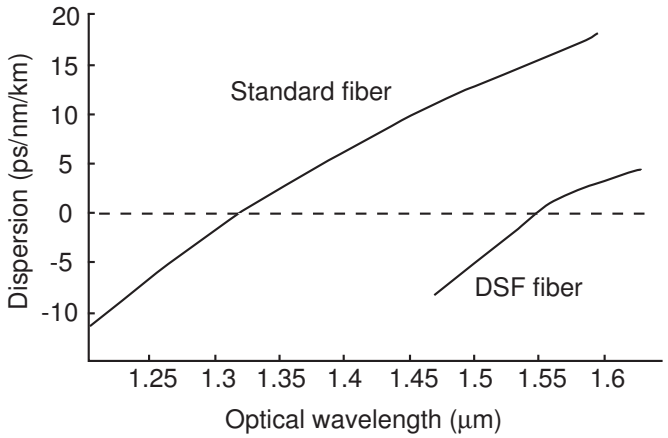

Figure 3: Typical dispersion curves for standard and dispersion shifted fibers (DSF).

For typical standard fibers (norm ITU-T G.652), used in most of metropolitan and wide area networks, dispersion at 1310 nm is zero and it is 17 ps/nm/km at 1550 nm. However, by carefully designing the waveguide, it is possible to obtain zero dispersion at 1550 nm.

These fibers are called dispersion shifted fibers (DSF, norm ITU-T G.653). Figure 3 represents the typical dispersion curves for standard and dispersion-shifted fibers. A recent norm, called ITU-T G.656, adopted in April 2004, introduces fibers where the dispersion is small, but not zero: D is between 2 and 14 ps/nm/km from 1460 nm to 1625 nm. In this case the influence of non-linear effects is reduced. These fibers are called non-zero dispersion shifted fibers (NZ DSF).

Polarization mode dispersion If the fiber is not perfectly cylindrical due to the fabrication process or if the fiber is put under mechanical or thermal stress, this waveguide will behave as a birefringent element. The fiber core becomes elliptic and the two orthogonal polarization components (birefringent axes) of the field acquire a differential group delay. This effect, called polarization mode dispersion (PMD), varies randomly along the fiber. It is quantified by measuring the standard deviation of the group delay between the two components. Standard fibers have a PMD of 0.2 ps/ $\sqrt{\text{km}}$.

Fiber lasers are sensitive to spurious birefringence as the cavity must be as stable as possible to avoid drift in the emission. To counteract this problem, special high birefringence fibers have been designed [7], e.g., PANDA fiber. Then, artificially induced birefringence maintains the original degree of polarization by keeping the spurious birefringence caused by PMD negligible.

2.1.4 Non-linearities

All the above effects are linear, i.e., they were independent of the intensity of light. When the intensity becomes sufficiently intense, non-linear effects appear [8, 9].

Kerr effect In electromagnetics, the electric induction $\mathbf{D}$ is equal to $\mathbf{D} = \varepsilon_0\mathbf{E} + \mathbf{P}$, where ε_0 is the vacuum permittivity, $\mathbf{E}$ the electric field and $\mathbf{P}$ the polarization. To take into account the non-linearities, the optical polarization must be expanded

$$\mathbf{P} = \varepsilon_0\chi^1 \times \mathbf{E} + \varepsilon_0\chi^2 \times \mathbf{EE} + \varepsilon_0\chi^3 \times \mathbf{EEE} + \ldots, \tag{4}$$

where χ^i is a i^{th} tensor and $\times$ denotes the tensor product. The first term χ^1 corresponds to the linear susceptibility while the higher order terms account for the non-linear contribution. In centrosymmetric media, such as silica, the optical polarization must verify the same symmetry condition as the medium, and so all even-order components are equal to zero. Thus, the next non-zero term is the third order and it causes most of the non-linear effects affecting light propagation in optical fibers: they are called the Kerr effects, or χ^3 effects. In the following paragraphs, we will briefly discuss the most important phenomena due to third-order non-linearities.

Self-phase modulation In optical fiber, the refractive index depends on the optical intensity of signals propagating through the fiber. The non-linear variation of the refractive index Δ_{NL} is proportional to its intensity $I(t)$

$$n(t) = n_0 + \Delta_{\mathrm{NL}} = n_0 + n_2 I(t). \tag{5}$$

where n_0 is the nominal value of the refractive index and n_2 is related to the non-linear susceptibility. Hence, a field traveling in the fiber will experience a phase shift proportional to its intensity: for this reason, this effect is called self-phase modulation (SPM).

Cross-phase modulation Cross-phase modulation (XPM) refers to the non-linear variation of the refractive index, i.e., the non-linear phase shift, induced by the co-propagating signals at different wavelengths or with different polarizations. When the two waves are at the same frequency but with orthogonal polarization states, the non-linear variation of the refractive index is given by [8]

$$\Delta_{NL} = n_2\left(I_1(t) + \frac{2}{3}I_2(t)\right), \tag{6}$$

where I_1 and I_2 are the respective intensities of the two signals. When two beams of same polarization are at different frequencies, the variation is given by [8]

$$\Delta_{NL} = n_2\left(I_1(t) + 2I_2(t)\right). \tag{7}$$

Since the phase fluctuations introduced by XPM, and also SPM, are intensity dependent, different parts of a pulse will undergo different phase shifts. It leads to frequency chirping,

in which the rising edge of the pulse suffers from a red shift in frequency (toward higher frequencies), whereas the trailing edge of the pulse experiences a blue shift in frequency (toward lower frequencies).

Four-wave mixing Four-wave mixing (FWM) occurs when two or more signals at different frequencies are launched into a fiber. For instance, when two signals interact with a third one, a fourth signal is created at another frequency. Similarly, when two optical signals at frequencies f_1 and f_2 are co-propagating along a fiber, they mix and generate signals at $2f_1 - f_2$ and $2f_2 - f_1$. In general, for N wavelengths launched into a fiber, the number of new generated wavelengths M is

$$M = \frac{1}{2}(N^3 - N^2). \tag{8}$$

These new signals are called sidebands and can cause interference if they overlap with frequencies used for data transmission. However, FWM can be used for wavelength conversion [10] or demultiplexing [11].

Non-instantaneous non-linearities Apart from the previous non-linearities presented so far, there also exists non-instantaneous effects that couple light with the vibration modes of the medium, called phonons. We can distinguish two types of such interactions. Both effects cause energy to be transferred from a high-power optical pump to a weaker signal, accompanied by either the creation or the annihilation of a phonon.

The stimulated Brillouin scattering effect (SBS) involves acoustic phonons that have a very low group velocity, lower than the speed of light in the medium. SBS occurs at relatively low input powers for wide pulses (greater than 1 μs) and has negligible effect for short pulses (less than 10 ns). The frequency range of SBS is low ($\approx$10 GHz in silica) and its gain bandwidth is only on the order of 100 MHz.

The stimulated Raman scattering (SRS) involves optical phonons that propagate in the lattice at a velocity close to that of light. This effect covers a large bandwidth of around 30 THz below the frequency of the input light in silica. It has a maximum gain at a frequency of around 13 THz less than the input signal frequency.

2.2 Optical amplifiers

Although manufacturing technology has made a lot of progress, attenuation and losses are still detrimental to long-haul telecommunication systems, as the number of photons in the signal becomes too small to be detected after long propagating distances. It is thus necessary to boost the power of the signal periodically. The first solution was to use opto-electronic amplification: the optical signal was first converted into an electric current and then regenerated using a transmitter. This solution presents many drawbacks in terms of effectiveness, complexity, and cost. All-optical amplifiers, using the principle of stimulated emission or non-instantaneous non-linear effects, have been developed to mitigate these issues. This section gives a general overview of the two basic types of optical amplifiers: fiber amplifiers and semiconductor optical amplifiers.

2.2.1 Fiber amplifiers

Fiber amplifiers are optical amplifiers which use an optical fiber, which bears the data signal. Two main categories of such components exist: rare-earth doped fiber amplifiers, based on stimulated emission, and non-linear optical amplifiers, based on phonon-photon interaction.

Rare-earth doped fiber amplifiers These amplifiers were introduced by Koestner and Snitzer in 1964 [12] and became commercially available 25 years later. The idea is to dope the core of the fiber with a rare-earth element, such as erbium, ytterbium or thulium, during its manufacturing process [13]. These dopants are excited into a higher energy level by an optical signal, referred to as pump signal, at a wavelength lower than that of the communication signal. This allows the data signal to stimulate the excited atoms to release photons.

Many variations have been proposed on this basic theme, in order to optimize many criteria, such as gain efficiency (measurement of the gain as a function of input power in dB/mW), gain bandwidth (range of wavelengths over which the amplifier is effective), saturated gain (gain when the value of output power no longer increases with an increase

in the input power), polarization sensitivity (dependence of the gain on the polarization of the signal)...

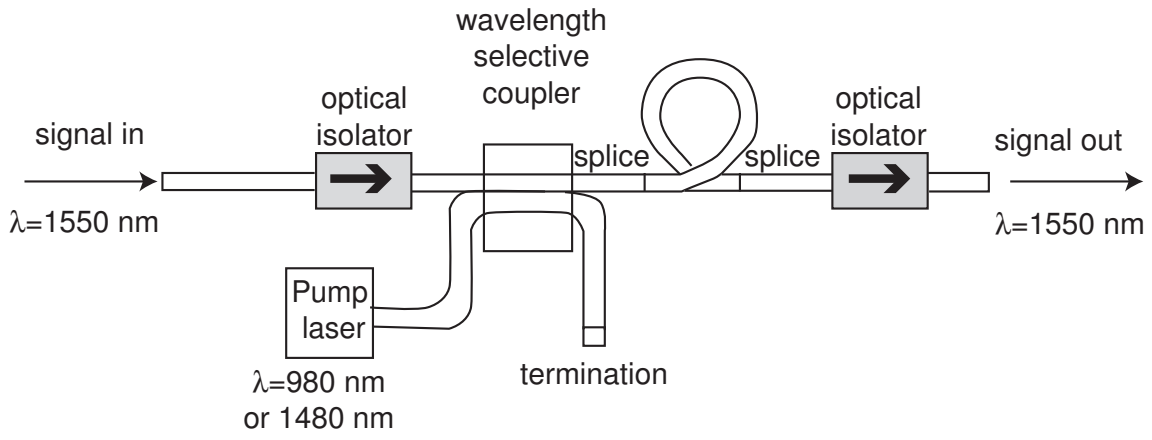

Figure 4: Schematics of an erbium-doped fiber amplifier.

As far as optical communications are concerned, the most frequent dopant is erbium ion (Er^{+}). These amplifiers are called erbium-doped fiber amplifiers (EDFA) [14]. They typically provide gain amplification over the C-band (conventional band from 1530 nm to 1565 nm) with a peak around 1535 nm, but recent EDFAs can also cover the L-band (long-wavelength band from 1565 nm to 1625 nm) [15]. Most EDFAs are pumped by lasers with a wavelength of either 980 nm or 1480 nm. Typical maximum gains are on the order of 30-50 dB. The gain saturation power is around 10 dBm and the 3-dB gain bandwidth is around 35 nm. As compared to other means of optical amplification, EDFAs have a large number of advantages, including fiber compatibility, reduced insertion losses (0.1-2 dB), low noise figure (<5 dB), polarization insensitivity and bit-rate transparency. In most cases, non-linearities are negligible and as the carrier lifetime is on the order of 10 ms, any phenomenon shorter than this value will not affect the equilibrium of the system.

The dominant source of noise is amplified spontaneous emission (ASE), which arises from the spontaneous emission of photons in the active region of the amplifier. Amplifier noise can be a problem especially when multiple optical amplifiers are cascaded: each amplifier will amplify the noise generated by the previous amplifiers. Another limitation

is the unequal gain spectrum of these optical amplifiers. It means that an optical amplifier will not necessarily amplify all wavelengths equally. This limits the performance of optical amplifiers, particularly when a multiwavelength optical signal is considered.

A number of solutions have been proposed to flatten the gain of an EDFA. For instance, a notch filter centered at around 1535 nm can be used to suppress the peak of the EDFA gain [16]. Another approach is to employ several pump signals.

Non-linear amplifiers Non-linear amplifiers differ from the previous ones in that they utilize non-instantaneous non-linear effects, such as SRS or SBS. In particular, in Raman amplifiers, gain can be obtained over a large band (around 100 nm), but it is relatively small (10-15 dB) [17]. The first observation was made by Stolen and Ippen in 1973 [18].

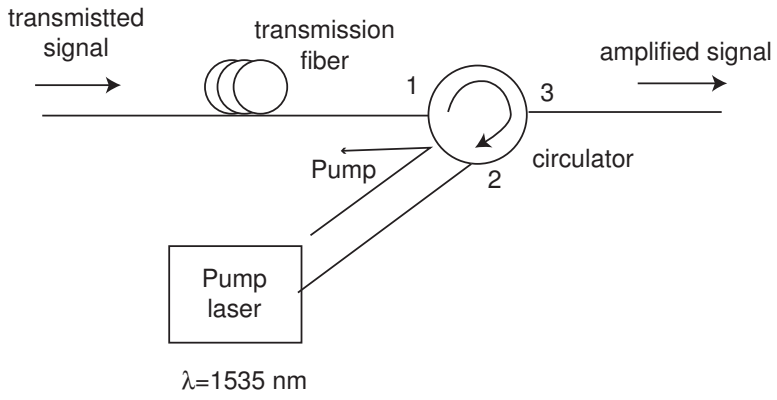

Figure 5: Typical Raman amplifier configuration.

The optical amplification occurs in the transmission fiber itself, distributed along the transmission path. This is a major difference and advantage compared to EDFAs. They can also be used in any installed transmission fiber; the only requirement being to inject a high-intensity pump signal. Pump power of several hundreds of milliwatts is necessary, and pump power from 1 W to 2 W is common. These amplifiers have also a low noise figure.

2.2.2 Semiconductor optical amplifiers

Semiconductor optical amplifiers (SOA) are essentially laser diodes, without end mirrors but with anti-reflection (AR) design at the end faces [19]. They have fiber attached to both ends. They amplify any optical signal coming from either fiber and transmit the amplified signal out of the second fiber: they can transmit bidirectionnally. Even if the SOA is showing great promise for use in future optical communication networks, the actual conventional systems are still dominated by EDFAs. Many recent advances in fabrication techniques and device design result in improvements of their performances, but their utilization is not yet industrial.

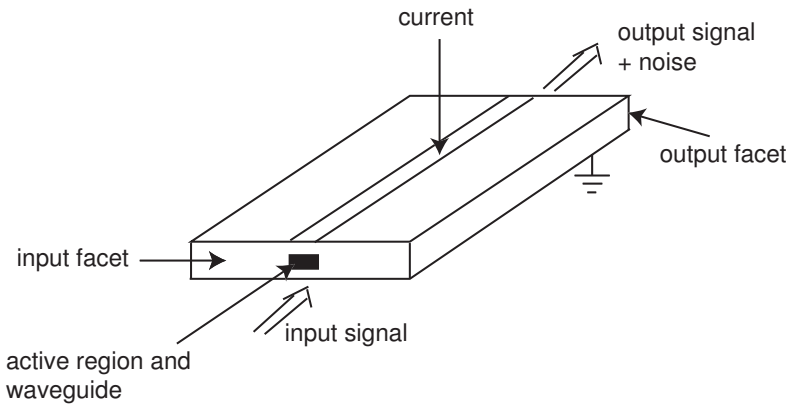

Figure 6: Schematic diagram of a semiconductor optical amplifier.

SOA is of small size and electrically pumped. Potentially, it can be less expensive then EDFA and can be integrated with other devices. However, the actual performance is still not competitive with EDFA. Typical maximum gains are on the order of 30 dB. The gain saturation power is between 5 and 20 dBm and the 3-dB gain bandwidth is between 30 and 80 nm, especially when using a multiple quantum wells design. This design increases the differential gain by confining the electrons in microscopic sections of the waveguide. SOAs also suffer from high insertion losses (6-10 dB), a high noise figure (7-12 dB), and a short carrier recombination lifetime (<1 ns). These fast gain dynamics make the amplifier gain react quickly to changes in the input signal. This characteristic can cause signal distortion

and make SOAs non bit-rate transparent. SOAs are polarization sensitive due to a number of factors including the waveguide structure and the gain material. Polarization sensitivity can be reduced (<2 dB) by the use of square-cross section waveguides and strained quantum well material. SOAs also exhibit non-linear behavior. These effects can cause problems such as frequency chirping and generation of inter-modulation products. They can also be exploited to perform all-optical signal processing [20].

Table 1: Comparison between EDFA and SOA.

characteristic	EDFA	SOA
gain (dB)	30-50	30
insertion loss (dB)	0.1-2	6-10
3-dB gain bandwidth (nm)	35	30-80
saturation output power (dBm)	10	5-20
noise figure (dB)	<5	7-12
carrier lifetime	<10 ms	<1 ns
pump source	optical	electrical
polarization sensitivity	no	yes
non-linear effects	negligible	yes

As a matter of fact, SOAs can be used for basic network applications, such as booster amplifiers to increase a high power input signal prior to transmission, pre-amplifiers to increase the power level of an optical data signal before detection, or in-line amplifiers to compensate for fiber loss during transmission. Moreover, SOA is a versatile candidate technology for executing many other operations that leverage its non-linearity, e.g., cross gain modulation (XGM) when a strong signal at one wavelength affects the gain of a weak signal at another wavelength, XPM, SPM, and FWM.

Among others, SOAs can be used in the following situations:

- wavelength conversion: it can increase the flexibility and capacity of a network using a fixed set of wavelengths. It can be used to centralize network management. Development of optical wavelength converters avoids the need to transfer the data into the electric domain before being resent on the new targeted wavelength and thus any electrical processing bottleneck.

- all-optical switching: by simply turning the device current on or off, an SOA can be used as an optical gate, or switch. An unbiased SOA becomes heavily absorbing and stops any signal. The switching time of a current switched SOA is on the order of several hundreds of picoseconds, but faster switching times can be obtained by using SOAs inserted in non-linear loop mirrors for data routing based on a packet-by-packet decision.

- optical logic: different configurations can create optical logic gates, useful for all-optical signal processing applications in high-speed optical networks.

2.3 Lasers

Previously, we presented how to guide light in optical fiber, but also how to amplify such a signal. In this section, we will focus on how to produce the light to be launched in them. We will introduce some of the fundamental principles of lasers and discuss various types of lasers, especially detailing fiber lasers that are at the core of our research.

2.3.1 Fundamentals

The word laser is an acronym for Light Amplification by Stimulated Emission of Radiation. As indicated in its name, a laser produces intense high-powered beams of coherent light by stimulated emission [21].

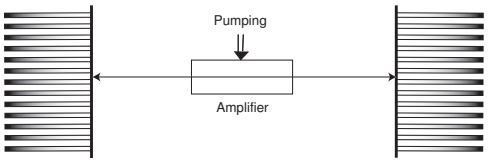

Figure 7: Fabry-Perot laser cavity.

A laser is composed of an optical cavity in which light can circulate, and within this cavity is placed a gain medium, which serves to amplify the light. Figure 7 shows a typical basic laser cavity, called Fabry-Perot cavity: two mirrors, one reflective and one partially-transmitting, form the resonant optical cavity. The basic idea is to excite electrons in the gain medium to produce photons and to accumulate the energy in the cavity. For this purpose, an external device, called pump, brings energy to the gain medium. This energy is absorbed by the medium and its electrons are excited to an upper state: absorption is at the origin of population inversion. When these electrons are excited, they tend to drop back to the ground state by spontaneous emission. Meanwhile, an incident photon of appropriate frequency can provoke emission of a cascade of photons by stimulated emission; so the beam is amplified. Emitted photons have the same direction and coherency as the stimulating photon. When the gain obtained after one round-trip is larger than the losses, laser threshold is reached. Laser light is emitted out of the cavity [22].

Once laser effect is achieved, only specific waves can be supported in the optical resonant cavity: they are called the longitudinal (or axial) modes of oscillation. These privileged waves are those satisfying the resonance condition: the optical distance of one cavity round-trip must be equal to an integer multiple of the wavelength (or in other terms, the round-trip phase shift must be a multiple of 2π). It means that if L is the optical length of the cavity and λ the wavelength, the relationship is

$$L = q\lambda, \tag{9}$$

where q is an integer. As shown in Figure 8, in the case of a Fabry-Perot configuration,

L is equal to twice the optical distance between the two mirrors. We can also note that in the case of a ring cavity, L is equal to the length of one loop. This implies also that for reasonable size cavities a large number of modes are theoretically possible; but the real number of emitted modes depends on several parameters, e.g., energy introduced in the laser, cavity length, gain spectrum, and type of gain.

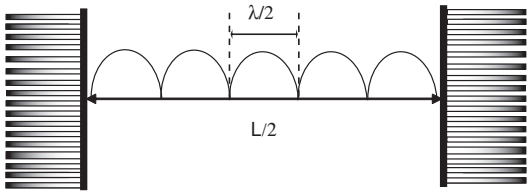

Figure 8: Representation of a wave propagating in a Fabry-Perot cavity.

A longitudinal mode is characterized by its optical wavelength. The q order mode, where q is an integer, is at the frequency ν_q, with

$$\nu_q = \frac{qc_0}{L}. \tag{10}$$

The spectral spacing between two successive modes $\Delta\nu$ is called axial mode separation and is given by

$$\Delta\nu = \frac{c_0}{L}. \tag{11}$$

This parameter plays a key role when using mode-locking technique to generate optical pulses with a laser.

Laser light presents many properties:

- monochromaticity: laser light is concentrated in a narrow range of wavelengths.
- coherence: all the emitted photons bear a constant phase relationship with each other in both time and space.
- low divergence: all light is concentrated into a narrow spatial band.

The gain medium is a critical element of a laser. Different media can generate different behaviors. We can separate them into two categories. Some are called “homogeneous” (case of doped fibers) when all the elements of the medium react in the same way. Thus, a signal applied to such a group of atoms will have the same effect on any atom. In fact, homogeneous broadening is an increase of the linewidth of an atomic transition caused by effects which equally affect different radiating or absorbing atoms. All the elements of a same group will have the same central frequency. Other media are called “inhomogeneous” (case of gases because of Doppler effect) when all the elements of a same group react differently. For instance, this can be caused by the different velocities of the atom of a gas or by different lattice locations of atoms in a solid. In this case, all the atoms of a same group will have slightly different resonant frequencies: inhomogeneous broadening will thus result in a larger increase of the linewidth of an atomic transition but of smaller amplitude at the central frequency than in the case of a homogeneous broadening. The homogeneous characteristic of erbium-doped fiber, in the order of 10 nm, can be a drawback for a closely-spaced multiwavelength generation. Indeed, in such circumstances, one mode will prevail over the others and will fix the gain for the other wavelengths.

2.3.2 Categories of lasers

Townes and Schawlow extended the principle of the maser (microwave amplification by stimulated emission of radiation) to the optical domain [23]. In 1960, Maiman invented the first ruby laser [24]. Since then, many lasers have been developed and built. They can be differentiated by the type of active medium used.

- Solid-state lasers: the active medium is a solid at room temperature, e.g., crystal, glass or optical fiber. Generally, the medium will consist of a glass or crystalline host material to which is added a dopant such as neodymium, chromium, or erbium. Common dopants are rare earth elements. Common solid-state lasers are Nd:YAG, Ti:sapphire and Yb:glass lasers.

- Semiconductor lasers: although semiconductor lasers are also solid-state devices, they are often classified in another category than solid-state lasers. Laser diodes produce wavelengths from 405 nm to 1550 nm. Low power laser diodes are used in laser pointers (1mW-5mW), laser printers, and CD/DVD players. The highest power industrial laser diodes, with power up to 10 kW, are used in industry for cutting and welding. Vertical cavity surface-emitting lasers (VCSELs) are semiconductor lasers whose emission direction is perpendicular to the surface of the wafer. VCSEL devices typically have a more circular output beam than conventional laser diodes, and potentially could be much cheaper to manufacture. VECSELs are external-cavity VCSELs. Quantum cascade lasers are semiconductor lasers that have an active transition between energy sub-bands of an electron in a structure containing several quantum wells.

- Gas lasers and excimer lasers: their active media are gases which are typically excited with electrical discharges. Frequently used gases include CO_2, argon, and gas mixtures such as helium/neon. Common excimers are ArF, KrF, and F_2: typically a noble gas (rare gas) and a halogen. For instance, carbon dioxide lasers are used in industry for cutting and welding.

- Chemical lasers: they are powered by a chemical reaction, and can achieve high powers in continuous operation. They are used in industry for cutting and drilling. Common examples of chemical lasers are the chemical oxygen iodine laser (COIL), and the hydrogen fluoride laser and deuterium fluoride laser, both operating in mid-infrared region.

- Dye lasers: they use an organic dye as the gain medium, usually as a liquid solution. Some of the dyes are fluorescein, coumarin, stilbene, umbelliferone, and tetracene.

In the next paragraph, we will focus on fiber lasers because our work in this dissertation deals with this particular type of lasers.

2.3.3 Fiber lasers

Fiber lasers are referred to as lasers with optical rare-earth doped fibers as gain media. Some lasers with a semiconductor gain medium and a fiber cavity are also called fiber lasers. Many configurations can be used for these lasers:

- Linear configuration: it is a type of Fabry-Perot cavity. For instance, end mirrors determining the laser cavity can be fiber Bragg gratings directly etched into the core of an optical fiber [25]. See Figure 9 (a).
- Ring configuration[26]. See Figure 9 (b).
- Figure-eight configuration [27]. See Figure 9 (c).
- σ configuration[28]. See Figure 9 (d).

These three latter configurations are the most common, since they enable short pulse generation and high repetition rate. In these architectures, the isolator is inserted to force light to circulate in an unique direction.

Fiber lasers have a lot of advantages compared to bulk lasers. They are compact and easy to build, to manipulate, and to transport. Fiber laser setups can be very robust when they are made with fibers only. They are easy to integrate and do not require any complex alignment or coupling. They are also less expensive and have the potential for high output powers (several kilowatts with double-clad fibers) with excellent beam quality [29, 30] due to high surface-to-volume ratio and the guiding effect which avoids thermo-optical problems. These fiber lasers can also operate with small pump powers. Their axial mode separation can be small (2 to 100 MHz for optical lengths of 3 to 150 m).

On the other hand, fiber lasers suffer from various problems: stability, power fluctuations, complicated temperature-dependent polarization evolution, and non-linear effects which may limit performance. Significant dispersion effects due to long length of fibers can be detrimental.

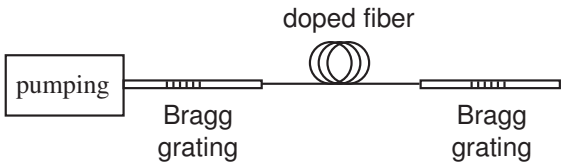

(a) linear structure

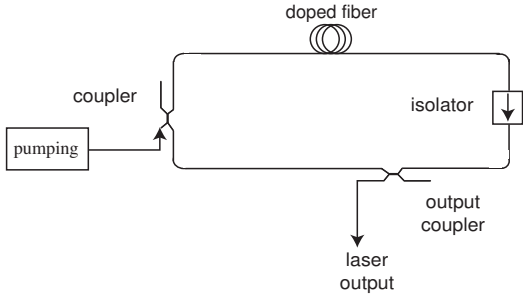

(b) ring strucutre

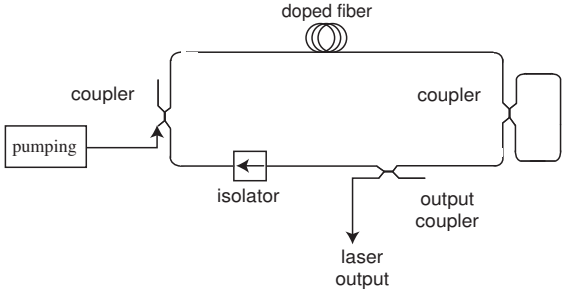

(c) figure-eight structure

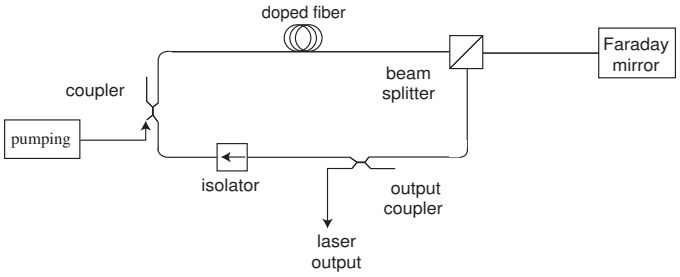

(d) σ structure

Figure 9: Different configurations for fiber lasers.

The application fields of fiber lasers range from telecommunications to car industry, but also include medicine and aerospace [31, 32, 33].

2.4 Pulse generation

The output of a laser may be a continuous, constant-amplitude output (known as CW or continuous wave), or pulsed, by using the techniques of Q-switching, mode-locking, or gain-switching. In pulsed operation, much higher peak powers can generally be achieved.

2.4.1 Pulse carving

To emit optical pulses, a straightforward solution includes a continuous light source and uses a fast modulator which periodically lets the light pass for a short period of time. This method is called pulse carving. This modulator acts as a switch. It can be an electro-absorber or a Mach-Zehnder interferometer, driven by an electrical signal to carve the desired optical pulses [34, 35]. The laser in itself does not have any influence on pulses characteristics, except if the modulator and the laser diode are integrated on the same substrate [36].

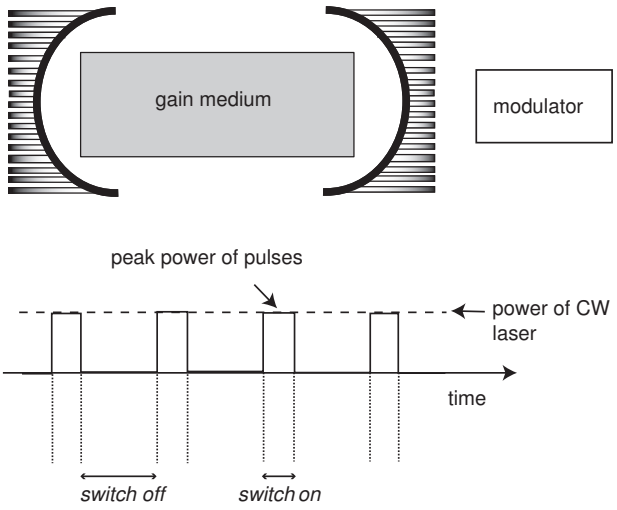

Figure 10: Pulse carving principle: cavity and laser output as a function of time.

This method is simple and easy to implement. However it has some drawbacks. With this technique duty cycles are large (between 30% and 50%) and so pulsewidths are significant compared to repetition rates. Moreover, the maximum pulse power cannot exceed the power of the used continuous laser diode. Since most of the light is lost at the modulator and since the pulse duration is limited by the speed of the modulator, other techniques based on intra-cavity modulation have been developed.

2.4.2 Q-switching

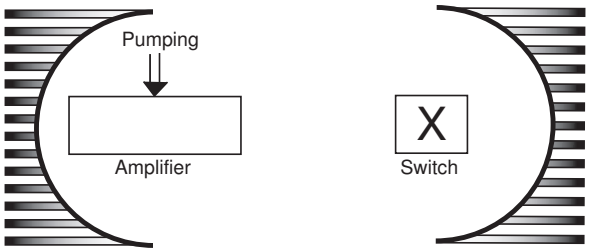

Figure 11: Q-switching laser cavity.

The idea of this method is to put an element that will play the role of a shutter inside the cavity. It leads to a change of loss parameter α. It creates short pulses of high energy. This method is called Q-switching because the decrease of loss corresponds to an increase of the Q-factor of the cavity. The analysis can be parted into two steps, as shown in Figure 12.

Step one:

- *The shutter is off.* The gain increases as energy in the amplifier is stored and losses are high, maintained equal to α_1. the pump power is equal to R and is used to increase the inversion of population without reaching the laser condition. The difference in population between electronic levels $\Delta N(t)$ stays at a value $R\tau_{inc}$, where τ_{inc} is the exponential time constant of increase of ΔN.

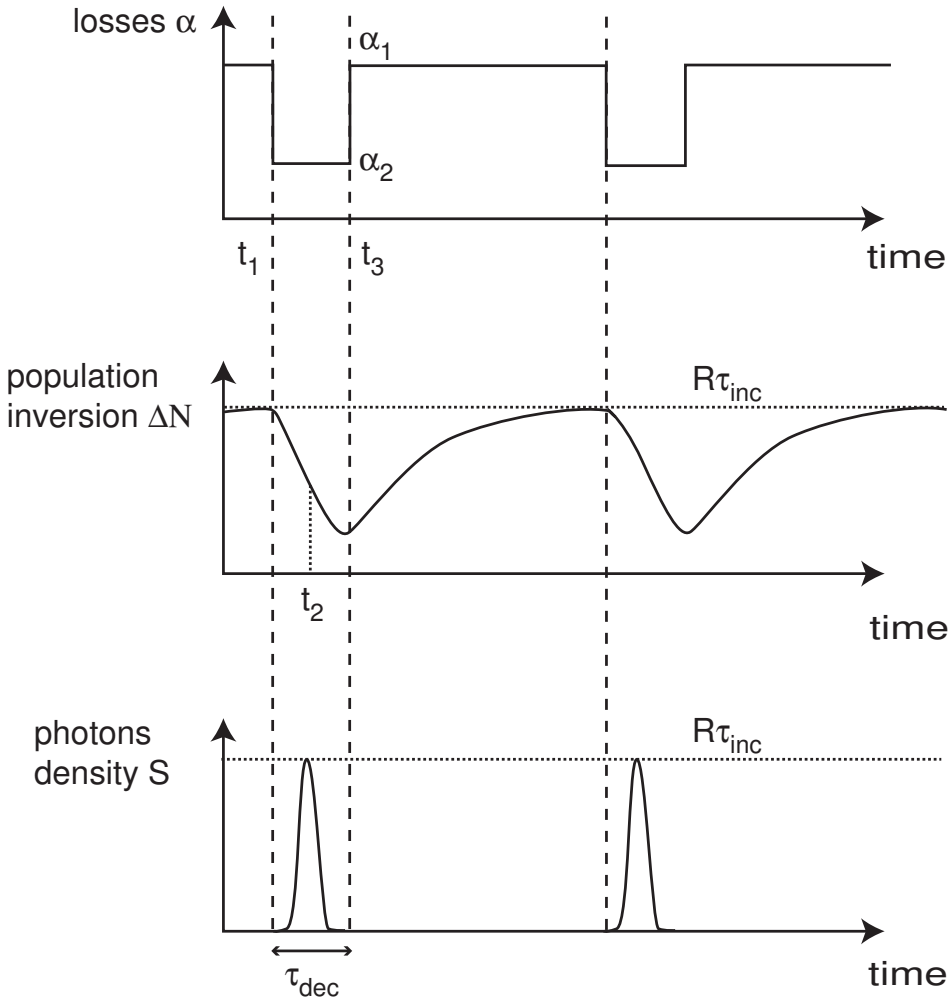

Figure 12: Q-switching principle.

Step two:

- *The shutter is on.* At time t_1, losses become suddenly low and reach a value α_2. The overall gain is greater than the laser threshold. There is emission. The emitted photons density, $S(t)$, and the optical power increase. They rapidly reach saturation. The resulting overall gain abruptly decreases and becomes less than the laser threshold at t_2. The photons density $S(t)$ decreases to 0 with a time constant τ_{dec}.

This technique generates short pulses of approximate duration τ_{dec}. At t_3, losses are set again at α_1 and the same process restarts after a certain period of time (around τ_{dec}), when the difference in population is back to equilibrium.

The maximum emitted photons density is $S_{\max} \approx R\tau_{inc}$ in Q-switched lasers, whereas in CW lasers it is $S_{\text{cont}} \approx R\tau_{dec}$. Ratio between these two values is $\frac{\tau_{inc}}{\tau_{dec}} \gg 1$, showing that peak power can be significantly large.

Two types of shutters are commonly used:

- rotative mirror;
- electro-optic switch (Pockels cell).

2.4.3 Gain-switching

Gain switching is a method for pulse generation by quickly modulating the laser gain with a varying pump power that will be alternatively turned on and off.

The principle of this technique is depicted in Figure 13:

- Pumping begins at t_1, and goes from R_1 below the laser threshold value R_{th} to a value R_2 above the threshold.
- The difference in population $\Delta N(t)$ begins to increase exponentially, with a time constant τ_p, and reaches the threshold limit ΔN_{th} at t_2. The photons density, $S(t)$, begins to increase.

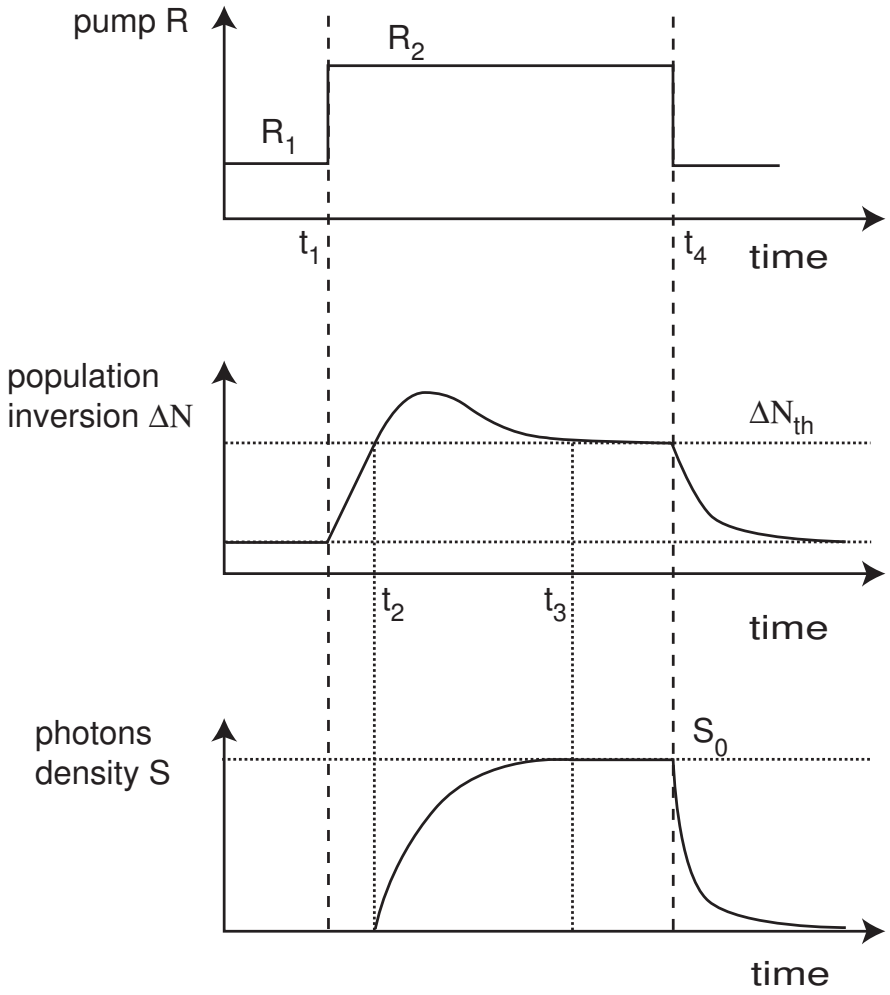

Figure 13: Gain switching pinciple.

- When reaching saturation, $\Delta N(t)$ decreases and stabilizes around ΔN_{th}. Therefore $S(t)$ stabilizes to a fixed value S_0 at t_3.

- At t_4, pump is back to its initial value R_1, and so $S(t)$ decreases to 0.

This method is easy to implement and short pulses (around 10 ps) can be generated. However, they are usually chirped and compression techniques are used, especially for long-haul transmissions [37, 38].

2.4.4 Mode-locking

The basic main idea of mode-locking is to coherently add several longitudinal modes and to concentrate the energy of these interferences at a specific location in the cavity to create pulses at a specific wavelength, as shown in Figure 14. This location propagates through the cavity and cavity modes are locked together. A phase relationship links the longitudinal modes in the cavity; for instance, the propagating optical signal is modulated at a frequency equal to the inverse of the round-trip time of the cavity.

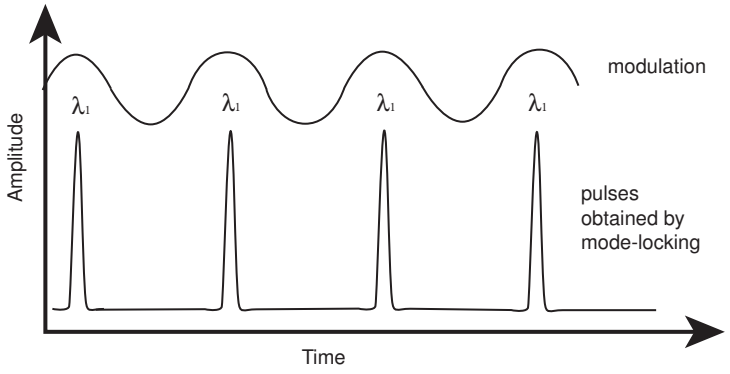

Figure 14: Mode-locking principle.

2.4.4.1 Basic concepts

To combine energy of several modes to form a pulse train, a phase relationship should be imposed to the optical signal propagating in the cavity.

Any modulating signal at a frequency f_m generates sidebands around each mode q (at a

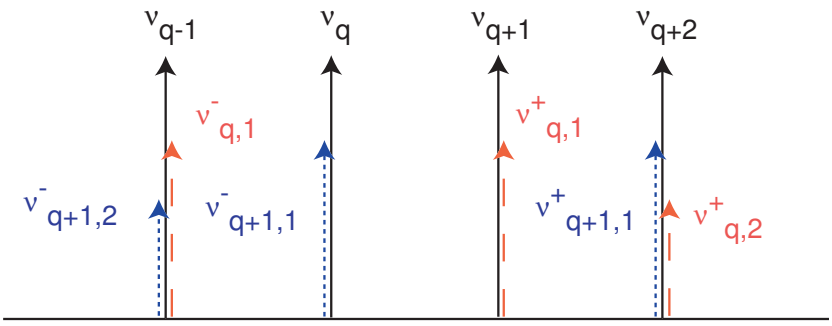

Figure 15: Modulation sidebands synchronization.

frequency ν_q). These sidebands are at frequencies $\nu^+_{q,k}$ and $\nu^-_{q,k}$, equal to

$$\nu^{\pm}_{q,k} = \nu_q \pm k f_m, \tag{12}$$

where k is an integer. If the modulation frequency is

$$f_m = \frac{k_{mod,n}\Delta\nu}{k_{mod,d}} \tag{13}$$

($k_{mod,n}$ and $k_{mod,d}$ are integers and $\Delta\nu$ is the axial mode separation, as in Equation 11), sidebands frequencies of mode q for $k = k_{mod,d}$ correspond to frequencies of modes of order $q + k_{mod,n}$ and $q - k_{mod,n}$. If the sidebands energy is large enough, coupling is achieved. The generated pulses are produced at a repetition rate equal to the frequency spacing between two successive coupled modes, i.e. $k_{mod,d}\, f_m$.

The relationship between the phase of the electromagnetic field, ϕ, and its frequency, ν, is

$$\nu = \frac{1}{2\pi}\frac{d\phi}{dt}. \tag{14}$$

Therefore

$$\phi_{q+1} - \phi_q = \frac{2\pi}{T}t + \phi_{cte}, \tag{15}$$

where ϕ_{cte} is a constant, ϕ_i is the phase of the mode i, and T is the cavity round-trip time.

Thus, if modes are in phase at $t = 0$, e.g., if they fulfill the mode-locking condition, they will also be in phase at all times $t = NT$. At $t = 0$, we can describe the mode-locking

condition by

$$\phi_{q+1} - \phi_q = \phi_{cte}, \tag{16}$$

which is equivalent to

$$\phi_q = q\phi_{cte} + \phi_0. \tag{17}$$

The non constant value of the spectrum gain curve of the amplifying medium causes non uniform amplification of frequencies. Hence only some modes are amplified enough to satisfy the lasing condition. Therefore, let us assume without loss of generality that $2M + 1$ modes are emitted. In this case, the electric field is

$$E(t) = \sum_{q=-M}^{M} E_q e^{(i\phi_q - i\omega_q t)}, \tag{18}$$

where E_q, ϕ_q, and ω_q represent magnitude, phase and frequency of mode q. In a first approach, let us consider that all modes have the same magnitude E_0. Using Equation 17, we obtain

$$|E(t)|^2 = \left[\frac{\sin\left(N\pi\,\Delta\nu\, t + \dfrac{\phi_{cte}}{2} \right)}{\sin\left(\pi\,\Delta\nu\, t + \dfrac{\phi_{cte}}{2} \right)} \right]^2 |E_0|^2, \tag{19}$$

with $N = 2M + 1$.

This leads to a series of pulses with temporal pulsewidth of value

$$\Delta t_p = \frac{1}{N\Delta\nu} \tag{20}$$

and the pulses are spaced by

$$\tau_{\mathrm{rt}} = \frac{1}{\Delta\nu}. \tag{21}$$

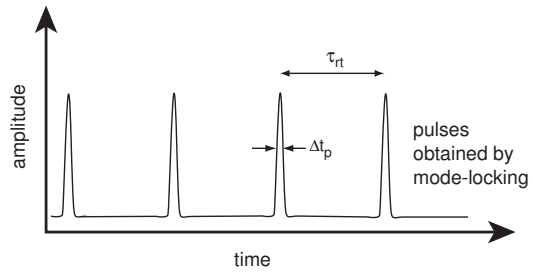

Figure 16: Mode-locked pulses characteristics.

This approach of the mode-locking technique allows us to understand how pulses can be generated when locking in phase the modes of the cavity. A more detailed analysis of this concept will be presented in the next paragraph.

2.4.4.2 Theoretical mode-locking analysis

We will consider a Gaussian approach to study pulse propagation in the cavity [39]. While this study considers transmission occurring at a maximum of the modulator transfer function, it describes quantitatively and qualitatively the generation of pulses. As represented in Figure 17, the cavity we consider has a ring configuration and has two components: gain medium and loss cell.

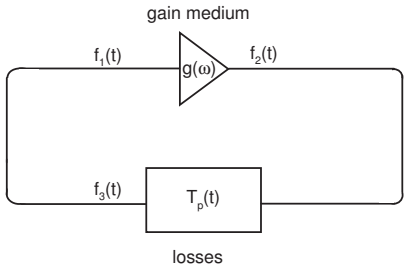

Figure 17: Schematics of mode-locking principle.

Gain medium transfer function Let us suppose that the input optical signal, $E_{in}(t)$, traverses an homogeneous gain medium represented by its transfer function $g(\omega)$. The output signal in frequency domain $E_{out}(\omega)$ satisfies

$$E_{out}(\omega) = E_{in}(\omega)g(\omega), \tag{22}$$

where $E_{in}(\omega)$ is the Fourier transform of $E_{in}(t)$.

It is assumed that the gain $g(\omega)$ of the medium is Gaussian

$$g(\omega) = \exp\left(-\frac{(\omega - \omega_0)^2}{\Delta\omega^2}\right), \tag{23}$$

where ω_0 is the reference angular frequency and $\Delta\omega$ is the 3 dB gain bandwidth.

Loss cell transfer function The losses are introduced by an intensity modulator. Its transfer function $T_p(t)$ is

$$E_{out}(t) = E_{in}(t)T_p(t) = E_{in}(t)\cos\left(\frac{\omega_0\tau(t)}{2}\right), \tag{24}$$

where

$$\tau(t) = \Delta\tau_p \sin(\Omega_p t), \tag{25}$$

$\Delta\tau_p$ being the modulation depth and Ω_p the modulation frequency, as we drive the modulator with a sinusoidal signal.

Considering first order approximations, this transfer function around $t = 0$ is

$$\begin{aligned} T_p(t) &\sim \cos\left(\frac{\omega_0}{2}\Delta\tau_p\Omega_p t\right) && (26)\\ &\sim 1 - \frac{1}{8}\omega_0^2\Delta\tau_p^2\Omega_p^2 t^2 && (27)\\ &\sim \exp\left(-\frac{1}{8}\omega_0^2\Delta\tau_p^2\Omega_p^2 t^2\right). && (28) \end{aligned}$$

Main analysis Figure 17 represents propagation of the optical signal through the diverse elements in the cavity. The initial pulse is assumed to be Gaussian and with optical frequency ω_0

$$f_1(t) = A\exp(i\omega_0 t - \Gamma t^2), \tag{29}$$

where $\Gamma = \alpha_1 - i\beta_1$ is the complex Gaussian pulse parameter.

By computing its Fourier transform, we obtain

$$F_1(\omega) = \frac{A}{2}\sqrt{\frac{1}{\pi\Gamma}}\exp\left(-\frac{(\omega - \omega_0)^2}{4\Gamma}\right). \tag{30}$$

Let's denote

$$B = \frac{A}{2}\sqrt{\frac{1}{\pi\Gamma}}. \tag{31}$$

After amplification, the pulse is described in the spectral domain by

$$\begin{aligned} F_2(\omega) &= F_1(\omega)g(\omega) && (32)\\ &= B\exp\left(-\frac{(\omega-\omega_0)^2}{4\Gamma}\right)\exp\left(-\frac{(\omega-\omega_0)^2}{\Delta\omega^2}\right) && (33)\\ &= B\exp\left(-(\omega-\omega_0)^2\left[\frac{\Delta\omega^2+4\Gamma}{4\Gamma\Delta\omega^2}\right]\right) && (34)\\ &= B\exp\left(-\frac{(\omega-\omega_0)^2}{4\Gamma'}\right), && (35) \end{aligned}$$

where

$$\begin{aligned} \Gamma' &= \frac{\Gamma\Delta\omega^2}{\Delta\omega^2+4\Gamma} && (36)\\ &= \frac{(\Delta\omega^4\alpha_1+4\Delta\omega^2(\alpha_1^2+\beta_1^2))-i\beta_1\Delta\omega^4}{(\Delta\omega^2+4\alpha_1)^2+(4\beta_1)^2} && (37)\\ &= \alpha_1'-i\beta_1'. && (38) \end{aligned}$$

In the temporal domain, we find that

$$f_2(t) = 2B\sqrt{\pi\Gamma'}\exp(i\omega_0 t-\Gamma' t^2). \quad (39)$$

After the intensity modulator, we have

$$\begin{aligned} f_3(t) &= f_2(t)T_p(t) && (40)\\ &\sim 2B\sqrt{\pi\Gamma'}\exp(i\omega_0 t-\Gamma' t^2)\exp\left(-\frac{1}{8}\omega_0^2\Delta\tau_p^2\Omega_p^2 t^2\right) && (41) \end{aligned}$$

As the signal should be the same after one round-trip for steady-state operation, f_3 and f_1 should be equal, and so

$$\begin{aligned} \alpha_1 &= \alpha_1'+\frac{1}{8}\omega_0^2\Delta\tau_p^2\Omega_p^2 && (42)\\ \beta_1 &= \beta_1' && (43) \end{aligned}$$

Using Equation 37, we obtain

$$\beta_1 = \frac{\beta_1\Delta\omega^4}{(\Delta\omega^2+4\alpha_1)^2+(4\beta_1)^2}. \quad (44)$$

Assuming that Γ is not zero, we have

$$\beta_1 = 0, \tag{45}$$

meaning there is no chirp effect. Thus, the second parameter α_1 is

$$\alpha_1 = \frac{(\Delta\omega^4\alpha_1 + 4\Delta\omega^2\alpha_1^2)}{(\Delta\omega^2 + 4\alpha_1)^2} + \frac{1}{8}\omega_0^2\Delta\tau_p^2\Omega_p^2. \tag{46}$$

Considering the typical values of the different parameters, ($\alpha_1 \approx \beta_1 \approx 10^{21}\ s^{-2}$ and $\Delta\omega \approx 10^{12}\ rad/s$), we have:

$$4\Delta\omega^2\alpha_1^2 \ll \Delta\omega^4\alpha_1, \tag{47}$$

and we find, after expansion of $(\Delta\omega^2 + 4\alpha_1)^{-2}$,

$$\alpha_1 = \frac{\omega_0\Delta\tau_p\Omega_p\Delta\omega}{8}. \tag{48}$$

As a result, the full width at half maximum (FWHM) is

$$\tau_p = (2\ln 2)^{\frac{1}{2}}\alpha_1^{-1/2} \tag{49}$$

$$= \frac{4\sqrt{\ln 2}}{\sqrt{\omega_0\Delta\tau_p\Omega_p\Delta\omega}}. \tag{50}$$

If phase modulation is considered instead of intensity modulation, similar results are obtained concerning temporal pulsewidth. However, a chirped pulse is generated and in this case, absolute values of α_1 and β_1 are equal [39].

2.4.4.3 Practical implementation techniques

To obtain this locking of modes, two methods can be used:

- *active mode-locking*: a modulator is introduced in the cavity to modulate in phase or in intensity at a frequency f_m, equal to $\Delta\nu$ [40, 41];

- *passive mode-locking* : a non-linear all-optical method is able to produce ultra-short pulses without any active component within the cavity. Usually, saturable absorbers or Kerr lenses are employed [42, 43, 44, 45]. A saturable absorber is a non-linear

optical component with an optical loss that decreases at high optical intensities. Laser emission can only occur if and only if modes are locked together to produce high intensity light to pass through the saturable absorber. The main drawback is lack of synchronization from an external clock.

2.4.4.4 Fundamental, harmonic, and rational mode-locking

When modulation frequency is equal to the axial mode separation, i.e., to the inverse of the cavity round-trip time T, the technique is called fundamental mode-locking.

If modulation frequency is equal to an integer multiple of the axial mode separation, mode-locking can still be achieved. This situation is called harmonic mode-locking [46]. Then, if the signal is modulated at a frequency $\omega_m = 2\pi N\Delta\nu$, with $N \in \mathbb{N}$, it can produce up to N pulses in the cavity. The temporal spacing between two successive pulses is then T/N. Obtained repetition rates can be high. All the modes within the gain bandwidth are thus grouped into N sets, called *supermodes*. The energy shifts among these groups and the relative phase-slides among them are the main source of amplitude fluctuations of the emitted pulses. It can lead to suppressions of pulses: this is the pulse drop-out phenomenon [47, 48, 49].

Equation 13 can also be satisfied for a modulation frequency equal to a rational of $\Delta\nu$. It is called rational mode-locking [50, 51].

2.5 Conclusions

This chapter was dedicated to the introduction to fiber optics communications. After a review of the fundamentals of optical fibers, we detailed the basics of optical amplifiers and laser sources. In the next chapter, we will introduce the different broadband access networks as well as the challenges they have to face. We will focus in particular on passive optical networks. We will emphasize the need of adequate light sources for this particular type of access network.

CHAPTER 3

BROADBAND ACCESS NETWORKS

Over the last few years, the area of data communications has experienced rapid development. As a result of the information superhighway, the growth rate in bandwidth demand is very high. Actual telecommunications networks have widely adopted optical fiber as the backbone transmission medium. Fiber is also a promising candidate for access networks. An important research activity has also been undertaken in the field of coding and multiplexing. Among all possibilities, WDM techniques have led to a great interest in fiber optic communication systems. However, to be practically implemented, these methods need adequate sources.

In this section, we introduce the background of the proposed research. First, we give a brief overview of actual telecommunications access networks. Then, we focus on the issues to solve for passive optical networks (PON). To conclude, we present diverse typical laser sources that may be used in these systems.

3.1 Types of access networks

With the expansion of services offered by the Internet, the last mile, also known as the first mile or broadband access, still represents a bottleneck problem. Depending on the competitors, different solutions are imagined and deployed. These can be classified into two main categories: wired and wireless. This section provides a brief overview of the different solutions, particularly emphasizing passive optical networks.

3.1.1 General considerations

Access networks connect business and residential customers to metropolitan area networks (MAN) and wide area networks (WAN). As shown in Figure 18, tomorrow's network is very dense and complicated. Because of the multiplicity of broadband multimedia applications, a huge demand for bandwidth has been imposed to the telecommunications

companies. Nowadays, access networks represent the bottleneck for end-to-end broadband applications. Unlike long-haul networks, access networks must serve a more diverse and cost-sensitive customer base. A good adequacy has to be found between a good quality of service (QoS), the offer bandwidth to the premises, cost, and performance.

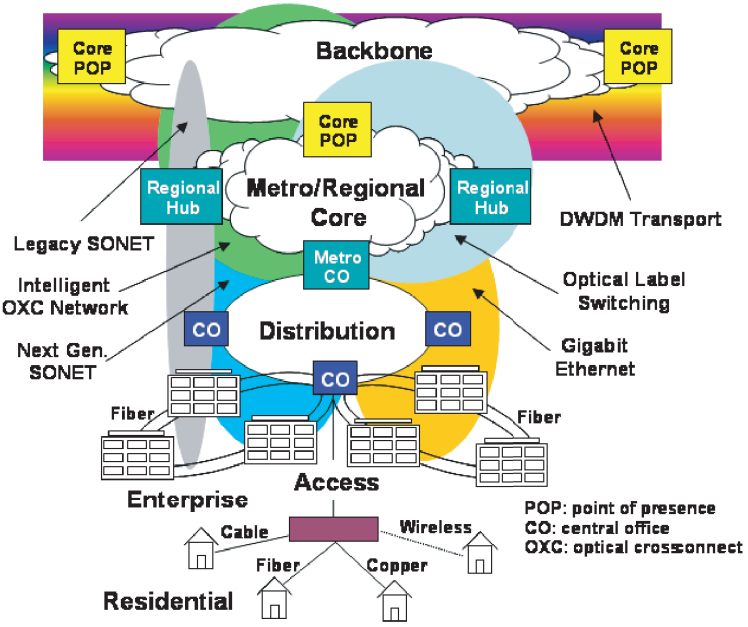

Figure 18: Tomorrow's network.

For the moment, the two most popular solutions are digital subscriber line (DSL) techniques deployed by telephone companies and cable modems from cable companies. Telecommunications companies try to take benefits of their installed infrastructure to eliminate deployment costs and to increase their return on investments to the maximum. For these reasons, DSL and cable are still the globally, mass-market, broadband access technologies. However, cable modems suffer from ingress noise and DSL systems from crosstalk. For these reasons, and because they are bandwidth limited, these solutions appear to be temporary. Even if wireless technologies are good for bandwidth scalability in terms of number of users and if mobility is their main asset, these solutions are prone to security problems and interference.

A new technology is steadily creeping up on the market: optical fiber. Fiber offers the

best guarantee that a network provider will have the infrastructure needed to deliver desired next-generation services, stay competitive, and retain customers. As a matter of fact, it is one major objective of these companies: to reduce churn, because the acquisition of a new customer is a very expensive hunt in a highly competitive environment. But to be a viable access network choice, fiber-based solutions need to face many challenges. The main one concerns the deployment costs. Fortunately, impressive advances in fiber splicing, trenching, and connectors have reduced installation costs. These new technologies and processes made also fiber installation easier and less time consuming, thereby reducing labor costs [52]. However, cost-effective solutions are still required in terms of light sources.

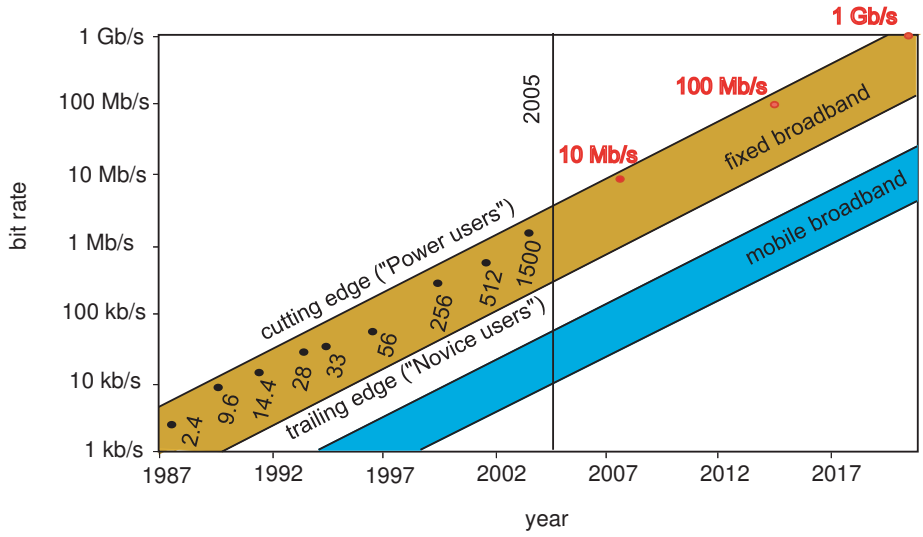

Figure 19: Data bandwidth projections (Source: Infonetics Research 2004).

Finally, we observe that the market is undergoing transformation from a broadcast one-way technology to an interactive, on-demand offering. Triple play services (voice, data, and video) are driving customers behaviors. To satisfy clients demands, the question is to know how much bandwidth will be enough in the future. With the upcoming necessary delivery of many high definition television (HDTV) channels and video-on-demand, consumer appetite for higher and higher speeds for high-speed Internet keeps outpacing market projections for growth in this service. Figure 19 projects the future expected needs in terms of data bandwidth. It seems that 25 Mb/s will suffice for a basic service offering in the near

term, but it will not be enough in the far future [53].

3.1.2 Digital Subscriber Line

Digital Subscriber Line (DSL) provides broadband access over twisted-pair copper phone lines. DSL separates the available frequencies to provide both voice and data services simultaneously over the same line. Different variants of DSL exist, such as asymmetric DSL (ADSL), High-Data-Rate DSL (HDSL), and Very High-Speed DSL (VDSL). The end users separate the data by using filters: a low-pass filter for voice and a high-pass filter for data.

DSL line rates are typically beyond 1.5 Mbps. The ADSL can reach 8 Mbps and uses the standard G. 992 issued by the International Telecommunication Union (ITU). The new standard released by the ITU in 2003, ADSL2+, increases the downstream data rates up to 24 Mbps on phone lines over 5 km and 20 Mbps over 10 km.

The main advantage of this solution is that it allows quick deployment because wiring is not required and is already installed. The connection is always on and there is no infringement on phone lines. However, because of its physical characteristics, copper cannot support high-bandwidth communication and has a high attenuation. As a consequence, DSL is restricted in data rate and distance of transmission. DSL is distance sensitive: performance is better when the subscriber is close to the central office. Thus, it can cause problems from a customer point of view. Another drawback is that DSL is not symmetric: the connection is faster for receiving data than for sending information through the network.

3.1.3 Hybrid Fiber Coax

The Hybrid Fiber Coax (HFC) network is a combination of two technologies and of two media: optical fiber and coaxial cable. Originally, HFC was a Cable TV (CATV) concept. CATV was invented to solve the issue of TV broadcasting and reception in rural areas. It makes use of the 50 to 750 MHz frequency spectrum, each channel occupying a 6 MHz band.

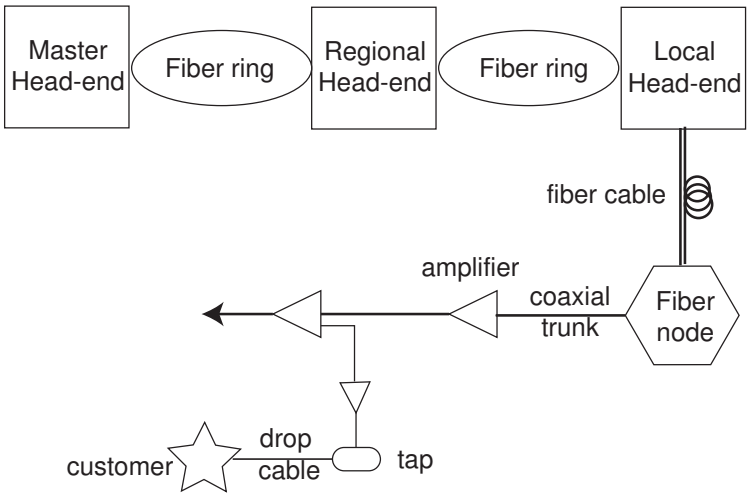

Figure 20: HFC configuration.

Pure coax systems are not able to provide high-speed residential broadband services. Moreover, they are difficult to design and maintain. Transmission degradations also occur during transmissions because of the limitations of amplifiers. To overcome these problems, cable operators suggested using fiber as a trunk medium and a coaxial cable network between the customer and the fiber node. It makes use of both optical fiber and coaxial cable, as depicted in Figure 20. The information is transmitted from a master head-end to the customer set top box via fiber rings, local head-ends, fiber nodes, coaxial cables, and amplifiers. The standard used is made by Cabelabs and is called DOCSIS. Version 1.0 was published in 1997, version 1.1 in 1999, and version 2.0 in 2002. The per-user bandwidth is about 10 Mbps.

In this network, the services are shared and always on. On average, the speed is ten times faster than with a telephone line. However, HFC has a limited upstream bandwidth: this is a major problem for important applications like peer-to-peer, video telephony, or web servers.

3.1.4 Wireless access network

The wireless access network has a major difference from the previous ones: there is no wiring. This solution is very attractive because it allows consumers to communicate

without the installation of wires. This offers a significant advantage: mobility. Initially, wireless was confined to voice communication, but with its tremendous success, its use rapidly expanded. Wireless access is excellent for the scalability of the network architecture in terms of number of users. From the service provider point of view, a large percentage of the deployment cost arises when a new customer subscribes.

As a matter of fact, the standardization of the 802.11 WiFi format by the Institute of Electrical and Electronics Engineers (IEEE) has paved the way for the deployment of this type of access network. The per-user bandwidth is 1.5 Mbps. Even if the idea is very appealing, the wireless spectrum seems too small for data traffic. There is a bottleneck between the data transported over fiber and the signals that have to be fed into a wireless channel. To solve this problem, a new solution is emerging: World Interoperability for Microwave Access (WiMax), known as standard IEEE 802.16. This uses a large frequency band, from 2 to 66 GHz, and should provide a per-user bandwidth of 70 Mbps up to a distance of about 50 km.

Other developments concern the use of infrared and free space optics. These techniques include the modulation of data onto an electromagnetic wave. The limitation mainly comes from the fact that free-space optics means point-to-point communication and is consequently limited by line of site.

Finally, the main drawback of this wireless technology concerns security: these systems are more prone to eavesdropping, attacks, and traffic analysis than the other systems.

3.1.5 PON: a promising candidate

A passive optical network is a point-to-multipoint optical network with no active element in the signal path between the source and the destination. It is mainly based on optical fiber and a power splitter. A PON configuration is shown in Figure 21. The passive elements are located in the distribution network (also called the outside plant) and the active elements at the endpoints of the network. The source endpoint is called the optical line terminal (OLT) and at the receiver side, the endpoint is called Optical Network Unit (ONU) [54]. Typically,

the PON is deployed in a single fiber tree configuration; the main fiber is called the trunk fiber and the last drop fibers are called the branches.

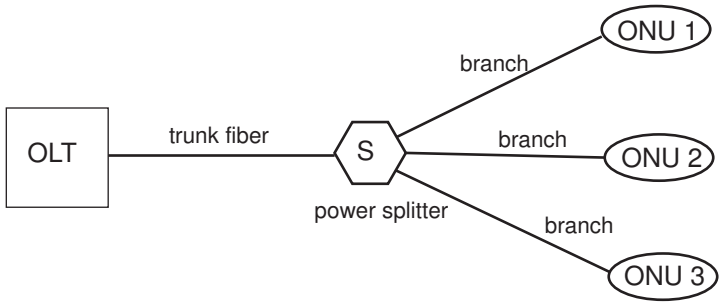

Figure 21: PON configuration.

Compared with the first and currently mass deployed access network systems, PON appears as a very promising candidate to provide high bit rate and symmetric-bandwidth distribution. Regarding its competitors, the PON approach presents a lot of advantages [55]:

- It makes use of the total bandwidth available in fibers. It will provide more bandwidth to the customer.
- It allows for longer distances between source and destination than with DSL. Typically, a PON can operate at distances over 20 km.
- It minimizes fiber deployment costs. Service providers share their costs of fiber and equipment at the OLT among several susbcribers.
- It reduces the capital expense of outside plants and related operation costs. Maintenance is simplified and is not a critical point.
- It provides greater flexibility. Service providers can upgrade or add new services by changing only some pieces of equipment at the OLT on a per-customer basis.

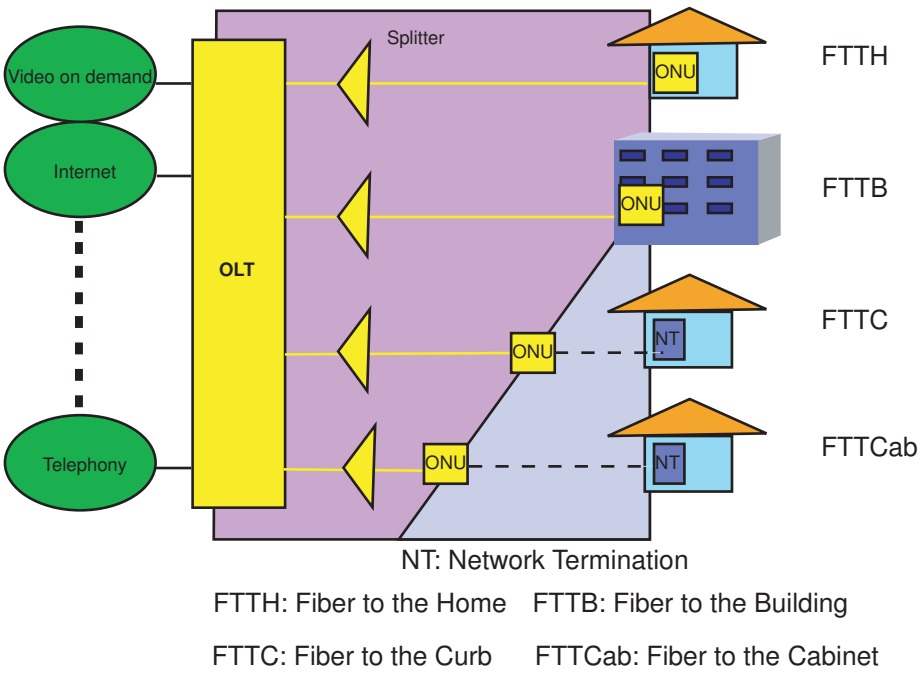

Figure 22: Different approaches of passive optical access networks.

PON technology includes different categories and approaches of access networks, as shown in Figure 22. For intense, researchers commonly speak about FTTP (Fiber-to-the-Premises), FTTH (Fiber-to-the-Home), FTTB (Fiber-to-the-Building), FTTC (Fiber-to-the-Curb), or FTTCab (Fiber-to-the-Cabinet). Generically, they are called FTTx architectures. The closer fiber comes to the final user, the more expensive is the deployment.

PON-based technology is already being rolled out, but at different rates and with different standards depending on the part of the world. The main regions are currently Asia, North America, and also Europe. As of September 2005, Japan had 2.7 million FTTP subscribers, Europe 892,000, and North America 322,700. In Japan, NTT announced in 2004 a plan under which it is to spend $48 billion to reach 30 million subscribers with EPON by 2010. In the United States, Verizon and SBC launched FFTP and FFTN using BPON. In Europe, Deutsche Telekom announced the deployment of FTTC for 50 cities in Germany. In France, France Telecom has just revealed its strategy to deploy FTTH using GPON in strategic urban areas to study the market.

3.2 Design issues for PON

With all the characteristics detailed in the previous paragraph, PONs lead to an intense interest for broadband access networks. Among all the propositions and research, many challenges still have to be solved. In particular, design considerations and issues have to be clarified, like frame format, Medium Access Control (MAC) protocol, or topology.

3.2.1 Frame format

Different data-link technologies can be used for transmission in PONs. The final choice of frame format and related protocol will not only depend on the types of services to be delivered, but also on the interfaces with the metro and long-haul area networks. Currently, three formats are in question: asynchronous transfer mode (ATM), Ethernet, and generic framing procedure (GFP).

ATM PON (APON)/Broadband PON (BPON) Until now, most of the deployments have been based on APONs. These proven PON technologies are based on the first specifications defined by a consortium formed by seven network operators in 1995. This initiative is called the Full Service Access Network (FSAN) [56, 57], which uses ATM as its layer-2 protocol. It was originally thought that ATM would become the prevalent technology in the different networks. Later, the name APON was replaced by the term Broadband PON (BPON) to emphasize the system's support of broadband services, such as video distribution. The original standard was defined by the ITU under the recommendation G.983. It specified an architecture with symmetric 155 Mbps upstream and downstream bit rates. The original recommendation was improved in 2001 to allow asymmetric 155 Mbps upstream and 622 Mbps downstream transmission. The transmission protocol uses a downstream frame of 56 ATM cells of 53 bytes each for the rate of 155 Mbps and of 224 cells for 622 Mbps. At the beginning and the middle of a downstream frame, Physical Layer Operation and Maintenance (PLOAM) cells are inserted: it is used by the OLT to control the communication with the ONUs. In each upstream slot, a three-byte overhead header and a 53-byte ATM cell are transmitted to allow for burst transmission and reception. In each ATM cell,

five bytes are for the header and 48 bytes are for the payload.

Finally, ATM has the advantage of allowing the implementation of various quality of service (QoS) policies and guarantees. It also appears to be a good choice to support real-time traffic. However, data has the form of Internet Protocol (IP) packets. To traverse the network, the packets have to be broken and put together at the end user; this induces complexity and cost. The overhead of ATM for carrying variable length IP packets is high and therefore is a major drawback for Internet traffic. Also, if an ATM cell is corrupted, it will affect an entire transmission and will consume ressources inefficiently. Moreover, the data rates appear relatively slow compared to other techniques and ATM has not become an inexpensive technology, as was promised.

Ethernet PON (EPON) Ethernet PON is a PON using Ethernet frames as defined in the IEEE 802.3 standard [58] released in mid-2004. It uses eight data bits encoded as ten line bits and operates symmetrically at a standard Ethernet speed of 1 Gbps. It is very convenient to carry IP packets via Ethernet frames: the protocol overhead for IP services is very small. Data transmission occurs in variable-length packets of up to 1518 bytes. The scalability is very high, up to 10 Gbps. Moreover, the hardware is cheap; EPON deployment is a cost-effective solution. Ethernet technology has now become a widely used standard, offering enormous economies of scale. Ninety-five percent of local area networks (LAN) use Ethernet and Ethernet has become very popular also in Metropolitan and Wide Area Networks (MAN and WAN). Ethernet deployment is growing rapidly and 10 Gigabit Ethernet products are available. As a consequence, the choice of Ethernet as a frame protocol would ease the integration and the interconnection of PONs with existing networks. With the EPON standard, there is no limit on the number of ONUs reached, but it is supposed to deliver up to 64 ONUs when using forward error correction.

Gigabit PON (GPON) With the emergence of EPON, the FSAN group realized that its architecture would require higher bit rates and a more efficient scheme of data transmission. Being limited by the intrinsic characteristics of the ATM frame format, the FSAN

group decided to adopt GFP, allowing a mix of variable-sized frames and ATM cells. It is referred as GPON [59], the ITU G.984 standard. GFP has the advantage of being SONET compatible, enabling service providers to link their voice connection into the PON without adding IP. The requirements include the following:

- full service support, including voice (TDM, both SONET and SDH), Ethernet, ATM, etc.
- physical reach distance of 20 km, at least.
- support for various bit rates using the same protocol, including 622 Mbps, symmetrical 1.25 Gbps, and 2.5 Gbps downstream / 1.25 Gbps upstream.
- security at the protocol level for downstream traffic.
- support up to 128 ONUs.

For all these reasons, GPON is a fierce competitor of EPON for the future deployed architecture.

3.2.2 MAC protocol

As a PON is a point-to-multipoint system, when different ONUs transmit data at the same time, collisions may occur. Then, a medium access control (MAC) protocol must be used to avoid this phenomenon and to fairly share the ressources among the different users. Two protocols are described here: time division multiplexing (TDM) and wavelength division multiplexing (WDM).

TDM Currently, the MAC protocol that has been intensively studied is TDM. The method is to put multiple data streams on the same medium by separating the signal into short time intervals. One segment is entirely dedicated to a specific user. It combines many advantages. In particular, it implies low cost and low maintenance. All ONUs can transmit over only one wavelength and so all the components in the different ONUs are identical.

For this reason, OLT only needs one receiver. In a TDM-PON, it seems easy to change the bandwidth allocated to each user, by only changing the time slot length assigned.

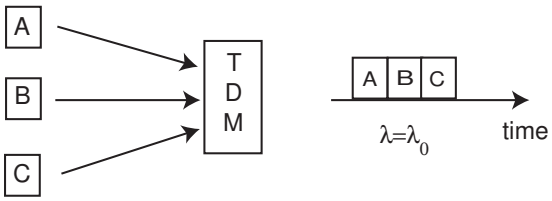

Figure 23: Time division multiplexing.

Despite all of these features, TDM-PONs face many challenges. In particular, end terminals must be accurately synchronized; the clock recovery can be challenging. The prime problems of TDM-based access network are faced in burst mode reception at OLT and synchronization within overhead period of each upstream slot. It seems difficult to easily upgrade and scale these TDM-based optical access networks.

WDM To extend the capacity of access networks without changing the fiber infrastructure too much, a method where each data signal is modulated onto a different optical wavelength has been considered: WDM.

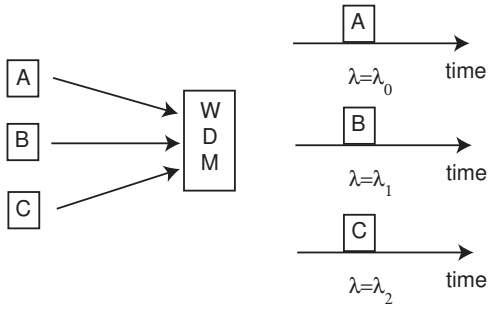

Figure 24: Wavelength division multiplexing.

In such a configuration, WDM makes full use of the large bandwidth of optical fiber [60]. By using different channels, WDM networks are easy to scale and to upgrade. The connection between source and destination is independent of the line rate and of the

frame format. WDM-PONs are still expensive architectures because specific wavelength-dependent devices, like dedicated transceivers for each end user, are required. A WDM-PON system also needs filters at the receiver side, which must be tuned very precisely to match the signal to its subscriber. Thus, inventory and maintenance become issues. Therefore, the cost of such a network appears prohibitive. However, the deployment costs are expected to decrease when the components become more mature and are mass produced.

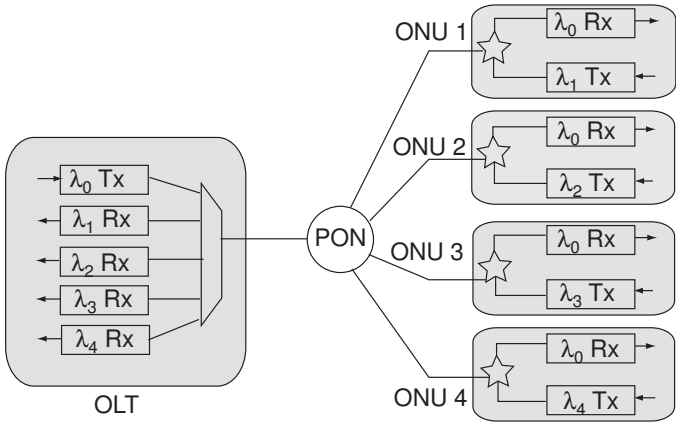

Figure 25: Hybrid TDM/WDM PON configuration.

With WDM, an important choice still has to be made regarding wavelength assignment: between coarse WDM (CWDM) and dense WDM (DWDM). CWDM uses 18 channels between 1290 nm and 1610 nm. The spacing between the channels is of 20 nm, with a channel bandwidth of 13 nm. The main advantage of the CWDM solution is its cost. CWDM components are cheap because their requirements are not stringent. The emitted wavelengths may vary. There is no need for temperature control and stabilization. However, the number of channels is limited to 18. Some channels suffer the peak absorption of water in the optical fiber. Attenuation will differ from one channel to another. Moreover, there is a lack of good optical amplification for these different channels. On the other hand, DWDM imposes a separation between wavelengths of 50 GHz (0.4 nm for the C-band) or 100 GHz (0.8 nm for the C-band). It achieves better spectral efficiency and, by using the C-band, fully exploits the commercially available optical amplifiers. It can also provide longer reach. For all these reasons, the performances with this method are very good and this technology

appears to be the best option in the long-term future. However, cost remains a problem.

A pragmatic scenario for the transition from current TDM-PONs to future DWDM-PONs uses a hybrid TDM/WDM access network architecture [61], as shown in Figure 25. It consists of a shared TDM downstream link on a dedicated wavelength (for instance 1310 nm) and a set of specific WDM upstream links (for instance over the C-band between 1530 and 1565 nm).

3.2.3 Physical topology

PON is basically a point-to-multipoint architecture. To implement such a network, many topologies have been proposed, some of which we present here. PONs can be deployed in a tree, ring, or bus configuration, as shown in Figure 26. Using couplers and splitters, PONs can easily be used in any of these architectures.

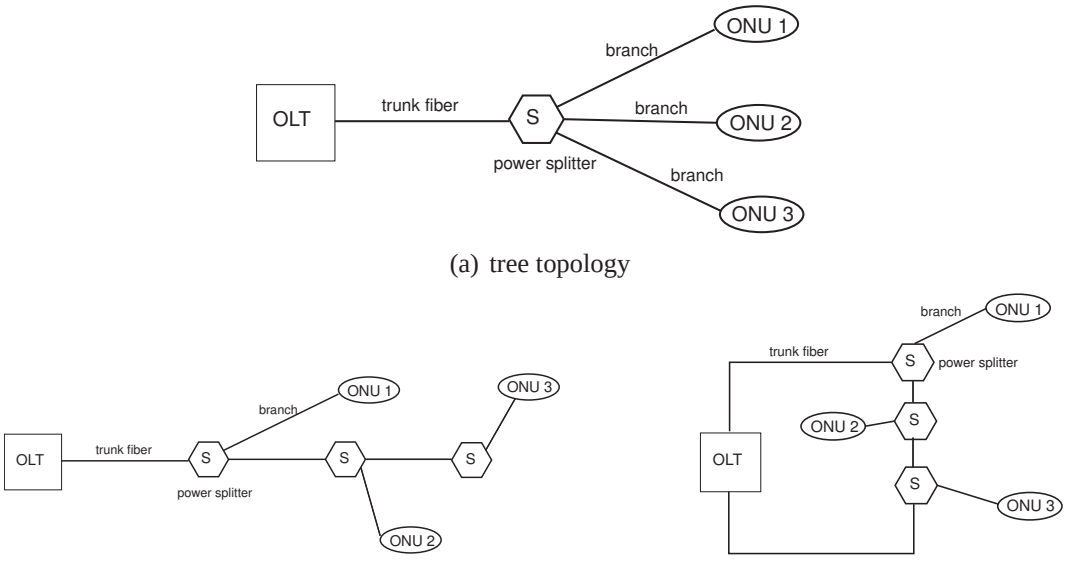

(a) tree topology

(b) bus topology

(c) ring topology

Figure 26: PON topologies.

In the field, two scenarios can be implemented with WDM-PON: single or dual fiber systems. In the single-fiber case, one fiber cable will support both downstream and upstream signals, whereas in the multiple fiber case, one fiber is dedicated to the downstream transmission and another one to the upstream transmission. Sometimes, one fiber can be

used for broadcast and another one for data. Figure 27 shows different scenarios for optical bands allocations in the two cases. The differences are mostly economical, in the sense that there is less fiber deployed in the first case. However, in the second proposition, the terminal components are less complicated to design and manufacture.

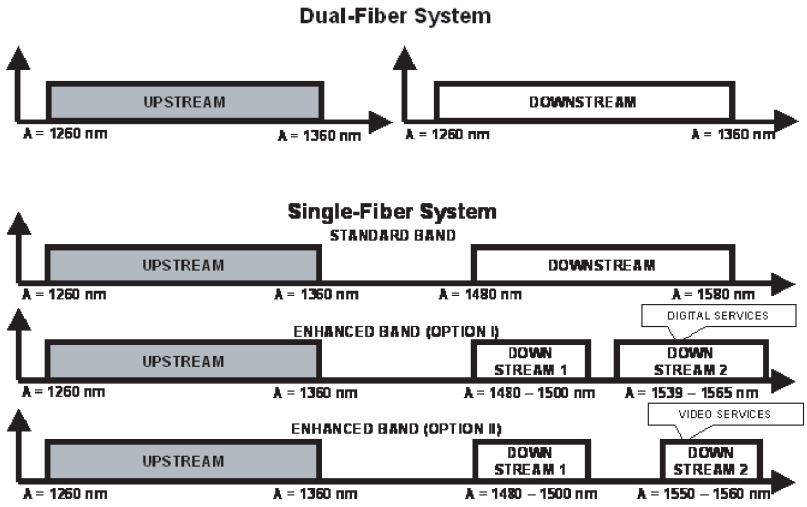

Figure 27: Typical downstream and upstream optical bands for single and dual fiber PON systems.

The successful deployment of PONs requires diverse enabling technologies, such as low cost and high-speed filtering. In this area, research focuses on tuning mechanism, devices design and fabrication. Then, wavelength multiplexers / demultiplexers will play a key role in the implementation of PONs. Switches and splitters are also investigated to optimally route the information to the subscriber. Also, optical transceivers operating at high bit rates have to be made suitable for access networks. Finally, especially in the case of WDM-PON, adequate sources are required to emit the light at specific wavelengths.

3.3 Light sources

To pratically implement such multiplexing techniques and optical network architectures, adequate emitters are required. Three categories of optical sources can be distinguished: fixed wavelength, tunable, and multiwavelength sources.

3.3.1 Fixed wavelength sources

In WDM networks, the multiplexing of different wavelength channels in a single fiber requires laser sources generating these wavelengths. The simplest idea consists of considering many emitters, each producing one specific fixed wavelength.

Currently, Fabry-Perot (FP) laser sources are cheap solutions. However, if there is no control of the temperature, FP lasers cannot emit at specific and calibrated wavelengths. Moreover, these sources suffer from mode partition noise. One solution is to use an injection-locking technique to adjust the wavelengths [62, 63].

There are also three other types of such sources: distributed feedback lasers (DFB), distributed Bragg reflectors (DBR), and vertical-cavity surface-emitting lasers (VCSEL). In all cases, these three different types of lasers are monolithic semiconductors. The fixed

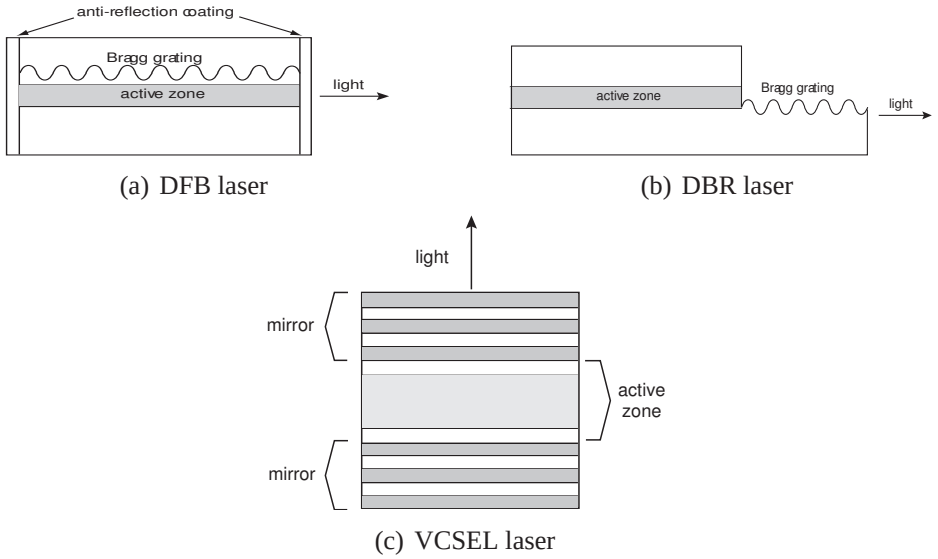

(a) DFB laser (b) DBR laser

(c) VCSEL laser

Figure 28: Types of fixed wavelength lasers.

wavelength emission is obtained by inserting an intracavity optical filter. A Bragg grating will notably be incorporated in the laser to control the laser diode wavelength. When the grating is integrated within the active zone, this is a DFB laser; otherwise it is a DBR laser. These two categories of sources emit in the plane of the PN junction: they are called edge-emitting lasers. These lasers have excellent wavelength stability.

These lasers have difficult coupling with optical fibers. Therefore, another source has been developed: source emitting in a direction perpendicular to the PN junction, known as VCSEL. The active zone is generally made of quantum wells and the length of a VCSEL is small compared to its width. On both ends, DBR lasers act as mirrors.

3.3.2 Tunable sources

The main drawback with the previous sources is that one specific laser can only generate one single wavelength. This leads to obvious cost, manufacturing, and inventory concerns. For these reasons, tunable lasers have been developed. There are mainly two tuning methods and many practical implementations.

Tuning techniques Two ways of reaching optical wavelength tunability are conceivable. The first and simplest one consists of using an optical filter that will move to select different longitudinal modes under the gain curve; this is mode hopping tuning. On the contrary, the second method is to change the positions of the longitudinal modes; this is continuous tuning.

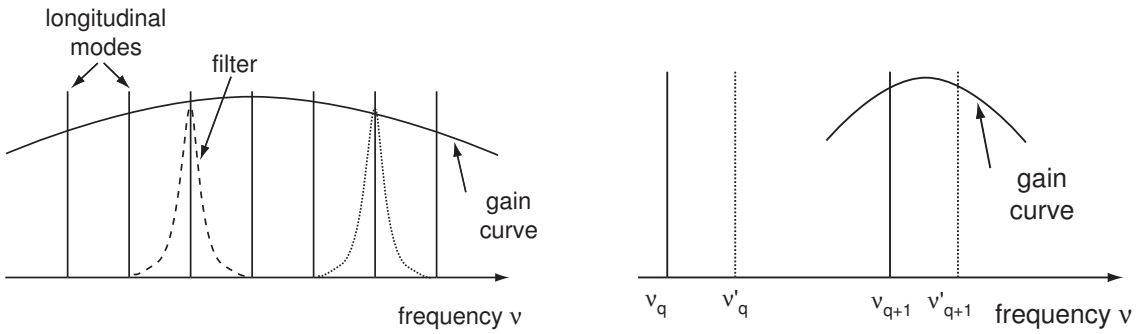

(a) mode hopping tuning (b) continuous tuning

Figure 29: Wavelength tuning methods.

Practical implementation Two categories of tunable lasers are described: semiconductor lasers and fiber lasers.

In semiconductor lasers, a widely used technique is to make the refractive index vary via current or temperature fluctuations [64]. A filter can also be added to the laser, such as sampled Bragg gratings [65]. A second method takes advantage of the insertion of the

laser in another cavity, called an external cavity. These lasers are known as extended cavity lasers. For instance, concerning VCSELs, one idea is to mount a micro- electro mechanical system (MEMS) on one mirror to change the cavity length by simply applying a voltage [66]. For the moment, VCSELs are commercially available for wavelengths at 850 nm and 1310 nm, but not yet for 1550 nm. However, VCSEL shows great promise as it has the potential for low-cost mass production and for high-level integration.

Regarding fiber lasers, the different solutions mostly incorporate an intracavity filter. Many types of filters have been studied: Bragg filters [25] Fabry-Perot filters [67], unbalanced Mach-Zehnder interferometers [68], acousto-optic filters [69], etc.

The tunability range of these different techniques depends on the considered gain medium.

3.3.3 Multiwavelength sources

Tunable sources appeared to have a great interest for WDM communications systems. Nevertheless, in many cases, they are not optimal. Another type of source has been explored by researchers: multiwavelength laser sources. Instead of tuning the emitted wavelength for one source, this approach consists of generating all the different channels via a single device.

Categories of multiwavelength sources When speaking about multiwavelength sources, two main categories can be identified: continuous wave [70, 71] and pulsed [72, 73] sources. Within the pulsed sources, research studies have focused on two types of operation. Indeed, as shown in Figure 30, wavelengths can be emitted:

- *simultaneously* [74, 75]: all the wavelengths are contained in each pulse.
- *alternatively* [76, 77]: successive pulses are at different wavelengths.

Practical implementation Many methods have been proposed to implement these multiwavelength sources. This section gives a general overview of the possible involved mechanisms.

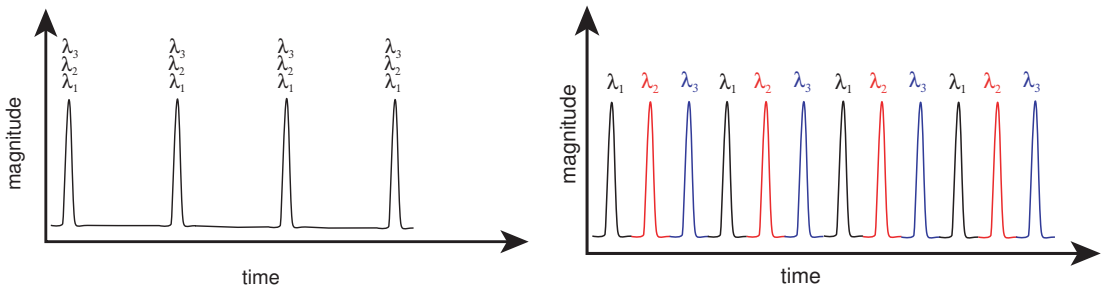

(a) simultaneous generation (b) alternate generation

Figure 30: Categories of multiwavelength pulsed sources.

Lasers array The simplest idea consists of choosing many semiconductor lasers producing different optical wavelengths and then mounting them together to form an array of lasers [78]. To miniaturize the source, the lasers can be put on the same wafer [79]. Zah et al demonstrated the design and fabrication of an array of 20 DFB laser diodes with integrated combiner and optical amplifier. The chip size was 4.3 mm x 1.4 mm [80]. Even if the compactness of this array is very attractive, some effort are still needed to reduce the facet reflectivity and cross-gain modulation before simultaneous modulation becomes practical.

As a matter of fact, the potential of these laser arrays is uncertain because manufacturing these sources becomes more and more complex with the number of integrated lasers. One of their main drawbacks is the high insertion loss into the optical fiber. Moreover, when one laser diode is broken, it causes a major problem of maintenance to replace and fix it. It also means that the user must have many DFB lasers for backup. Using one DFB laser for each channel requires complicated procedures for monitoring and controlling either temperature or injection current to inhibit wavelength shifts and power fluctuations.

Supercontinuum generation The use of many laser diodes to form a multiwavelength source appears to be cost-inefficient, especially when the number of desired wavelengths becomes large. An other candidate was proposed: supercontinuum generation. The supercontinuum generation is a phenomenon in which an intense pump optical pulse spectrum is broadened over a continuous range due to non-linear effects in an optical fiber [81].

The generated spectra extend to both longer and shorter wavelengths from the pump wavelengths and can exhibit an almost flat profile by choosing adequate parameters. By using an arrayed-waveguide-grating (AWG), one mode can be extracted, forming CW light for transmission.

Even if the number of wavelengths can be very large (up to 1000 channels with 12.5 GHz spacing), their use is limited by the noise performance. The combination of FWM and ASE during the supercontinuum generation process results in degradation of the coherence and decrease of the signal-to-noise ratio [82].

Spectrum slicing The use of numerous lasers to form a single multiwavelength source turns out to be expensive. Efforts have been made to create a single source directly producing many wavelengths. One technique consists of using a wide spectrum source, such as a broadband light-emitting diode (LED) or an amplified spontaneous emission (ASE) source, and an adequate filter to select the wavelengths; this method is known as spectral slicing [83, 84].

This technique using broadband light source with spectrum slicing suffers from the need for the high power front end, as well as the power efficiency of discarding much of the available spectrum in the filtering process. Moreover these sources may have high packaging costs.

A similar method consists of building a simple fiber ring laser cavity consisting of just a gain medium and an intracavity filter [85]. The generated laser output is thus a multiwavelength CW light. Many filters are commonly employed. For example,

- Fabry-Perot filters [71].
- delayed interferometer: when the two arms of the Mach-Zehnder interferometer have different path lengths, it acts as a periodic filter [86, 87].
- chirped ladder filter [88].
- Bragg gratings: if sampled or chirped, they act as spectral filters [89]. These chirped

gratings allow the separation of the pulses at different wavelengths before their amplification.

- filters resulting from nonlinear effects [90]. For instance, in [91], a sampled fiber Bragg grating initiates the multiple wavelength generation and the number of wavelength increases through FWM in a high non-linear photonic crystal fiber.

- high-birefringence fiber loop mirror [92, 93]. The idea is to split the input optical signal equally into two counter-propagating signals which interfere at the coupler after propagating around the loop. This interference will be constructive or destructive depending on the birefringence of the cavity. The loop reflection is indeed wavelength dependent. This is also called a Sagnac interferometer [94, 95].

- intracavity polarizer [96, 97]. In this simple method, a polarizer is inserted in the cavity containing a birefringent gain fiber. Because of the wavelength dependence of the phase shift induced by fiber birefringence, wavelength selection occurs.

Gain medium management In the previous methods, erbium-doped fiber amplifiers were largely represented and used as gain media because of their high gain with broad gain bandwidth and compatibility with fiber-communication systems. The number of wavelengths that can be generated in a fiber laser is critically important as it is directly proportional to the system trasnmission capacity. However, the homogeneous character of the erbium normally poses a major barrier to obtaining a stable multiwavelength emission [14] at room temperature. Consequently many gain medium management techniques have been investigated to combat against this limitation. As a matter of fact, scientists observed that by inserting an intracavity filter associated with an acoustooptic frequency shifter in the laser cavity, multiwavelength operation was feasible [98]. This frequency shifting forbids the existence of a stationnary state in the cavity. By cooling the gain medium in liquid nitrogen at 77 K, homogeneous broadening of erbium is largely reduced. The disadvantage

is that this technique is not easily integrated in industrial systems [99]. It is an inconvenient method and it may impact the device durability, leading to complexity in component configuration. In [100], a single piece of erbium-doped twincore fiber is used to provide an inhomogeneous gain medium through macroscopic spatial hole burning. As the available gain at each lasing wavelength is partially decoupled from the others, simultaneous operation of several single frequency modes can be reported.

Compared with EDFA, SOAs can suppress mode competition at room temperature because of their inhomogeneous gain broadening and facilitate multiwavelength oscillation with ITU-grid spacing [72, 101]. Unfortunately, SOAs are still not deployed in industrial networks, even if they are intensively studied in research laboratories. However, they have a lot of potential for next-generation networks, even if they still possess relatively high insertion loss. Some other schemes propose to form a hybrid gain medium by inserting a SOA into a EDFA-based ring cavity to increase the bandwidth of the gain medium to increase the number of emitted wavelengths: in such a situation, a uniform and broadband gain spectrum can be obtained and a stable simultaneous multiwavelength laser operation can be achieved at room temperature [102, 103]. Recent studies also focus on Raman optical amplifiers [104] and linear optical amplifiers [105, 106].

Dispersion tuning The previous methods were mainly dealing with multiwavelength CW light sources. To generate pulses, mode-locking is widely used and pulses are emitted when inserting a modulator in the cavity. By adding a modulator to a laser cavity with a gain medium and a comb filter, it is easy to produce simultaneous multiwavelength generation. A more difficult task is to emit alternate multiwavelength pulsed light. A method consists of using dispersion [77, 107, 108]. For instance, in [77], the technique relies on sequentially self-seeding the modes of a directly modulated laser diode in a dispersion-managed fiber loop. In this scenario, all the pulse trains arrive at the same time at the modulator and are then temporally separated when traveling through negative dispersive elements. These trains continue to propagate and when they arrive at the positive dispersive medium, they

will propagate at different speeds, so that they will fall into the same transmission window of the modulator.

This method requires a good optimization of the experimental parameters to synchronize correctly the different pulse trains at the modulator: tunability and upgradability are the weaknesses of this configuration. Moreover, the number of wavelength generated with this technique is still limited: between two and ten wavelengths.

Dispersion can also be used to control the emitted wavelengths. Spacing between two wavelengths emitted by the laser is linked to the modulation frequency, the cavity length, and the intracavity dispersion. For given two first parameters, an adjustment of the dispersion affects the wavelength spacing. It allows smooth wavelength tuning, which means that the oscillating wavelength can be continuously tuned by changing either the modulation frequency or the cavity length without interrupting the stable pulsing state. This approach offers the advantages of a relatively low cavity loss and a wide tuning range, but only dual-wavelength pulses have been experimentally demonstrated [109].

Diverse methods Optical sources capable of generating multiple wavelengths have been intensively investigated and many techniques have been introduced. Here are some other examples of the methods developed.

A method developed by Chen et al generates dual-wavelength actively mode-locked pulses in an EDFA-based fiber ring laser. As shown in Figure 31, it uses two nearly identical serial arrays of fiber Bragg gratings having opposite orientation to spread the pulses before amplification and de-spread them before time-gating [110]: pulses generated at different wavelengths pass through the time-gating element simultaneously. Another demonstration was made with two nearly identical linearly chirped fiber Bragg gratings [76]. This principle is interesting but becomes less practical when the number of wavelengths increases. Moreover, fiber Bragg gratings generally result in highly chirped pulses.

In the case of multiwavelength mode-locked pulses, since the round-trip time for each wavelength is different, precise control of the cavity length is required to achieve optimum

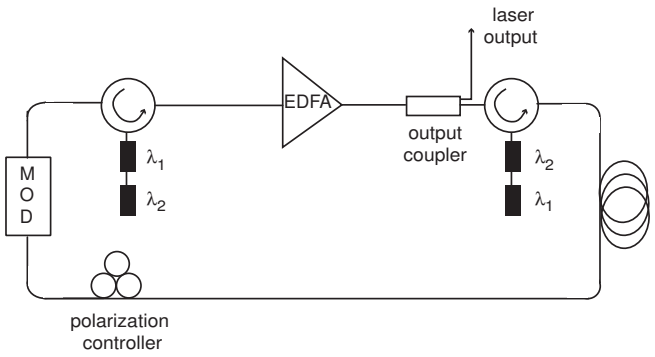

Figure 31: Schematic diagram of an alternate multiwavelength laser source using fiber Bragg gratings (MOD: modulator).

mode-locking condition for each wavelength: the arrival time of each pulse must be coincident. One solution is to use multi-cavities of different lengths with only one gain medium [111, 112]. The main drawback with this method is that it requires a lot of effort to adjust carefully the lengths of the different cavities.

A simultaneous generation of multiwavelength short pulses has been demonstrated by self-injection of a laser diode [113]. The idea is to use a gain-switched laser diode in an external cavity. Owing to the quasimonochromatic nature of the self-seeded gain-switched laser output, the multiwavelength operation can be reached by introducing many wavelengths elements back into the diode provided that the repetition frequency is a multiple of the round trip propagation frequency for each pulse. The wavelengths are selected by the use of multiple optical paths in an external cavity consisting of a grating, a beam splitter, and two mirrors. Three 0.9 nm spaced wavelengths are generated with tunability over 14 nm.

A widely used set-up uses sigma laser configuration. Typically, it comprises a loop in which an electro-optical modulator is included to create mode-locked pulses and at least one arm coupled to the loop by the means of a power beam splitter. In the arm of the laser, fiber Bragg gratings are used to play the simultaneous roles of wavelength-selective mirrors, tunable optical filters, and output fiber couplers. To obtain simultaneous multiwavelength operation, different schemes have been exposed: the gratings can be put in

series [114] or in parallel, forming multiple arms [115].

Recently time-lens compression has been proposed [116]. Pulses are formed by pulse carving before being sent into a time lens. In addition to pulse compression, it also displaces the pulses according to their center wavelengths. Alternating multiwavelength trains are thus produced.

3.3.4 Laser sources in WDM-PONs

Many issues have to be solved when deploying a PON system as we described previously. In a WDM context, the question of light sources is of prime interest because cost-effective solutions have to be found to be commercially competitive. As no active element is allowed in the distribution network, light sources represent an issue at the ONU (customer side) and at the OLT (central office side). In this paragraph, we will briefly describe the technologies that have already been studied.

To send an upstream signal, the most straightforward solution to implement the ONU transmitter is to use a stabilized laser source. A solution consists of employing dedicated lasers for each specific ONU. Fabry-Perot lasers are the less expensive sources, but the upstream bit rate will be limited and stabilization of the emitted wavelength might require bulky optics and power-hungry electronics [117]. Link reach can also be limited by the mode partition noise, because multiple longitudinal modes are excited in a Fabry-Perot laser. To excite only one designated wavelength, researchers have proposed an injection-locked technique [62]. In this case, the laser behaves as an oscillator that synchronizes with external excitation and modulation index, laser bias current, and the power of the injected signal must be carefully chosen to optimize the efficiency of the system. Moreover, using one specific source for each user becomes considerably expensive when the number of subscribers becomes large. The objective is to avoid wavelength specific ONUs to decrease the costs of operation, administration and maintenance functions. Since mass production becomes possible with just one specification, production costs will also decrease.

For these reasons, many alternatives have been proposed [60, 61]. The first one is to

use a tunable light source without wavelength stabilization at each ONU, but with wavelength monitoring functionality in the OLT. However, tunable lasers are still expensive for access networks solutions. In the future, VCSEL have the potential for low-cost mass production and when tunable VCSEL around 1550 nm will become a mature technology, it might be an ideal candidate for WDM-PON. A second approach is to employ a light source with broadband optical spectrum, such as light emitting diode, at each ONU. The signals generated by the ONUs are then spectrally sliced by AWGs [118]. This system is low cost, but the power after spectral slicing is low and thus the link reach can be limited. The last option is to use an external lightwave provided by the OLT and to simply employ a modulator in the ONU: the light source is centralized at the OLT. For this option, different configurations have been suggested and demonstrated. Many ONUs models have been suggested by using different modulation formats for upstream and downstream transmission or by using amplitude signal regeneration and advanced devices: for instance frequency-shift keying/intensity modulation [119] and differential phase-shift keying/remodulated on-off keying [120] have been demonstrated. One idea is to use a remodulating loop composed of a circulator, a modulator, and a gain medium to boost the signal [121]. Many schemes use reflective SOA (RSOA) for remodulation for the upstream transmission [122, 123, 124]. Prat et al use a single RSOA in the ONU performing two operations: detection but also modulation and amplification [125].

3.4 Conclusions

This chapter was dedicated to the introduction of broadband access networks techniques. We particularly emphasized the passive optical networks that are at the center of our study. We presented the different light sources that can be used in such networks. We pointed the interest and the need for multiwavelength laser sources to achieve cost-efficient systems. This kind of source is the main object of our work. In the next chapter, we will

introduce a new type of sources that we designed, developed, built, and tested: an alternate multiwavelength picosecond mode-locked erbium-doped fiber ring laser based on an unbalanced Mach-Zehnder interferometer.

CHAPTER 4

ALTERNATE MULTIWAVELENGTH PULSED FIBER LASER

Mode-locked lasers emitting picosecond pulses around the 1550 nm region are potential signal sources for high bit rate communication systems. To reduce the cost and increase the capacity of future systems, recent studies focused on the creation of multiwavelength sources. They are expected to find wide applications in the practical implementation of two-dimensional optical code-division multiple access (OCDMA) [126] and photonic analog-to-digital conversion [127]. The proposed work studies the design of a novel architecture with alternate multiwavelength behavior. The successive multiwavelength pulsed operation is reached in an actively mode-locked erbium-doped fiber laser in which an unbalanced Mach-Zehnder interferometer (UMZI) has been introduced.

The following sections introduce the general principle of this specific fiber laser setup. Then, we report the theoretical, numerical, and experimental results of the multiwavelength generation.

4.1 Presentation of the source

4.1.1 General principle

The main objective is to produce picosecond pulses at GHz repetition rates in the third telecommunication window, i.e., in the 1550 nm region. Spacing between emitted wavelengths should be on the order of some nanometers. As shown in Figure 32, the setup comprises an erbium-doped fiber amplifier (EDFA) as gain medium, a polarization controller, an output coupler, and an UMZI [128].

To generate the alternate multiwavelength emission, two basic operations are needed, pulse generation and wavelength selection. To do so, two different techniques are used: active mode-locking and tunable filtering. The originality of our scheme is to use the UMZI as a single device to realize both operations. A similar principle was first used by Olsson and Tang in a bulk laser, but with separated tunable filter and mode-locker elements [129].

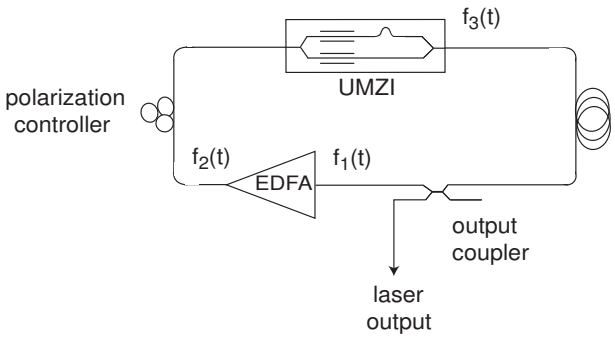

Figure 32: Schematic diagram of the alternate multiwavelength laser.

When no radio-frequency (RF) signal is applied onto the UMZI, it behaves as a spectral filter, with a sinusoidal frequency transfer function and a free spectral range (FSR) of 60 nm. Upon the application of a time-varying electrical signal, this transfer function shifts accordingly. Equivalently, each wavelength sees a different temporal transfer function that depends on the bias of the UMZI and the frequency and modulation depth used. This results in a wavelength-dependent mode-locking condition and in an alternate generation of pulses at different wavelengths. In the time domain, for a specific wavelength, the UMZI acts as an intensity modulator and thus will concentrate the energy of the cavity under the maxima of its transfer function. It will produce optical pulses by active mode-locking. To reach Gigahertz repetition rates, harmonic mode-locking is used, i.e., the UMZI is driven at a harmonic of the fundamental frequency of the cavity.

To obtain an alternate multiwavelength operation, it is necessary for the maxima of the ouput power of the UMZI for different wavelengths to alternate. Figure 33(a) shows an example of an alternate dual-wavelength pulse emission. In this situation, the maxima of the output power for wavelength λ_a correspond to the minima of the output power for λ_b. We can observe that the bias point of the modulator is on the positive slope linear part of the transfer function for λ_b and on the negative slope linear part for λ_a. Figure 33(b) shows the alternate generation of multiwavelength pulses when the bias point is near a maximum of the transfer function. It leads to a frequency doubling situation: the pulses are emitted at twice the modulation frequency of the UMZI.

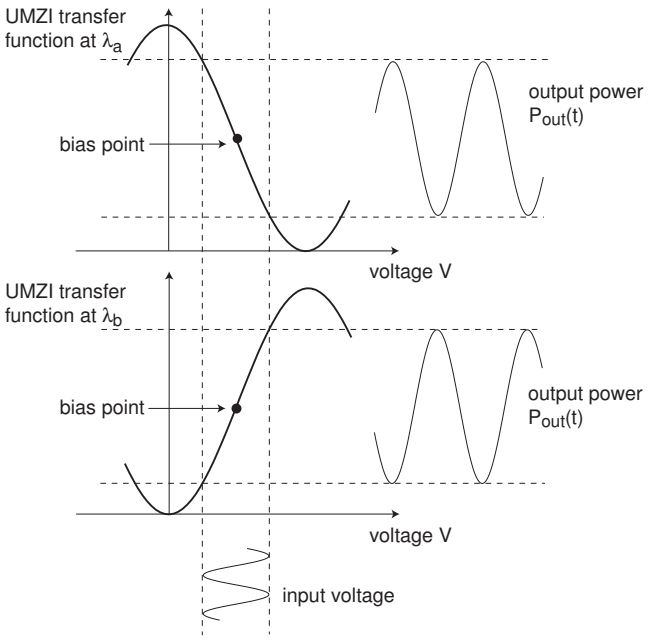

(a) bias on the linear part

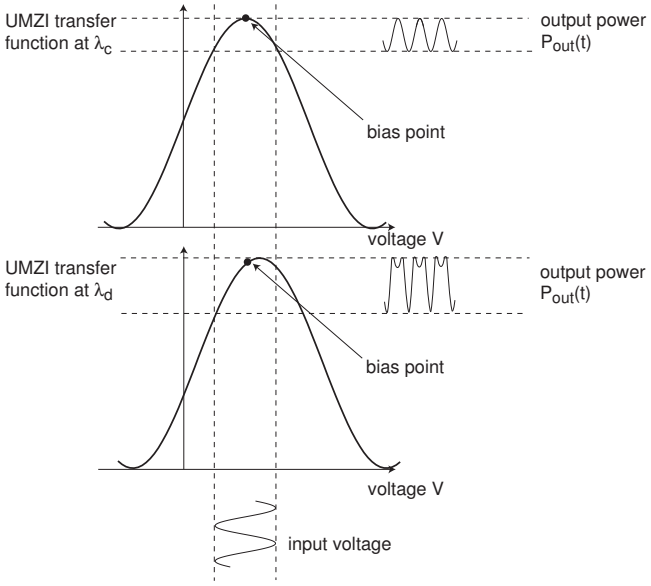

(b) bias at the maximum

Figure 33: Principle of the multiwavelength pulse generation with an UMZI.

4.1.2 Possible applications

Code Division Multiple Access To meet the dual demand for high speed and high security communications, an alternative all-fiber access network technology has been proposed: Code Division Multiple Access (CDMA). This spread spectrum (SS) technique is frequently used in radio networks. At the origin, SS systems have been developed for military applications, where resistance to jamming is obviously primordial. Other applications were found in the civilian domain, such as in multiple access communications.

In this type of architecture, transmitted signals have a bandwidth much greater than the effective message bandwidth. This appears to be a method of building the information bearing signal: it makes the signal have a noise-like appearance so as to blend it into the background.

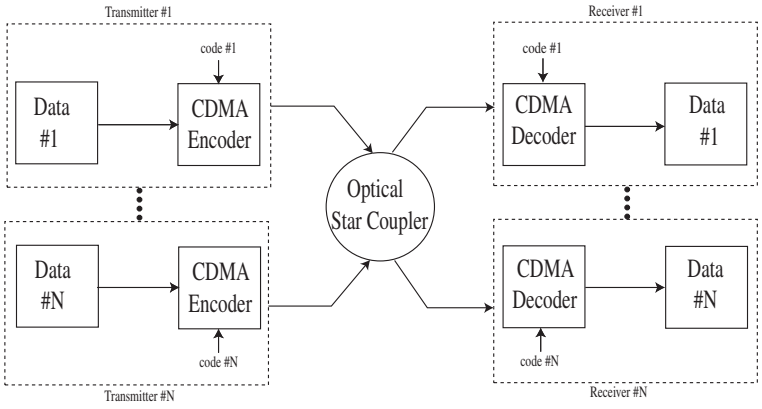

Figure 34: Typical CDMA architecture.

Multiplexing and band spread are achieved by assigning each user pair a different spreading code, generally called a pseudo-noise (PN) sequence, that is independent of the message. A typical schematic of CDMA systems is represented in Figure 34. Each transmitter sends data through a CDMA encoder, using a specific PN sequence. All the different signals are then transmitted simultaneously through the shared network. On the other side, each receiver collects its specific message as well as the other interfering signals. A CDMA decoder will employ a replica of the assigned code in order to despread the signal to recover the message corresponding to a specific user.

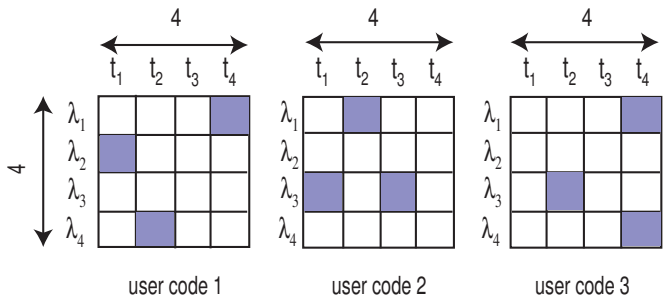

Figure 35: Examples of user codes for CDMA.

By emitting successive pulses at different wavelengths, codes associating one time slot with one wavelength can be implemented. The alternate multiwavelength source might enable the implementation of two-dimensional wavelength-time optical CDMA [130, 131, 132, 133]. This two-dimensional codes are generally represented by two-dimensional spatial signature patterns, as shown in Figure 35. In this case, codes use 4 time slots and 4 wavelengths. The code weight is thus equal to the number of black squares: in the example, the code weight is 3. We can notice there is no specific restriction: one time slot can have two wavelengths (multiple pulses per column), and one wavelength can be present at two different times (multiple pulses per row). We can note that research groups also work on three-dimensional codes: time, frequency, and space, for instance [134].

Photonic analog-to-digital conversion For real-time data transmission, ultra-high speed sampling is required. To overcome the electronics bottleneck, multiwavelength pulse trains can be used [127, 135, 136, 137]. The idea is to use the wavelength multiplicity to increase the sampling rate of analog-to-digital converters, as shown in Figure 36.

Optical demultiplexing The multiwavelength source generates alternate pulse trains at different wavelengths. This laser might be used to demultiplex a signal, as represented in Figure 37.

In this example, we suppose that at the emitter, three channels are multiplexed in the time domain in order to create the pulse train called “signal” at a fixed wavelength λ_s.

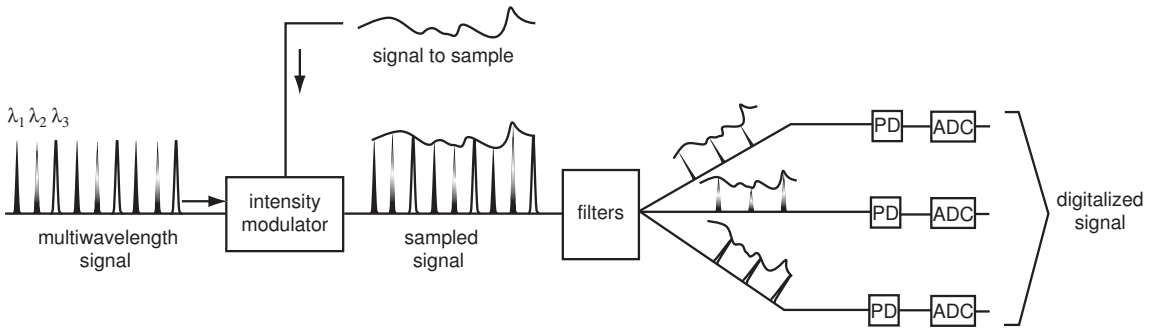

Figure 36: Photonic analog-to-digital conversion (PD: Photodiode, ADC: Electronic analog-to-digital converter).

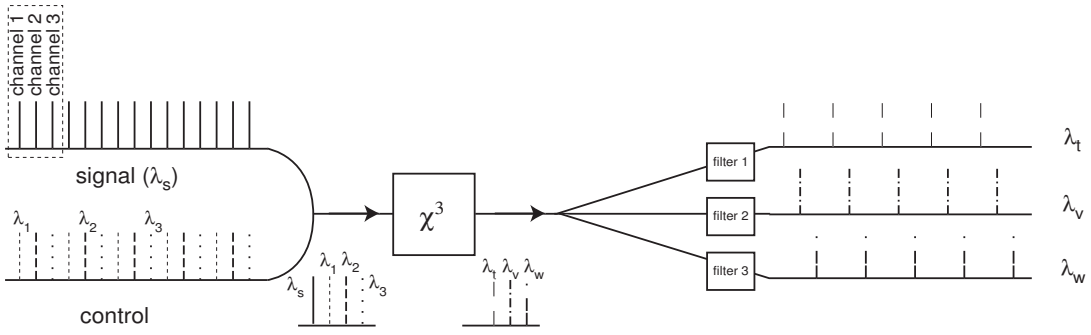

Figure 37: Principle of temporal demultiplexing by using a multiwavelength laser.

At the receiver, by using nonlinear effects (χ^3), this train will interact with the three-colors (λ_1, λ_2 and λ_3) train, called "control", produced by the multiwavelength laser. It leads to the generation of three new wavelengths (λ_t, λ_v and λ_w) that we can separate by using adequate filters: thus the signal is demultiplexed. Essential to the operation, we have to synchronize the trains "signal" and "control" at the receiver with a clock recovery system.

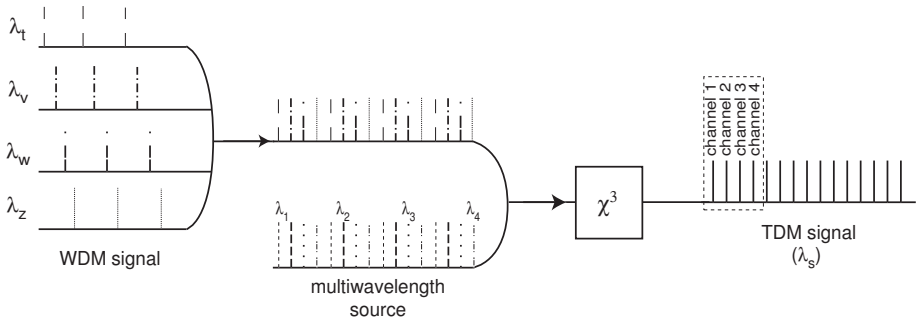

Figure 38: WDM/TDM converter.

By looking more precisely, this scheme might also be considered as an optical time division multiplexing (TDM) / wavelength division multiplexing (WDM) converter. By adapting this technique, as shown in Figure 38 with four channels, we might also think of a WDM/TDM converter, but the requirements seem to be more stringent. The different channels at the output of the converter should be exactly at the same wavelength. Thus, such a system might be difficult to practically implement.

Other applications This new type of laser might also be useful in other situations. Such a source can be used to test optical components. For instance, a tunable multiwavelength laser allows the measurement of the polarization-mode dispersion in optical fibers [138]. A multiwavelength laser is also employed for applications in differential absorption Lidars [139]: these devices are used to monitor trace gases. In [140], a system is introduced that combines a mode-locked fiber ring laser with intra-cavity spectroscopy to distinguish between different gas cells. It is a multiplexed network that would reduce the cost per point by sharing the same fiber source and the same signal-processing unit. When

the laser is locked at a gas absorption line, the cavity loss increases and the output power decreases because of absorption. The change of output power can be related to the change of gas concentration and in this way, the weak gas absorption can be amplified and easily measured.

The medical application of lasers is also an active field: for instance, for coagulating and anastomosing or for cutting and ablation. New applications are being explored because of the availability of new multiwavelength sources. Delivery of multiple energy sources to a tissue site thanks to one single device could be very helpful [141].

4.1.3 UMZI model

By inserting the UMZI in the cavity, pulses will be formed by active harmonic mode-locking. The chosen gain medium is an EDFA, leading to a gain bandwidth of approximately 40 nm. The free spectral range of this filter is related to the optical path length difference between the two arms of the interferometer and is chosen to be equal to 60 nm. Therefore, only one maximum of the transfer function will be located under the EDFA gain curve. By applying a sinusoidal voltage to the UMZI, the maximum of the filter will shift under the C-band and select one specific wavelength for each moment.

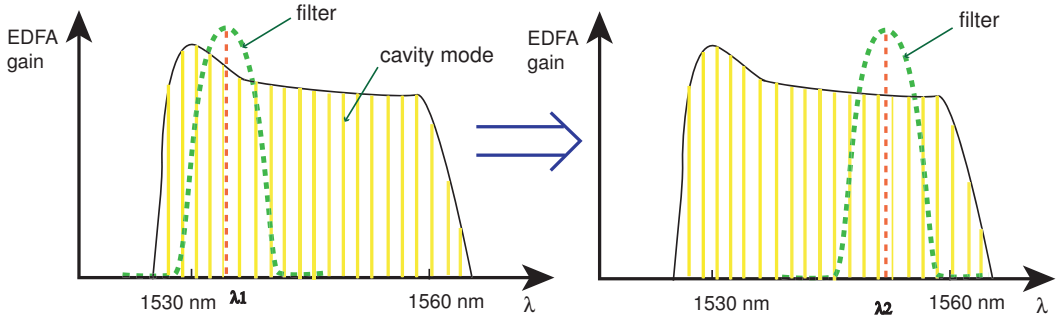

Figure 39: Wavelength selection by tunable filtering.

The complex amplitude field at the output of the UMZI, $\mathbf{E}_{\text{out}}(t)$, is related to the input field, $\mathbf{E}_{\text{in}}(t)$, and given by

$$\mathbf{E}_{\text{out}}(t) = \frac{1}{2}\left[\mathbf{E}_{\text{in}}\left(t - \frac{\tau}{2}\right) + \mathbf{E}_{\text{in}}\left(t + \frac{\tau}{2}\right)\right], \tag{51}$$

where τ is the delay introduced by the unbalanced interferometer, assumed to be of the form $\tau(t) = \tau_0 + \Delta\tau \sin(\Omega t)$, where Ω is the modulation frequency of the UMZI. Electric field amplitudes are equal to

$$E_{\text{out}}(t)e^{i\omega t} = \frac{1}{2}\left[E_{\text{in}}\left(t - \frac{\tau}{2}\right)e^{i\omega\left(t-\frac{\tau}{2}\right)} + E_{\text{in}}\left(t + \frac{\tau}{2}\right)e^{i\omega\left(t+\frac{\tau}{2}\right)}\right], \tag{52}$$

where ω is the angular frequency, in the neighboorhood of a reference ω_0. Considering that the low-frequency temporal envelope of the input field slowly varies during time τ, the ouput field amplitude is

$$E_{\text{out}}(t)e^{i\omega t} \approx \frac{1}{2}E_{\text{in}}(t)\left[e^{i\omega\left(t-\frac{\tau}{2}\right)} + e^{i\omega\left(t+\frac{\tau}{2}\right)}\right], \tag{53}$$

and so

$$E_{\text{out}}(t)e^{i\omega t} \approx E_{in}(t)e^{i\omega t}\cos\left(\frac{\omega\tau}{2}\right). \tag{54}$$

The UMZI transfer function is then evaluated as

$$H(t) \approx \cos\left(\frac{\omega\tau}{2}\right). \tag{55}$$

The extrema of H are given by the extrema of the cosine function, that is, the angular frequency has to be equal to

$$\omega_{max} = \frac{4k\pi}{\tau} = 2\pi f_{k_{max}}, \tag{56}$$

where $f_{k_{max}}$ is a frequency maximum of order $k \in \mathbb{N}$. Thus, we also have

$$\omega_{max} = \frac{4k\pi}{\tau_0 + \Delta\tau\sin(\Omega_m t)}, \tag{57}$$

$$= \frac{\omega_0}{\left[1 + \frac{\Delta\tau}{\tau_0}\sin(\Omega_m t)\right]}, \tag{58}$$

where ω_0 is chosen to be a maximum of transmission for the filter at $t = 0$: $\omega_0 = 4k\pi/\tau_0$. Using a Taylor expansion, ω_{max} can be evaluated as

$$\omega_{max} \approx \omega_0\left(1 - \frac{\Delta\tau}{\tau_0}\sin(\Omega_m t)\right). \tag{59}$$

If optical wavelengths are considered rather than angular frequencies, this relationship is

$$\lambda_{max} \approx \lambda_0\left(1 - \frac{\Delta\tau}{\tau_0}\sin(\Omega_m t)\right). \tag{60}$$

This allows the prediction of the theoretical evolution of the maximum of the transfer function of the UMZI as a function of time, and thereby of the emitted wavelength.

4.2 Theoretical analysis

In this section, we report the theoretical study of the proposed multiwavelength source [142]. Temporal and spectral parameters of the produced pulses are derived analytically by using a circulating Gaussian pulse analysis [39].

4.2.1 Extended UMZI transfer function

The signal at the input of the UMZI is assumed to be Gaussian:

$$X(t) = A\exp(i\omega_0 t - \Gamma t^2), \tag{61}$$

where $\Gamma = \alpha_1 - i\beta_1$ is the complex Gaussian pulse parameter and ω_0 the angular reference frequency. Being in a push-pull configuration, the UMZI output is given by

$$Y(t) = \frac{1}{2}\left[X\left(t - \frac{\tau(t)}{2}\right) + X\left(t + \frac{\tau(t)}{2}\right)\right], \tag{62}$$

and so

$$\begin{aligned} Y(t) &= \frac{A}{2}\left\{\exp\left[i\omega_0\left(t - \frac{\tau(t)}{2}\right) - \Gamma\left(t - \frac{\tau(t)}{2}\right)^2\right]\right. \\ &\quad \left. + \exp\left[i\omega_0\left(t - \frac{\tau(t)}{2}\right) - \Gamma\left(t + \frac{\tau(t)}{2}\right)^2\right]\right\} \qquad (63) \\ &= X(t)\exp\left[\frac{\tau^2(t)}{4}(i\beta_1 - \alpha_1)\right]\cos\left(\frac{\omega_0\tau(t)}{2} + t\tau(t)(\beta_1 + i\alpha_1)\right). \qquad (64) \end{aligned}$$

As ω_0 is chosen to be a maximum of transmission for the filter at $t = 0$ and since the delay introduced by the modulator is small compared to the pulse characteristic times $\alpha_1^{-\frac{1}{2}}$ and $\beta_1^{-\frac{1}{2}}$, the transfer function of the UMZI is proportional to

$$\frac{Y(t)}{X(t)} = T_p(t) \approx \cos\left(\frac{\omega_0\tau(t)}{2} + t\tau(t)\,(\beta_1 + i\alpha_1)\right). \tag{65}$$

In the neighborhood of $t = 0$, $T_p(t)$ can then be approximated by

$$\begin{aligned} T_p(t) &\approx \cos\left(\frac{\omega_0}{2}(\tau_0 + \Delta\tau\sin(\Omega t)) + t(\tau_0 + \Delta\tau\sin(\Omega t))(\beta_1 + i\alpha_1)\right) && (66)\\ &\approx \cos\left[\left(\frac{\omega_0\Delta\tau\Omega}{2} + \tau_0(\beta_1 + i\alpha_1)\right)t\right] && (67)\\ &\approx \exp\left[-\frac{1}{2}\left(\frac{\omega_0\Delta\tau\Omega}{2} + \tau_0(\beta_1 + i\alpha_1)\right)^2 t^2\right] && (68)\end{aligned}$$

Strictly speaking, this is not a true temporal transfer function as it depends on the input pulse parameters. Nevertheless, for clarity's sake, $T_p(t)$ will be designated as the UMZI extended transfer function.

4.2.2 Circulating Gaussian pulse analysis

As shown in Figure 32, the starting pulse in the cavity is described by a Gaussian envelope:

$$f_1(t) = A\exp(i\omega_0 t - \Gamma t^2), \tag{69}$$

where $\Gamma = \alpha_1 - i\beta_1$ is the complex Gaussian pulse parameter and ω_0 the angular reference frequency. By computing its Fourier transform, we obtain

$$F_1(\omega) = B\exp\left(-\frac{(\omega - \omega_0)^2}{4\Gamma}\right), \tag{70}$$

with

$$B = \frac{A}{2}\sqrt{\frac{1}{\pi\Gamma}}. \tag{71}$$

The pulse propagates through the EDFA, modeled as a Gaussian spectral transfer function:

$$g(\omega) = \exp\left(-\frac{(\omega - \omega_0)^2}{\Delta\omega^2}\right), \tag{72}$$

where $\Delta\omega$ is the gain bandwidth. At the ouput of the gain medium, the resulting pulse is described in the spectral domain by

$$\begin{aligned} F_2(\omega) &= F_1(\omega)g(\omega) && (73)\\ &= B\exp\left(-\frac{(\omega - \omega_0)^2}{4\Gamma'}\right), && (74)\end{aligned}$$

with

$$\Gamma' = \frac{(\Delta\omega^4\alpha_1 + 4\Delta\omega^2(\alpha_1^2+\beta_1^2)) - i\beta_1\Delta\omega^4}{(\Delta\omega^2+4\alpha_1)^2+(4\beta_1)^2} \quad (75)$$

$$= \alpha_1' - i\beta_1'. \quad (76)$$

The pulse is then

$$f_2(t) = C\exp(i\omega_0 t - \Gamma' t^2), \quad (77)$$

with

$$C = 2B\sqrt{\pi\Gamma'}. \quad (78)$$

The pulse then goes through the UMZI and as $\alpha_1' \approx \alpha_1$ and $\beta_1' \approx \beta_1$, it can be depicted at its output by

$$f_3(t) = f_2(t)T_p(t) \quad (79)$$

$$= 2B\sqrt{\pi\Gamma'}\exp(i\omega_0 t - \Gamma' t^2)\exp\left[-\frac{1}{2}\left(\frac{\omega_0\Delta\tau\Omega}{2} + \tau_0(\beta_1 + i\alpha_1)\right)^2 t^2\right]. \quad (80)$$

For a steady-state mode-locked laser operation, f_3 and f_1 have to be equal. One must solve the following equations:

$$\begin{cases} \alpha_1 = \alpha_1' + \frac{1}{2}\left[\left(\tau_0\beta_1 + \frac{\omega_0\Delta\tau\Omega}{2}\right)^2 - \tau_0^2\alpha_1^2\right] \\ \beta_1 = \beta_1' - \tau_0\alpha_1\left(\tau_0\beta_1 + \frac{\omega_0\Delta\tau\Omega}{2}\right) \end{cases} \quad (81)$$

By using Γ' expression, we find that

$$\beta_1 = \frac{\beta_1\Delta\omega^4}{(\Delta\omega^2+4\alpha_1)^2+(4\beta_1)^2} - \tau_0\alpha_1\left(\tau_0\beta_1 + \frac{\omega_0\Delta\tau\Omega}{2}\right). \quad (82)$$

As $\frac{16(\alpha_1^2+\beta_1^2)}{\Delta\omega^4} \ll \frac{8\alpha_1}{\Delta\omega^2}$ and as $\frac{8\alpha_1}{\Delta\omega^2} \ll 1$, we find

$$\beta_1 = -\frac{\omega_0\Delta\tau\Omega}{2\tau_0}. \quad (83)$$

The non-zero value of β_1 indicates that the pulse is chirped.

We also calculate that

$$\alpha_1 = \frac{(\Delta\omega^4\alpha_1 + 4\Delta\omega^2(\alpha_1^2+\beta_1^2))}{(\Delta\omega^2+4\alpha_1)^2+(4\beta_1^2)} - \frac{1}{2}\tau_0^2\alpha_1^2. \quad (84)$$

By using the same approximations as previously, we obtain

$$\alpha_1 = \frac{\omega_0 \Delta\tau\Omega}{\tau_0} \sqrt{\frac{2}{8+\tau_0^2\Delta\omega^2}}. \tag{85}$$

Finally, the full-widths at half-maximum (FWHM) of the pulses in the time domain τ_p and in the spectral domain Δf are

$$\begin{cases} \tau_p = \sqrt{2\ln 2}\sqrt{\frac{\tau_0}{\omega_0\Delta\tau\Omega}}\left(\frac{8+\tau_0^2\Delta\omega^2}{2}\right)^{\frac{1}{4}} \\ \Delta f = \frac{\sqrt{2\ln 2}}{\pi}\left(\frac{8+\tau_0^2\Delta\omega^2}{2}\right)^{-\frac{1}{4}}\left[\frac{\omega_0\Delta\tau\Omega}{\tau_0}\left(2+\frac{\tau_0^2\Delta\omega^2}{8}\right)\right]^{\frac{1}{2}} \end{cases} \tag{86}$$

We can note that if the gain medium is infinitely flat, the value for β_1 does not change, whereas α_1 becomes zero, indicating a continuous laser emission with variable frequency.

4.3 Pulse characterization

To analyze the results obtained with the proposed laser, it appears necessary to introduce the different methods used to characterize the generated pulses.

4.3.1 Main parameters

The first objective of the laser is to generate picosecond optical pulses. Let us characterize them, both in the time and frequency domains.

Time domain An optical field can be described by an analytical signal

$$\mathcal{E}(t) = \Re\{\sqrt{P(t)}\exp[i\omega_0 t + i\phi(t)]\} = \Re\{E(t)\}, \tag{87}$$

where P(t) is the power and ϕ(t) the instantaneous phase. It leads to introduce the instantaneous frequency ω_i(t)

$$\omega_i(t) = \omega_0 + \frac{d\phi}{dt}. \tag{88}$$

Consequently, if the instantaneous phase is constant, the optical field oscillates at the carrier frequency. However, if this phase varies, the instantaneous frequency varies also. It is called the chirp phenomenon.

An optical pulse can be described by its intensity profile. We can focus on its peak or mean power. Another important characteristic is the pulse duration. We will consider the full width at half maximum (FWHM) pulsewidth in this document.

In the case of a linearly chirped Gaussian pulse, the field satisfies [21]

$$\mathcal{E}(t) = \Re\{\sqrt{P(t)}\exp(-\Gamma t^2)\exp(i\omega_0 t)\}, \tag{89}$$

where $\Gamma = a - ib$. The pulse width at half maximum is

$$\Delta\tau = \sqrt{\frac{2\ln 2}{a}}, \tag{90}$$

and the instantaneous frequency is

$$\omega_i(t) = \omega_0 + 2bt. \tag{91}$$

It explains the term of linear chirp used in this case.

Frequency domain Similarly, the field can be expressed in the frequency domain by taking the Fourier transform of its temporal expression

$$\widehat{E}(\omega) = \int_{-\infty}^{+\infty} E(t)\exp(-i\omega t)\,dt, \tag{92}$$

and so

$$\widehat{E}(\omega) = \sqrt{\widehat{P}(\omega-\omega_0)}\ \exp(-i\widehat{\phi}(\omega-\omega_0)), \tag{93}$$

where $\widehat{\phi}(\omega-\omega_0)$ is called spectral phase. In this frequency domain, we also define pulsewidth at half maximum Δf. Hence, we can define the time bandwidth product (TBP), equal to

$$\text{TBP} = \Delta\tau\Delta f. \tag{94}$$

In the Gaussian case, the field is

$$\widehat{E}(\omega) = \frac{1}{2\sqrt{\pi\Gamma}}\ \exp\left[-\frac{(\omega-\omega_0)^2}{4\Gamma}\right], \tag{95}$$

and the frequency pulsewidth Δf is

$$\Delta f = \frac{\sqrt{2\ln 2}}{\pi}\sqrt{a\left[1+\left(\frac{b}{a}\right)^2\right]}. \tag{96}$$

The time-bandwidth product is then

$$\Delta\tau\Delta f = \frac{2\ln 2}{\pi}\sqrt{1+\left(\frac{b}{a}\right)^2}. \tag{97}$$

As a consequence, an unchirped Gaussian pulse (for which b=0), TBP is about 0.44.

Evolution of the spectral pulsewidth as a function of the temporal pulsewidth is given by the sign of

$$\frac{d(\Delta f)}{d\Delta\tau} = \frac{d(\Delta f)}{da}\frac{da}{d\Delta\tau}. \tag{98}$$

According to Equation 90, $\frac{da}{d\Delta\tau}$ is negative, and according to Equation 96, we have

$$\frac{d(\Delta f)}{da} = \frac{1}{2}\frac{\sqrt{2\ln 2}}{\pi}\frac{a^2-b^2}{\sqrt{a^5+b^2a^3}}. \tag{99}$$

Finally, we can distinguish two cases:

- if a<b: chirp dominates. So, if the temporal pulsewidth increases, the spectral pulsewidth also increases.

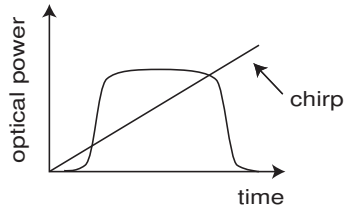

Figure 40: Case where chirp dominates.

- if a>b: chirp does not dominate. So, if the temporal pulsewidth increases, the spectral pulsewidth decreases.

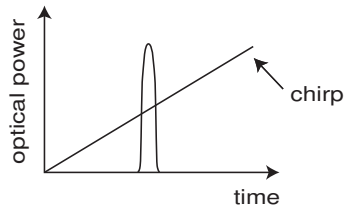

Figure 41: Case where chirp does not dominate.

Time, phase, and amplitude jitters Generated pulse trains are rarely perfect. They undergo many fluctuations, called jitter. It can affect time, phase, or amplitude [143, 144]. These variations are represented in Figure 42. Amplitude jitter ga_n corresponds to fluctuations in magnitude. Time jitter gt_n occurs when the pulse maxima are not regularly spaced. Lastly, phase jitter gp_n introduces phase changes between pulses. These phenomena are random and can only be statistically studied.

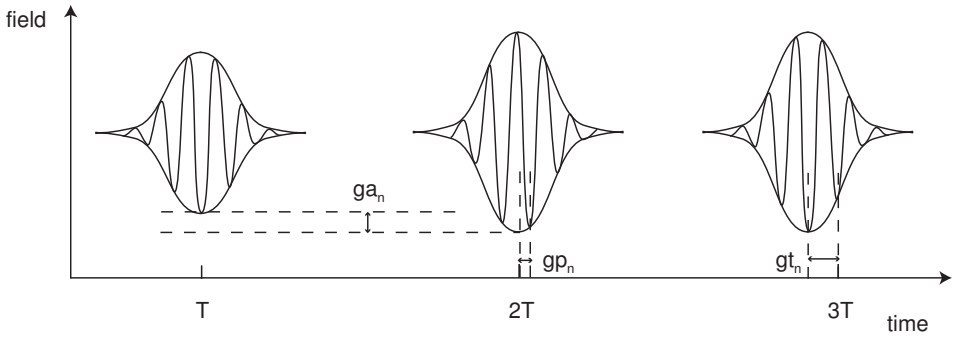

Figure 42: Scheme of time, phase, and amplitude jitters.

4.3.2 Used techniques

We will focus now on these parameters measurements. A method to evaluate them uses the intensity autocorrelation function by second-harmonic generation [145]. Assuming the pulse shape, its intensity profile can be found. Although this technique is sensitive and easy to use, it cannot characterize skewness. Moreover, this method does not give information on the phase profile of the signal.

As direct measurements of the phase are impossible, indirect techniques are used. One of the most popular technique if the frequency resolved optical gating (FROG) technique [146]. It is based on the autocorrelation spectra at different temporal positions. The amplitude and phase of the signal are then reconstructed.

In our study, the main goal is to validate the alternate multiwavelength operation. Two methods can be employed. The first technique is to perform a temporal windowing and to record the spectrum of every temporal optical pulse. The second method consists of

implementing a spectral windowing. It simply consists of inserting a filter at the laser output and to observe its behavior in the temporal domain. We will use this technique. The bandwidth of the filter must be carefully chosen to correctly isolate each pulse.

In the temporal domain, a 30 GHz photodiode and a sampling oscilloscope are used to detect pulses up to 10 or 20 ps, at repetition rates of several GHz. In the spectral domain, the main characteristic is the central emitted wavelength for each pulse. An optical spectrum analyzer with 0.07 nm resolution will be used and a 1.2 nm bandpass tunable optical filter will be employed at the laser output to operate the spectral windowing. The spectral windowing is chosen to accurately determine the spectral content of each pulse train. If the laser output is sent to an adequate demultiplexer to use as many oscilloscope inputs as channels, all pulse trains at different wavelengths could be displayed simultaneously on the screen. However, this method is limited to small number of wavelengths.

To validate the alternate multiwavelength operation of our system, we will also use spectrogram that represents instant frequencies present in a signal as a function of time. This representation can be very helpful as chirp and pulsewidth can be evaluated.

4.4 Multiwavelength generation

The key element of our setup is the UMZI. We describe in detail and present some numerical and experimental results that validate the principle of the alternate multiwavelength mode-locked fiber laser [147, 148].

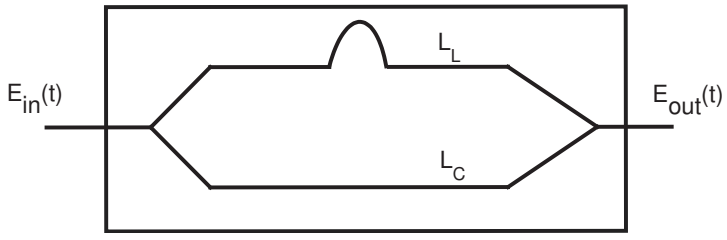

Figure 43: Scheme of an unbalanced Mach-Zehnder interometer.

4.4.1 UMZI practical description

The device used in the experiments is a component specially designed by us and fabricated by Photline Technologies for our application. It is made of two Y-junctions linked together by two arms of different lengths: one short linear arm of length L_S and one long one of length L_L.

The interferometer is in a push-pull configuration for radio-frequency (RF) electrodes, i.e., voltages applied on both arms are equal but opposite. However, direct current (DC) electrodes are only applied on a single arm.

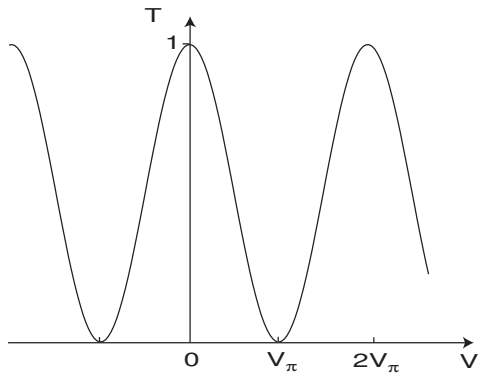

Figure 44: Transmission of a Mach-Zehnder interferometer.

Transmission of a Mach-Zehnder interferometer is given by the ratio of optical powers at its input, $P_{in}(t)$, and output, $P_{out}(t)$. The half-wave voltage V_π corresponds to the voltage applied to cause a phase shift of π. In our case, for RF electrodes, V_π is equal to 5 V, whereas it is 15 V for DC electrodes. Experimentally, we can measure the half-wave voltage of DC electrodes by applying different bias voltages to make a maximum of transmission become a minimum, as shown in Figure 45.

This interferometer is an integrated annealed proton exchanged $LiNbO_3$ 10-Gb/s intensity modulator that includes a fixed optical path length difference of 40 μm between its two arms. Its free spectral range is 60 nm. The used crystal is in a X-cut, Y-propagation configuration. The insertion losses, without connectors, are about 6 dB.

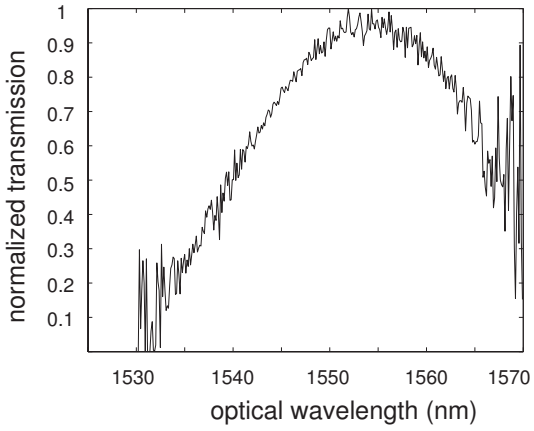

(a) voltage V=0 V

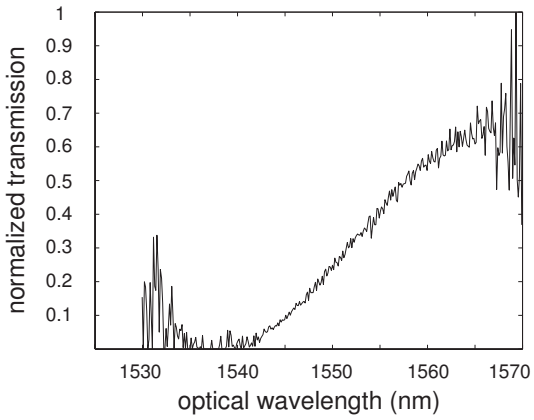

(b) voltage V=6 V

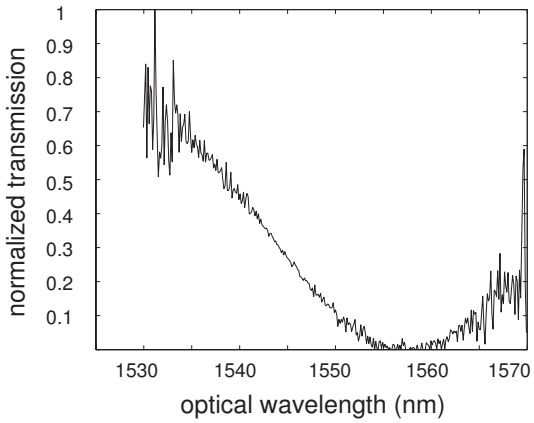

(c) voltage V=15 V

Figure 45: Transmission of the UMZI for different DC bias voltage to measure V_π for DC electrodes.

Scattering parameters, or S-parameters, are the reflection and transmission coefficients between the incident and reflection waves. Parameters S_{11}, reflection coefficient at the input, and electro-optic transmission coefficient were measured with a vector analyzer and are depicted in Figure 46. The second coefficient was obtained by using a photodetector at the output of the modulator to convert the optical signal into an electrical signal.

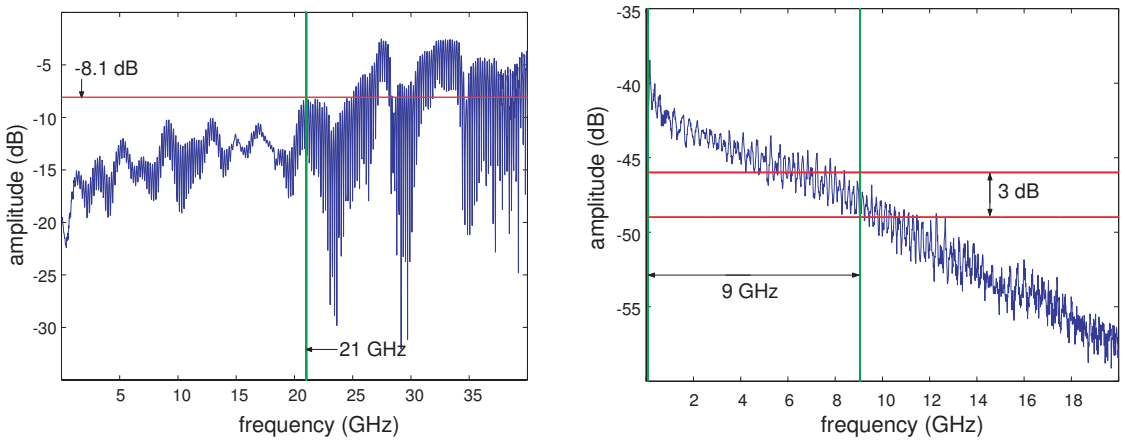

(a) S_{11} parameter (b) electro-optic transmission coefficient

Figure 46: Experimental parameters of the UMZI.

4.4.2 Numerical simulations

4.4.2.1 Modeling

Numerical simulations of the laser operation are undertaken to give a qualitative behavior and a physical description of the multiwavelength source [149]. They are carried out by injecting a weak noise field and allowing it to numerically evolve to a steady state subject to the action of the various components shown in Figure 32.

EDFA To model the EDFA gain medium, we need to consider the gain factor by itself, but also the amplified spontaneous emission (ASE) noise. To take into account the gain saturation phenomenon, the amplifier power gain is assumed to be

$$g = \frac{g_0}{g_0 - (g_0 - 1)e^{-\frac{P_{mean}}{Psat_{in}}}}, \tag{100}$$

where g_0 is the small-signal gain, P_{mean} the mean power, and $P_{sat_{in}}$ the saturation power at the EDFA input. Using a first order Taylor expansion of the exponential function, we find

$$g \sim \frac{g_0}{1 + \frac{P_{mean}}{P_{sat_{in}}}}. \tag{101}$$

The used model corresponds well to the expected behavior:

$$\text{when } P_{mean} \to 0, \quad \text{we have} \quad g \to g_0, \tag{102}$$

$$\text{when } P_{mean} \to \infty, \quad \text{we have} \quad g \to 0. \tag{103}$$

If $(P_{mean_n})_{n\in\mathbb{N}}$ represents the series of the signal mean powers for loop n and $(g_n)_{n\in\mathbb{N}}$ the series of EDFA gains for loop n, we obtain

$$P_{mean_n} = P_{mean_{n-1}} g_{n-1}, \tag{104}$$

$$= \frac{g_0}{1 + \frac{P_{mean_{n-1}}}{P_{sat_{in}}}} P_{mean_{n-1}}. \tag{105}$$

Finally, when $n \to \infty$, we have $P_{mean_n} \to A$, with

$$A = \frac{g_0}{1 + \frac{A}{P_{sat_{in}}}} A, \tag{106}$$

and so

$$A = (g_0 - 1) P_{sat_{in}}, \tag{107}$$

$$\approx P_{sat_{out}}, \tag{108}$$

where $P_{sat_{out}}$ is the saturation power at the output of the EDFA.

In our simulations, the small signal gain g_0 is 30 dB and the saturation power at the EDFA input $P_{sat_{in}}$ is -10 dBm.

The ASE noise of the EDFA $n(t)$ is modeled by a white Gaussian field with an autocorrelation function given by

$$< n(t) n^*(t') >= 2(g - 1)\hbar\omega_0 n_{sp} \delta(t - t'), \tag{109}$$

where ω_0 is the reference optical frequency, n_{sp} is the spontaneous emission noise factor, $\hbar$ the Planck's constant and δ the Kronecker's symbol. If $E_{in}(t)$ is the input signal, the output signal $E_{out}(t)$ is given by:

$$E_{out}(t) = \sqrt{g}E_{in}(t) + n(t). \tag{110}$$

Light propagation To simulate light propagation in the ring cavity, and especially in the optical fiber, we use a non-linear partial differential equation as mathematical model and a classical numerical method to solve it.

NLSE The non-linear Schrödinger equation (NLSE or *Master Equation*) is a mathematical representation for the propagation of light through fiber. If the propagating field amplitude is given by

$$E(r,t) = F(x,y)A(z,t)e^{i(\beta z - \omega_0 t)}, \tag{111}$$

where A(z,t) is the slowly varying envelope component, the NLSE can be expressed from Maxwell's equations by [8]

$$\frac{\partial A}{\partial z} + \frac{\alpha}{2}A + \frac{i\beta_2}{2}\frac{\partial^2 A}{\partial T^2} - \frac{\beta_3}{6}\frac{\partial^3 A}{\partial T^3} = i\gamma\left[|A|^2 A + \frac{i}{\omega_0}\frac{\partial}{\partial T}(|A|^2 A) - T_R A\frac{\partial |A|^2}{\partial T}\right], \tag{112}$$

where α represents the absorption coefficient, $\gamma = \frac{n_2\omega_0}{c_0 A_{eff}}$ is called the non-linearity coefficient, A_{eff} is the effective core area, n_2 is the non-linear index coefficient, and T_R is defined as the first moment of the non-linear response function. In this equation, a frame of reference moving with the pulse at the group velocity v_g is used by making the transformation

$$T = t - \frac{z}{v_g}. \tag{113}$$

As we work with pulses larger than one picosecond, the last two terms of Equation 112 can be neglected.

Split-step Fourier method The NLSE equation is a non-linear partial differential equation, which in general does not have an analytical solution. Hence, a numerical approach is needed to solve this equation. The split-step Fourier method [150] is widely used to solve the pulse propagation problem in non-linear dispersive media. This is a finite-difference method, close to the beam propagation method.

The propagation equation is written as

$$\frac{\partial A}{\partial z} = \left(\widehat{D} + \widehat{N}\right) A, \tag{114}$$

where $A = A(z, T)$. The two operators are

$$\widehat{D} = -i\frac{\beta_2}{2}\frac{\partial^2}{\partial T^2} + \frac{\beta_3}{6}\frac{\partial^3}{\partial T^3} - \frac{\alpha}{2}, \tag{115}$$

$$\widehat{N} = i\gamma|A|^2. \tag{116}$$

$\widehat{D}$ is a differential operator that includes dispersion and losses in a linear medium. $\widehat{N}$ is a non-linear operator that includes the effects of fiber non-linearities.

If we consider that $\widehat{N}$ does not depend on distance z, we have:

$$A(z + h, T) \approx exp[h(\widehat{D} + \widehat{N})]A(z, T). \tag{117}$$

Dispersion and non-linearity are considered to act independently. The numerical method becomes:

- The fiber is divided in small segments of length h.
- The non-linearity part $\widehat{N}$ is computed at each segment.
- The dispersion $\widehat{D}$ is then computed on each segment.

Hence, for each segment

$$A(z + h, T) \approx exp(h\widehat{D})exp(h\widehat{N})A(z, T). \tag{118}$$

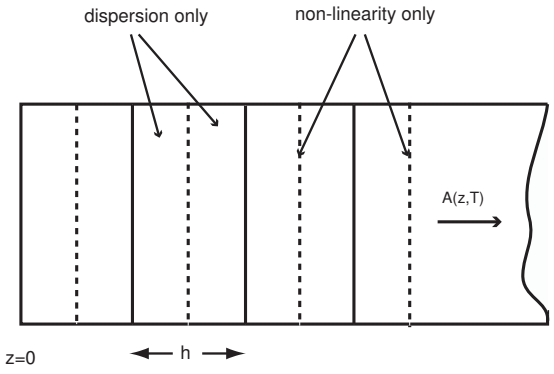

Figure 47: Split-step Fourier method principle.

The operators $\widehat{N}$ and $\widehat{D}$ are non-commuting, i.e.,

$$[\widehat{D}, \widehat{N}] = \widehat{D}\widehat{N} - \widehat{N}\widehat{D} \neq 0. \tag{119}$$

From the Baker-Hausdorff formula, for two non-commuting operators $\widehat{a}$ and $\widehat{b}$, we have

$$\exp(\widehat{a})\exp(\widehat{b}) = \exp\left[\widehat{a} + \widehat{b} + \frac{1}{2}\left[\widehat{a}, \widehat{b}\right] + \frac{1}{2}\left[\widehat{a} - \widehat{b}, \left[\widehat{a}, \widehat{b}\right]\right] + \ldots\right]. \tag{120}$$

Thus, in this case, this method is accurate to second order in the step size h.

Exponential operator $\exp(h\widehat{D})$ is analytically computed in the Fourier domain

$$\exp(h\widehat{D})B(z,T) = F_{T^{-1}}\exp[h\widehat{D}(j\omega)]F_T B(z,T), \tag{121}$$

where F_T is the Fourier transform and $F_{T^{-1}}$ its inverse.

The accuracy of the split-step Fourier method can be improved by adopting a symmetric form of exponential operator. Each segment is divided in two and

$$A(z+h,T) \approx \exp(\frac{h}{2}\widehat{D})\exp\left(\int_z^{z+h}\widehat{N}(z')dz'\right)\exp(\frac{h}{2}\widehat{D})A(z,T). \tag{122}$$

In this technique, the effect of non-linearity is concentrated in the middle of the segment rather than at the end of the segment. Since we use symmetric form of exponential operators, it si called the symmetrized split-step Fourier method. This approach is accurate to third order in the step size h.

Finally, in the simulations, the UMZI is modeled using a discretized version of Equation 62.

4.4.2.2 Simulation results

Figures 48(a) and (b) display the temporal trace and spectrum of the signal at the laser output when the parameters of the simulation are chosen to be $\tau_0 = 1.33\ 10^{-13}$ s, $\omega_0 = 1.216\ 10^{15}$ rad/s, $\Omega = 7.18\ 10^{10}$ rad/s, $\Delta\tau = 8.52\ 10^{-16}$ s, and $\Delta\omega = 23.55\ 10^{12}$ rad/s. In this case, the dispersion in the cavity is set to 0 ps/nm/km. The round-trip length of the cavity is 20 m, and the results shown are obtained after 200 loops, when the signal is stabilized to

a steady state. For this repetition rate of $f_m = \Omega/2\pi$ =11.33 GHz, two successive trains at two different wavelengths (λ_e=1540 nm and λ_f=1560 nm) are observed.

Table 2: Simulation parameters for alternate multiwavelength generation.

parameter	value
g_0	30 dB
τ_0	1.33 10^{-13} s
$\Delta\tau$	8.52 10^{-16} s
ω_0	1.216 10^{15} rad/s
Ω	7.18 10^{10} rad/s
$\Delta\omega$	23.55 10^{12} rad/s
dispersion	0 ps/nm/km
cavity length	20 m
A_{eff}	80 10^{-12} m^2
fiber loss	0.2 dB/km
n_2	3 10^{-20} m^2/W
γ	1.5 W^{-1}/km

The pulse widths are recorded to be 7 ps and 6.5 ps, yielding a time-bandwidth product (TBP) of 0.72 and 0.61, respectively. As expected in a mode-locked operation, two successive pulses of the same train are separated by $1/f_m$=88 ps. Figure 48(a) also indicates the temporal transfer function of the UMZI for λ_e and λ_f, and Figure 48(b) its spectral transfer function at t_1=-32 ps and t_2=-76 ps. It emphasizes the fact that each wavelength sees a different temporal transfer function and that a specific position of the filter corresponds to a precise moment.

The multiwavelength pulsed laser operation is conveniently examined in the time - frequency domain through the pulse spectrogram [146]. Figure 49(a) shows the spectrogram for the results shown in Figure 48.

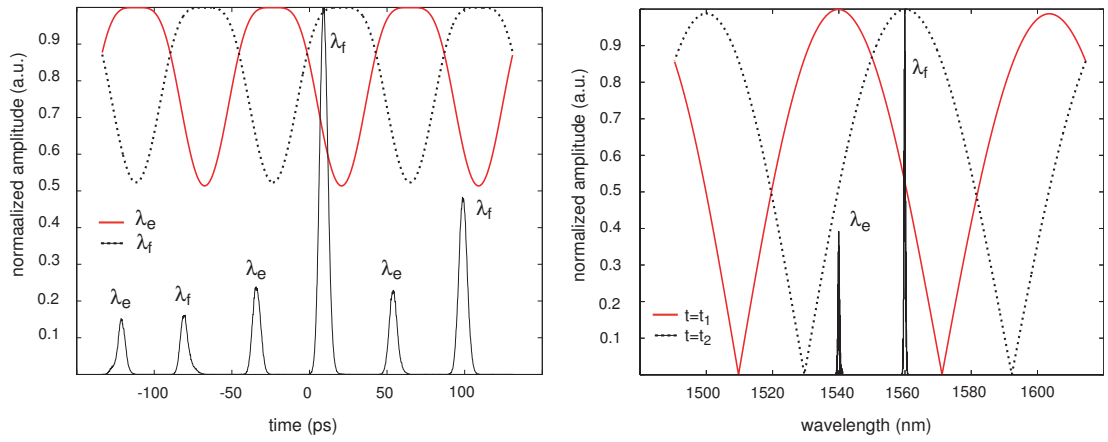

(a) time trace (b) spectrum

Figure 48: Laser output obtained by simulation with corresponding temporal and spectral transfer function of the UMZI

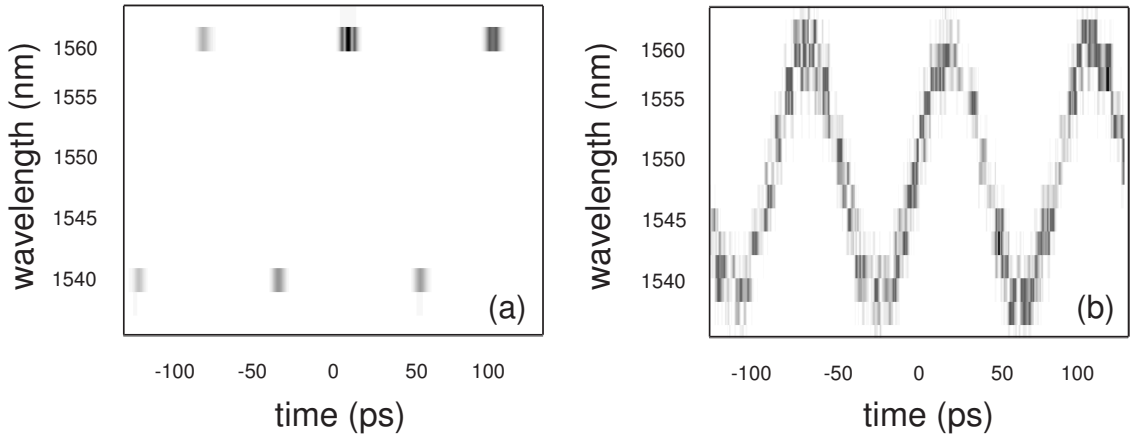

Figure 49: Spectrograms obtained by simulation with a (a) Gaussian and (b) an infinitely flat gain medium.

In comparison, Figure 49(b) shows the spectrogram obtained when the gain is not assumed to be Gaussian anymore, but infinitely flat. As expected in the previous circulating Gaussian pulse analysis, it can be observed that a continuous emission with changing frequency is produced. In this case, the UMZI is the only frequency-selective element in the cavity and thus imposes the emitted wavelength through the evolution of the maximum ω_{max} of its transfer function, as described by Equation 59. This observation indicates that the filtering action of the UMZI prevails in achieving multiwavelength operation, but that the Gaussian gain of the EDFA acts as an extra intra-cavity filter to select precise wavelengths at specific times.

4.4.3 Experimental results

A photograph of the experimental setup is shown in Figure 50. All the main components used in the following experiments are detailed. The amplifier used is a gain-flattened EDFA (Keopsys model 1 060 234). Figure 51 represents the EDFA small-signal gain (reached for an input power of -7 dBm) and the spontaneous emission noise (obtained for a pump current of 0.8 A).

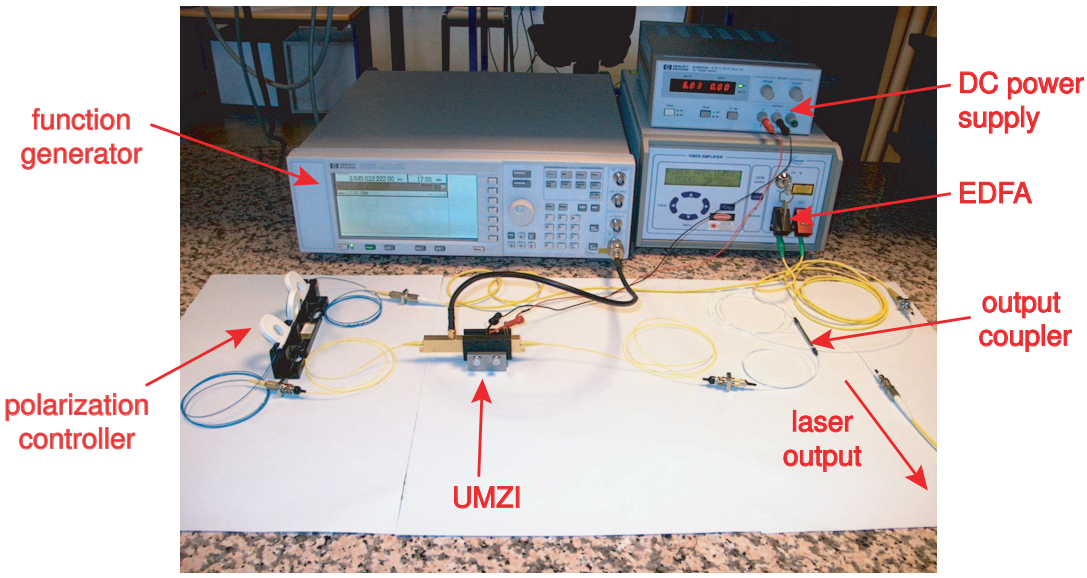

Figure 50: Photography of the experimental setup.

Figures 52 (a) and (b) display the temporal trace and spectrum of a signal at laser output, respectively. The experimental parameters are τ_0=1.33 10^{-13} s, $\Delta\tau$=1.9 10^{-15} s, and λ_0=1550 nm. The repetition rate is 3.8 GHz and the measured intracavity dispersion is less than 1 ps/nm/km [147, 151, 148].

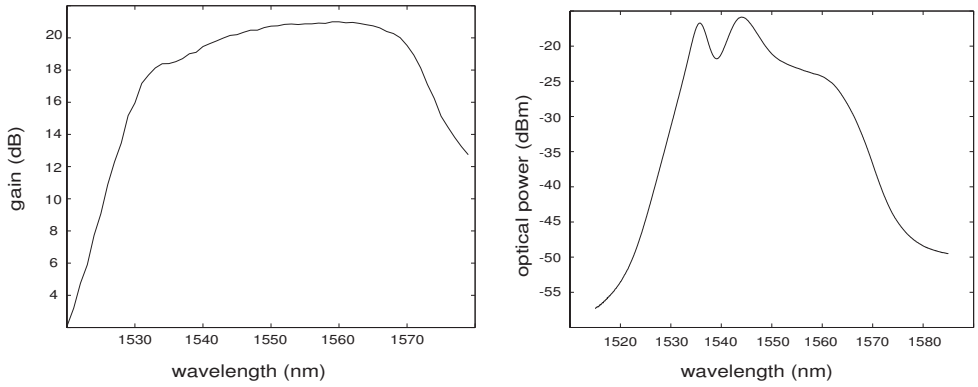

(a) small signal gain (b) spontaneous emission noise

Figure 51: EDFA experimental characteristics.

Three successive trains at three different wavelengths (λ_1=1543.2 nm, λ_2=1549.6 nm, and λ_3=1562.5 nm) are observed using an optical spectrum analyzer with 0.07 nm resolution and a sampling oscilloscope with a 30 GHz photodiode. The wavelength of each pulse is identified by adding a 1.2 nm tunable bandpass optical filter at the laser output, and the pulsewidths are recorded to be 24, 25, and 38 ps, yielding a time-frequency product of 0.81, 1.06, and 1.85, respectively. Since the center wavelength of the filter varies with time, the generation of chirped pulse is expected and verified. Theory and Equation 86 predict pulses of width equal to 3.4 ps with a time-bandwidth product of 0.89. The obtained values are slightly different in the experiment and may be attributed to two main factors: the behavior of the gain medium, both homogeneous and inhomogeneous, is more complex than our model and laser emission does not occur at a maximum of sliding as supposed in the theoretical circulating Gaussian pulse analysis. The three wavelengths' operation is stable for some hours at a constant room temperature. Nevertheless, since no stabilization system has been implemented, fluctuations of the peak power are observed.

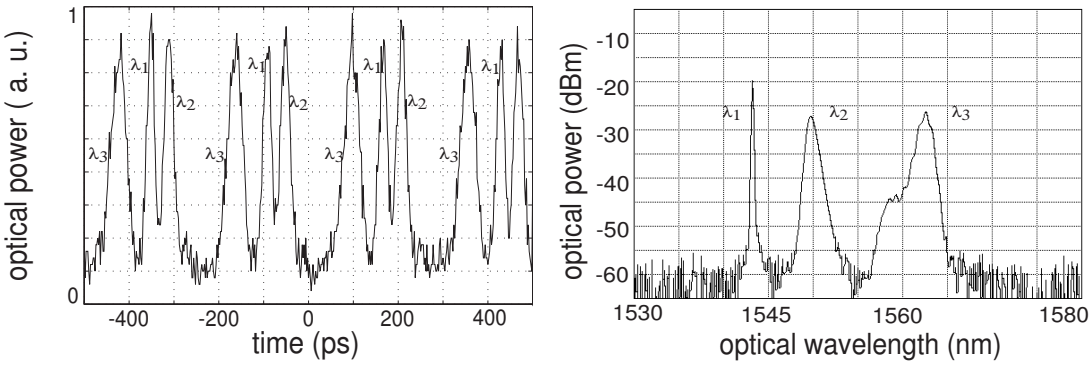

(a) time trace (b) spectrum

Figure 52: Experimental multiwavelength laser output.

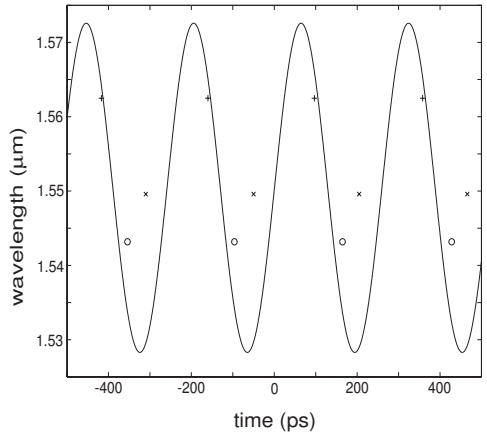

Figure 53: Theoretical evolution of the maximum of the transfer function of the UMZI as a function of time (solid line) and experimental behaviors (points).

The time locations of these emitted wavelengths are plotted in Figure 53, as well as the theoretical evolution of the maximum of the transfer function given by Equation 60. Experimental behaviors of λ_1 and λ_3 are in good agreement with the expected behavior. However, λ_2 is not accounted for by the filter transfer function. This might indicate that, for this filter position, the overall frequency selection is dominated by the EDFA transfer function.

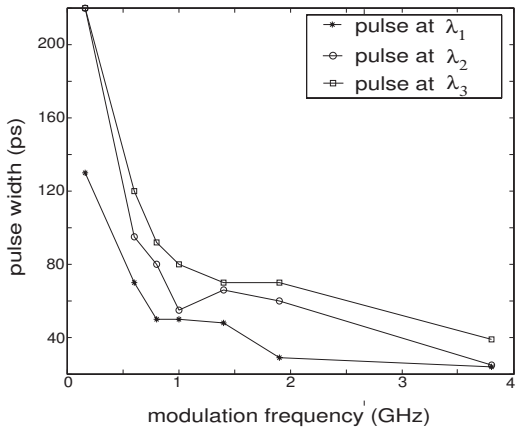

Figure 54: Full-width at half maximum pulsewidth as a function of modelocking frequency for the three emitted wavelengths.

As shown in Figure 54, the three pulse trains-three colors operation of the laser has been observed at different harmonics of the frequency axial mode separation for a range from some megahertz up to 3.8 GHz. As expected in a mode-locked configuration, the pulsewidth decreases with an increase of the modulation frequency [39].

Typically, the large homogeneous broadening occurring in the EDFA causes mode competition in a 10 nm window around each laser oscillation and prevents the emission of closely separated wavelengths [152, 153]. Nevertheless, as mentioned in [76], temporal-spectral multiplexing helps overcome homogeneous broadening in multiwavelength pulsed lasers. In this laser, the wide separation of the emitted wavelengths (about 6 and 13 nm) seems to be inherent to the specific mode-locking technique used. The large FSR of the UMZI and the necessary adequation between the location of the pulse in the time domain and its spectral content, in the absence of any other constraint, are imposing such widely

separated wavelengths. The exact emitted wavelengths are determined by local extrema of the gain curve of the EDFA.

4.5 Conclusions

In this chapter, a new original type of mode-locking has been demonstrated on the dual use of an unbalanced Mach-Zehnder interferometer that has been inserted inside an erbium-doped fiber ring laser. The UMZI serves both as active mode-locker and tunable filter. The design and the theoretical study of the laser display the anticipated alternate multiwavelength operation. The implemented prototype was able to generate pulse trains at three separate wavelengths.

The repetition of the pulses was set by the UMZI modulation frequency. And the optical wavelength of each pulse was determined by the interaction between the bandwidth of the erbium doped fiber amplifier gain and the UMZI modulation frequency.

This first proof of concept showed significant jitter on the amplitude of the optical pulses, as well as variations in temporal and spectral spacings between the different pulse trains. The following chapter will discuss methods and equipment solutions to address these shortcomings.

CHAPTER 5

IMPROVEMENTS OF THE MULTIWAVELENGTH PULSED LASER

In the previous chapter, we numerically and experimentally validated a technique to generate successive pulses at different wavelengths using an actively mode-locked fiber laser in which an UMZI is inserted. In this chapter, we will focus on the improvements that can be achieved for this new fiber laser source.

The drawback of the alternate multiwavelength source is that times and wavelengths at which the emission of pulses occur are not fully controlled. We demonstrate in this section a technique to set the emission of time-wavelength interleaved pulses on a predetermined grid.

Moreover the source is a mode-locked fiber laser, hence it suffers from many defects: jitter and lack of stability. This chapter will introduce a novel technique we developed to address this situation: the multi-harmonic phase modulation (MHPM).

Finally, we will present other possible improvements of the behavior of this alternate multiwavelength laser.

5.1 Control of the multiwavelength emission

From inspection of Figure 53, we can observe that pulses at λ_1 and λ_2 are separated by 6.4 nm in the Fourier domain and by 44 ps in the time domain, whereas those at λ_2 and λ_3 are separated by 12.9 nm and 147 ps. Besides, those at λ_3 and λ_1 are separated by 38 ps. It is clear that variations in both temporal and spectral spacings appear. It is primordial to overcome these fluctuations and to have a better control of the source for practical use and applications of such a laser source.

5.1.1 Control in the time domain

Emitted pulses can be controlled with an additional modulator. For instance, a conventional intensity modulator (IM), integrated on $LiNbO_3$, is added in the ring cavity, as shown in Figure 55. The IM is synchronously driven at a modulation frequency f_{im} equal to an integer multiple N of the UMZI modulation frequency. Thus, if k pulse trains at k different wavelengths are generated by the UMZI, these pulses will also have to satisfy the mode-locking condition for the additional intensity modulator. This new constraint imposed by the IM fixes the temporal spacing between two successive pulses to an integer multiple (within 1 and N) of the inverse of the modulation frequency f_{im}. It locks the emission of pulses on a temporal grid, while the central wavelength is still set by the UMZI.

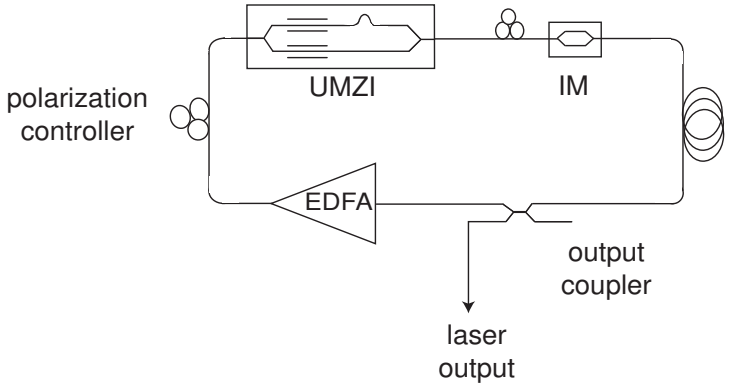

Figure 55: Multiwavelength laser controlled in time.

5.1.1.1 Modification of the Gaussian analysis

The theoretical analysis described in section 4.2 can be slightly modified to include the effect of the IM in the cavity.

The starting pulse in the cavity is still described by a complex Gaussian envelope

$$f_1(t) = Ae^{-\alpha_1 t^2} e^{i(\omega_0 t + \beta_1 t^2)}, \tag{123}$$

Equation 68 gives the exponential approximation of the transfer function of the UMZI

$$T(t) = \exp\left[-\frac{1}{2}\left(\frac{\omega_0 \Delta\tau \Omega_m}{2} + \tau_0(\beta_1 + i\alpha_1)\right)^2 t^2\right], \tag{124}$$

where Ω_m is the modulation frequency of the UMZI. Chirp is still considered to be maximum at ω_0. The intensity modulator has no path length difference between its two arms and so its transfer function T_{im} is

$$T_{\text{im}}(t) = \exp\left[-\frac{1}{2}\left(\frac{\omega_0 \Delta\tau_{\text{im}} \Omega_{\text{im}}}{2}\right)^2 t^2\right], \tag{125}$$

where $\Omega_{\text{im}} = N\Omega_m$ is the modulation frequency of the conventional modulator and $\Delta\tau_{\text{im}}$ its modulation depth. Thus, if we consider an infinitely flat gain, after one loop, the input pulse $f_1(t)$ becomes

$$f_3(t) = f_1(t)T(t)T_{\text{im}}(t). \tag{126}$$

The two signals have to be equal for a steady-state solution and

$$\begin{cases} \alpha_1 = \alpha_1 + \frac{\tau_0^2}{2}(\beta_1^2 - \alpha_1^2) + \frac{1}{8}\omega_0^2 \Delta\tau_{\text{im}}^2 N^2 \Omega_m^2 + \frac{1}{8}\omega_0^2 \Delta\tau^2 \Omega_m^2 + \frac{1}{2}\omega_0 \Delta\tau\tau_0 \Omega_m \beta_1 \\ \beta_1 = \beta_1 - \tau_0^2 \beta_1 \alpha_1 - \frac{1}{2}\omega_0 \Delta\tau\tau_0 \Omega_m \alpha_1 \end{cases} \tag{127}$$

By solving the second equation, we compute β_1. Finally, we derive that

$$\begin{cases} \beta_1 = -\frac{\omega_0 \Delta\tau \Omega_m}{2\tau_0} \\ \alpha_1 = \frac{\omega_0 \Omega_{\text{im}} \Delta\tau_{\text{im}}}{2\tau_0} \end{cases} \tag{128}$$

We can note that the value of β_1 computed in this case is equal to the one determined in section 4.2. Consequently, the temporal and spectral pulsewidths, Δt and Δf, are

$$\begin{cases} \Delta t = \sqrt{\frac{4 \ln 2 \tau_0}{\omega_0 \Omega_{\text{im}} \Delta\tau_{\text{im}}}} \\ \Delta f = \frac{\sqrt{2 \ln 2}}{\pi} \sqrt{\frac{\omega_0 \Omega_{\text{im}} \Delta\tau_{\text{im}}}{2\tau_0}\left[1 + \frac{1}{2}\left(\frac{\Delta\tau}{N\Delta\tau_{\text{im}}}\right)^2\right]} \end{cases} \tag{129}$$

If we consider a Gaussian gain represented by Equation 23, the system becomes

$$\begin{cases} \alpha_1 = \alpha_1' + \frac{\tau_0^2}{2}(\beta_1^2 - \alpha_1^2) + \frac{1}{8}\omega_0^2 \Delta\tau_{\text{im}}^2 N^2 \Omega_m^2 + \frac{1}{8}\omega_0^2 \Delta\tau^2 \Omega_m^2 + \frac{1}{2}\omega_0 \Delta\tau\tau_0 \Omega_m \beta_1 \\ \beta_1 = \beta_1' - \tau_0^2 \beta_1 \alpha_1 - \frac{1}{2}\omega_0 \Delta\tau\tau_0 \Omega_m \alpha_1 \end{cases} \tag{130}$$

where α_1' and β_1' are defined by Equation 75 and Equation 76. By using the same approximations as in section 4.2, we find

$$\begin{cases} \beta_1 = -\frac{\omega_0 \Delta\tau \Omega_m}{2\tau_0} \\ \alpha_1 = \frac{\omega_0}{\sqrt{8 + \tau_0^2 \Delta\omega^2}}\left[\frac{2\Delta\tau^2 \Omega_m^2}{\tau_0^2} + \frac{\Delta\omega^2 \Delta\tau_{im}^2 \Omega_{im}^2}{4}\right]^{\frac{1}{2}} \end{cases} \tag{131}$$

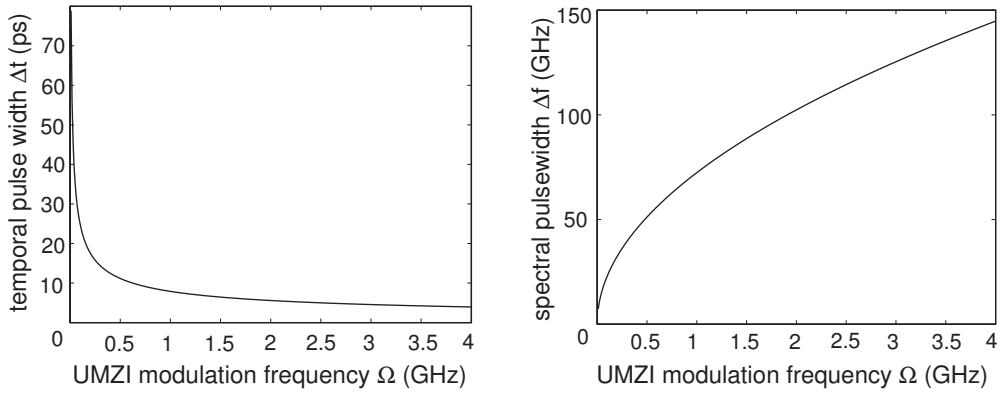

(a) temporal pulsewidth (b) spectral pulsewidth

Figure 56: Pulsewidths evolution as functions of the UMZI modulation frequency (with $\omega_0 = 1.216\ 10^{15}$ rad/s, $\tau_0 = 1.33\ 10^{-13}$ s, $\Delta\tau = 2\ 10^{-15}$ s, $\Delta\tau_{im} = 1.3\ 10^{-15}$ s, $\Delta\omega = 7.85\ 10^{12}$ rad/s and $\Omega_{im} = 3\Omega$).

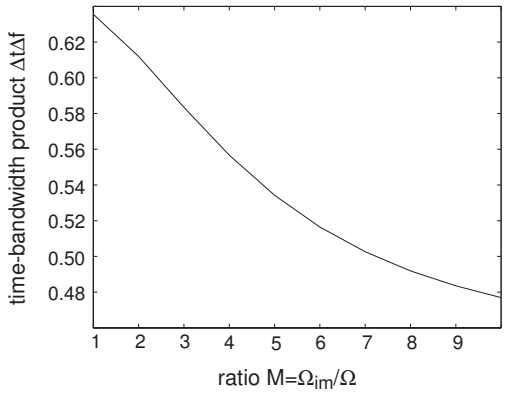

Figure 57: TBP evolution as a function of M (with $\omega_0 = 1.216\ 10^{15}$ rad/s, $\tau_0 = 1.33\ 10^{-13}$ s, $\Delta\tau = 2\ 10^{-15}$ s, $\Delta\tau_{im} = 1.3\ 10^{-15}$ s, $\Delta\omega = 7.85\ 10^{12}$ rad/s and $\Omega = 2\ 10^{9}$ rad/s).

The addition of the IM does not change the chirp value of β_1, but only the value of α_1, and thus of the pulsewidth. The chirp is solely due to the frequency sweeping of the UMZI.

The resulting pulsewidths are then given by:

$$\begin{cases} \Delta t = \sqrt{\frac{2\ln 2}{\omega_0}}\left(8+\tau_0^2\Delta\omega^2\right)^{\frac{1}{4}}\left[\frac{2\Delta\tau^2\Omega_m^2}{\tau_0^2}+\frac{\Delta\omega^2\Delta\tau_{mi}^2\Omega_{mi}^2}{4}\right]^{-\frac{1}{4}} \\ \Delta f = \frac{\sqrt{2\ln 2}}{\pi}\left\{\frac{\omega_0}{\sqrt{8+\tau_0^2\Delta\omega^2}}\left[\frac{2\Delta\tau^2\Omega_m^2}{\tau_0^2}+\frac{\Delta\omega^2\Delta\tau_{im}^2\Omega_{im}^2}{4}\right]^{\frac{1}{2}}\right. \\ \qquad \left.\left[1+\frac{\Delta\tau^2\Omega_m^2}{4\tau_0^2}\left(8+\tau_0^2\Delta\omega^2\right)\left[\frac{2\Delta\tau^2\Omega_m^2}{\tau_0^2}+\frac{\Delta\omega^2\Delta\tau_{im}^2\Omega_{im}^2}{4}\right]^{-1}\right]\right\}^{\frac{1}{2}} \end{cases} \quad (132)$$

Figure 56 shows the theoretical evolution of temporal and spectral pulsewidths as a function of the UMZI modulation frequency, when the IM modulation frequency is three times the UMZI modulation frequency. We observe that the TBP is independent of Ω when the other parameters are fixed. The TBP depends more on the ratio M=Ω_{im}/Ω, as shown in Figure 57.

5.1.1.2 Numerical simulations

The influence of a conventional IM in the cavity aids to control the timing of the emitted pulses. Synchronously driven at an integer multiple, *N*, of the UMZI modulation frequency, the IM locks the emission of pulses on a temporal grid, while the central wavelength is determined by the UMZI.

Figure 58 shows the simulation results after 200 loops, when the modulation frequency of the IM ($f_{im} = \Omega_{im}/2\pi = 34$ GHz) is three times the modulation frequency of the UMZI ($f_{UMZI} = \Omega/2\pi = 11.33$ GHz). The other parameters are set to $\omega_0 = 1.216\ 10^{15}$ rad/s, $\tau_0 = 1.33\ 10^{-13}$ s, $\Delta\tau = 1.29\ 10^{-15}$ s, $\Delta\tau_{im} = 1.29\ 10^{-15}$ s, and $\Delta\omega = 23.5\ 10^{12}$ rad/s.

Three series of pulses at three different wavelengths ($\lambda_g = 1538$ nm, $\lambda_h = 1554$ nm and $\lambda_i = 1567$ nm) are obtained. Two successive pulses are separated by $1/f_{im}$ and two pulses at the same wavelengths by $1/f_{UMZI}$, as expected. The pulse widths are recorded to be 1.9 ps, 2.5 ps and 1.7 ps, yielding a TBP of 0.57, 0.78 and 0.51. Theory predicts a pulsewidth of 1.49 ps and a TBP of 0.56. We can also observe that two pulses at the same wavelength are separated by 88 ps, corresponding to $1/f_m$.

Table 3: Simulation parameters in the case of time control.

parameter	value
g_0	30 dB
τ_0	1.33 10^{-13} s
$\Delta\tau_{im}$	1.29 10^{-13} s
$\Delta\tau$	1.29 10^{-15} s
ω_0	1.216 10^{15} rad/s
f_{im}	34 GHz
f_{UMZI}	11.33 GHz
Ω	7.18 10^{10} rad/s
$\Delta\omega$	23.5 10^{12} rad/s
dispersion	0 ps/nm/km
cavity length	20 m
A_{eff}	80 10^{-12} m^2
fiber loss	0.2 dB/km
n_2	3 10^{-20} m^2/W
γ	1.5 W^{-1}/km

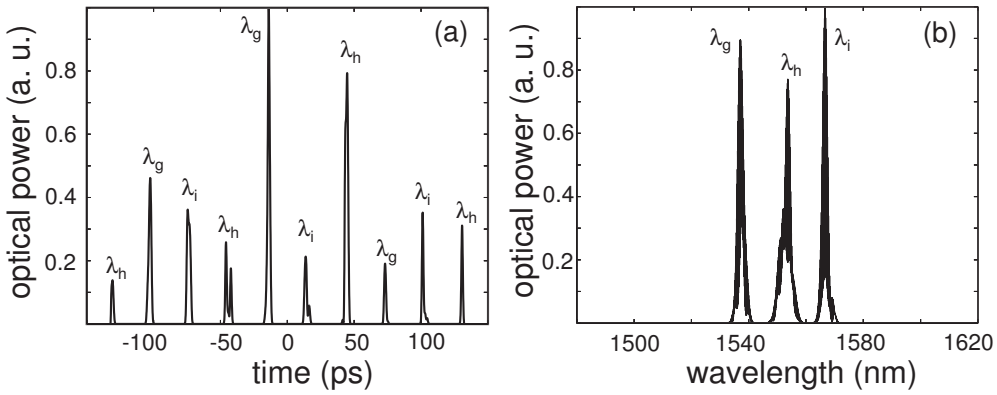

Figure 58: Simulation results in the presence of an additional intensity modulator in the (a) time domain and (b) spectral domain.

Two successive pulses are separated by 29 ps, i.e. by $1/f_{im}$. This behavior matches our expectations.

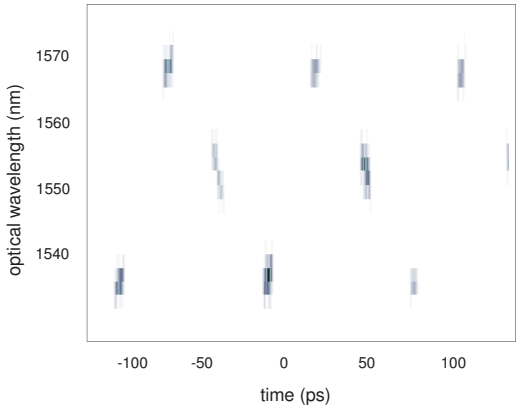

Figure 59: Spectrogram in the presence of an additional intensity modulator.

Based on our simulations, an intensity modulator in the cavity is able to control both the temporal spacing between two pulses at the same wavelength and the temporal spacing between pulses at different wavelengths. It imposes a temporal grid to the laser.

5.1.1.3 Experimental results

Based on the above results, experiments have been undertaken to verify the temporal control of the multiwavelength laser source. The IM used in our experiments is integrated on $LiNbO_3$, built using titanium in-diffused technology. The used crystal is in a X-cut, Y-propagation configuration. The electro-optic bandwidth at -3 dB is 10 GHz and the insertion losses, without connectors, are about 6.2 dB. The interferometer is in a push-pull configuration. The half-wave voltage V_π is equal to 5.6 V for RF electrodes and 6.1 V for DC electrodes.

Figure 60 shows the experimental results when the modulation frequency of the IM (f_{im} = 4.837 GHz) is five times the modulation frequency of the UMZI (f_{UMZI} = 967.4 MHZ). The other parameters are set to $\omega_0 = 1.216\ 10^{15}$ rad/s, $\tau_0 = 1.33\ 10^{-13}$ s, $\Delta\tau = 2\ 10^{-15}$ s, and $\Delta\tau_{\mathrm{im}} = 1.3\ 10^{-15}$ s.

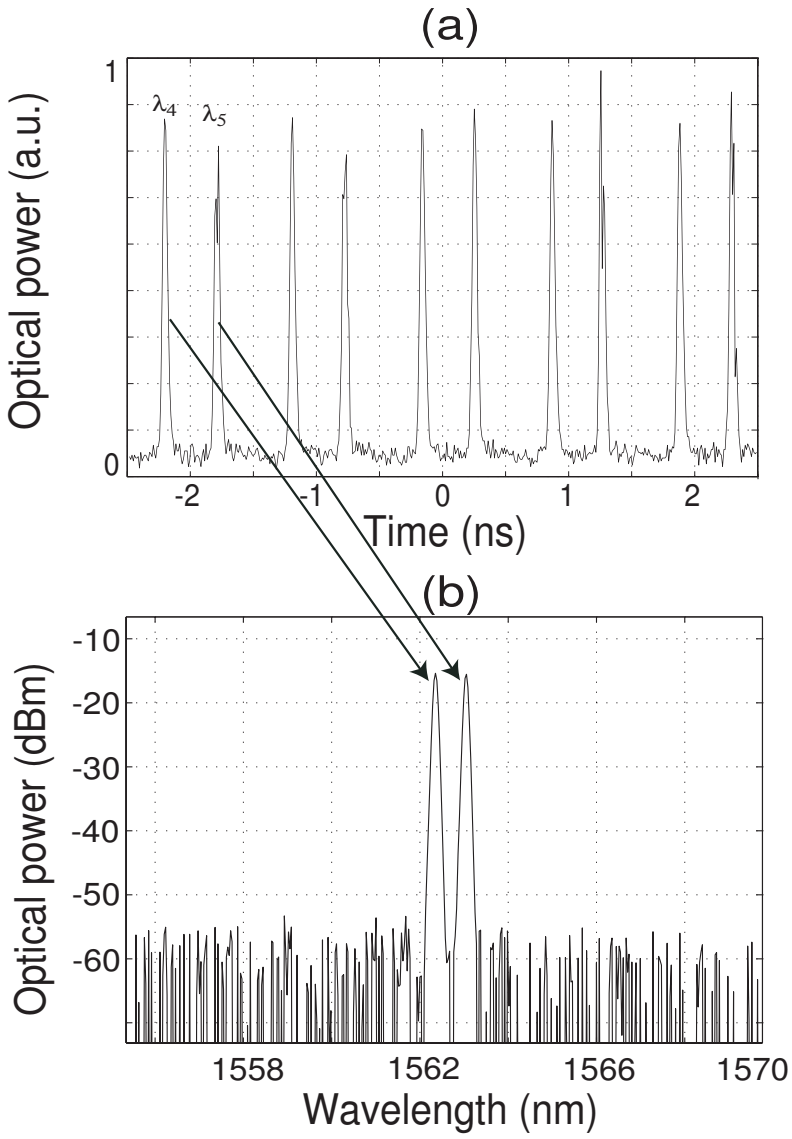

Figure 60: Time trace (a) and spectrum (b) at the laser output in the presence of a conventional intensity modulator.

Two series of pulses at two different wavelengths (λ_4 = 1562.3 nm and λ_5 = 1563 nm) are obtained. This confirms the ability to emit laser pulses at closely spaced wavelengths. The temporal pulses at λ_4 and λ_5 are separated by $2/f_{im}$. The other locations on the temporal grid are left unoccupied, probably because the two emitted wavelengths capture all the available gain. The pulse widths are recorded to be 50 and 45 ps, yielding a time-bandwidth product of 0.56 and 0.48, respectively. Theory predicts pulsewidths of 2.8 ps and a TBP of 0.46. We can thus observe the experimental TBPs are close to the theoretical ones, whereas the experimental pulsewidths are much larger. We attribute this fact to the homogeneous character of the EDFA that needs a better modeling in the theoretical equations.

The birefringence of the IM combined with the polarizing behavior of the UMZI acts as a filter that imposes a wavelength spacing of 0.7 nm. One could use this phenomenon to anchor the emitted wavelengths on the ITU grid.

5.1.2 Control in the spectral domain

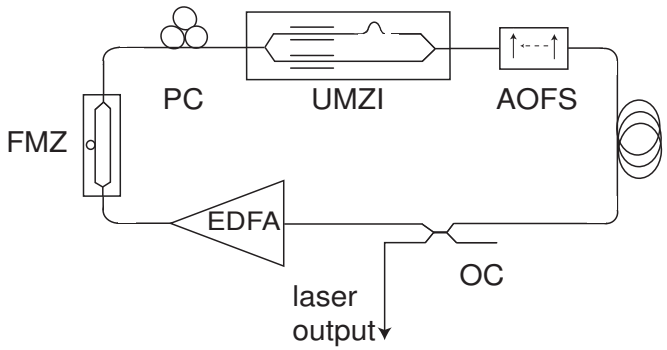

Figure 61: Improved experimental setup (FMZ: fiber Mach-Zehnder, PC: polarization controller, AOFS: acousto-optic frequency shifter, OC: output coupler).

By analogy with the time grid imposed to the laser output, we can impose a wavelength grid to control the spectral content of the generated pulses. Diverse methods can be investigated, such as birefringence [93], dispersion tuning [107], use of four wave mixing [90], arrayed waveguide gratings [154] or Sagnac loop filters [155]. One could also impose a constraint in the frequency domain by inserting a periodic filter in the cavity.

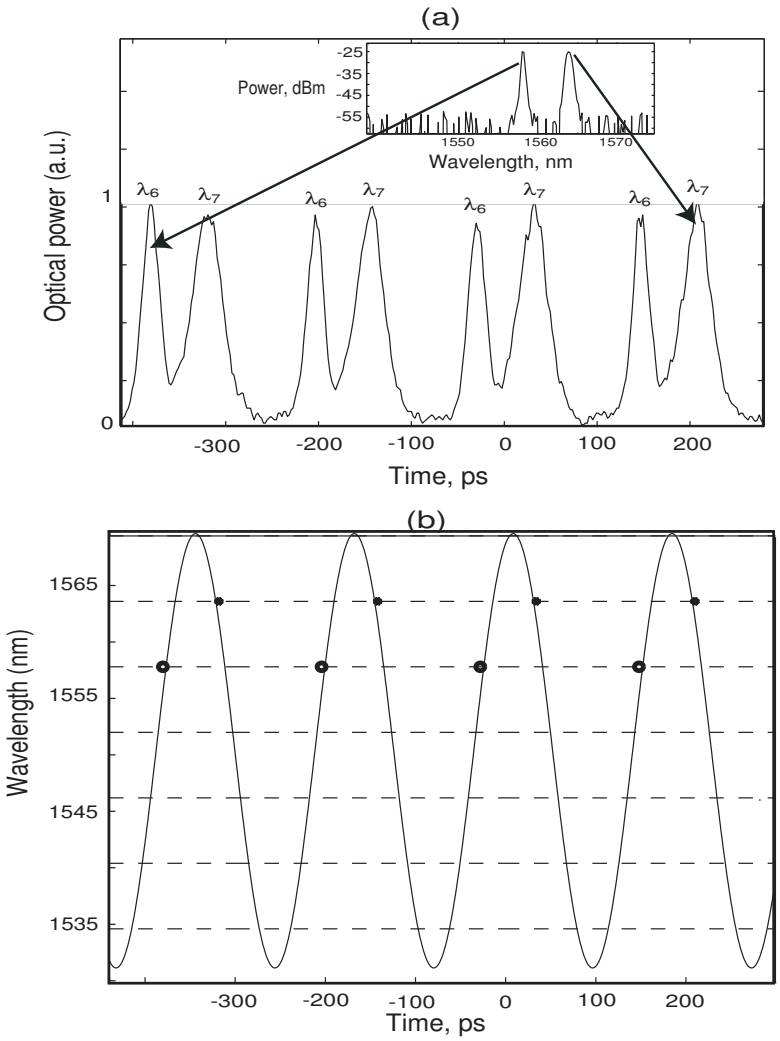

Figure 62: Time trace and spectrum (a) of the laser output and the corresponding spectrogram (b), with theoretical evolution of the maximum of the transfer function of the UMZI as a function of time (solid line) and experimental data (points).

In our case, to control wavelength spacings, a fiber Mach-Zehnder (FMZ) is inserted in the initial ring cavity as well as an acousto-frequency shifter (AOFS). The FMZ will play the role of a periodic filter and the AOFS will prevent gain saturation by a single wavelength to allow multiwavelength laser emission at room temperature [75].

In the experiments, the modulation frequency was set to 5.67 GHz and the FSR of the additional periodic filter is Δ_{FMZ} = 5.8 nm. The results are shown in Figure 62(a), both in the time and frequency domains. The spectal content of each pulse is also determined to prove the alternate multiwavelength operation. Two pulse trains at two different wavelengths (λ_6=1557.8 nm and λ_7=1563.6 nm) are obtained. As expected, even if only two wavelengths are generated, we note that the wavelengths are separated by Δ_{FMZ}: the emitted wavelength are anchored on the frequency grid imposed to the ring cavity. This grid is schematically represented in Figure 62(b) by the horizontal lines. The pulse widths are recorded to be 20 ps and 28 ps, respectively. The TBP of each pulse is 0.56 and 1.12. Once again, the chirp is due to the time variation of the center wavelength of the filter. Figure 62(b) shows the theoretical evolution of the maximum of the transfer function of the UMZI as a function of time (with $\tau_0 = 1.33\ 10^{-13}$ s, $\omega_0 = 1.216\ 10^{15}$ rad/s, $\Omega = 3.56\ 10^{10}$ rad/s and $\Delta\tau = 1.65\ 10^{-15}$ s as experimental parameters) and the corresponding experimental data points.

5.1.3 Time-wavelength mapping

5.1.3.1 Principle

In order to fully control the laser output, both previous types of control can be simultaneously operated. The emission is anchored on a time-wavelength map [156, 157, 158]. Figure 63 shows the setup used in this situation: a phase modulator (PM) is inserted as well as a comb filter with an AOFS.

To have better control on the timing of the emitted pulses, a conventional phase modulator (PM) is added in the cavity. By synchronously driving the PM at a harmonic of the

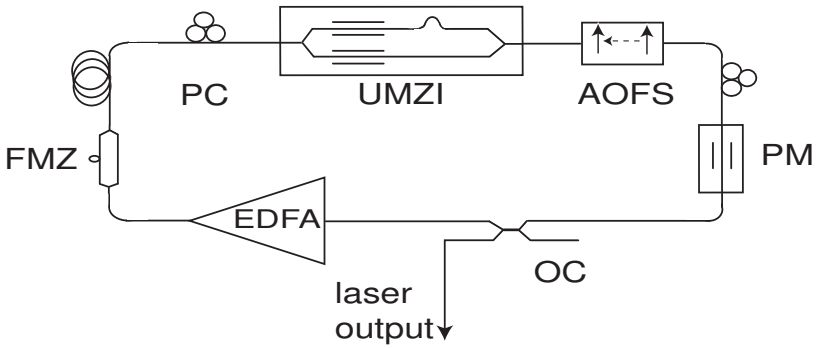

Figure 63: Improved experimental setup.

modulation frequency of the UMZI, pulse emission is locked on a temporal grid. In a similar way, by inserting an additional periodic filter in the cavity, the wavelength spacing of the possible emitted wavelengths is fixed to an integer multiple of its free spectral range. An acousto-optic frequency shifter is also introduced in the loop to prevent gain saturation by a single wavelength and to allow multiwavelength laser emission at room temperature [159]. As a consequence, the laser output is restricted to a time-wavelength map. Finally, these time and frequency locking conditions, along with the condition imposed by Equation 60, impose three constraints on the emitted pulses in the time-wavelength domain.

5.1.3.2 Simulation results

To validate this concept of time-wavelength mapping, numerical simulations have been undertaken. For the additional intra-cavity filter, a Fabry-Perot interferometer is considered. Its spectral transfer function is represented in Figure 64. The thickness of the substrate is 100 μm and the reflectance is $R = 0.4$. these characteristics imply a finesse of $F = \frac{\pi\sqrt{R}}{1-R} = 3.3$ and a FSR of 6 nm.

In this simulation, the FSR of the additional intracavity filter is chosen to be $\Delta_{\mathrm{FSR}} = 6$ nm. The other parameters of the simulation are $\tau_0 = 1.33\ 10^{-13}$ s, $\omega_0 = 1.216\ 10^{15}$ rad/s, $f_m = \Omega/2\pi = 11.33$ GHz, and $\Delta\tau = 1\ 10^{-15}$ s. The modulation frequency of the PM, f_{pm}, is three times the modulation frequency of the UMZI: $f_{pm} = 3 * f_m = 33.99$ GHz.

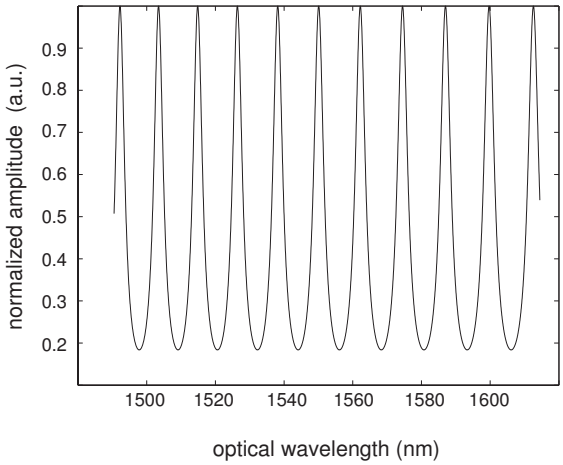

Figure 64: Transfer function of the filter used in the simulations.

Table 4: Simulation parameters in the case of time-wavelength mapping.

parameter	value
g_0	30 dB
τ_0	1.33 10^{-13} s
$\Delta\tau$	1 10^{-15} s
f_m	11.33 GHz
f_{pm}	33.99 GHz
ω_0	1.216 10^{15} rad/s
$\Delta\omega$	6 nm
dispersion	0 ps/nm/km
cavity length	20 m
A_{eff}	80 10^{-12} m^2
fiber loss	0.2 dB/km
n_2	3 10^{-20} m^2/W
γ	1.5 W^{-1}/km

The dispersion is fixed to be null. Figure 65 shows the numerical results of the simulation in the time and frequency domains; three pulse trains at three different wavelengths (λ_j = 1538.4 nm, λ_k = 1550.2 nm, and λ_l = 1562.2 nm) are observed. These values correspond to the maxima of the transfer function represented in Figure 64. The spectral content of each pulse is examined to be able to attribute every wavelength to every pulse.

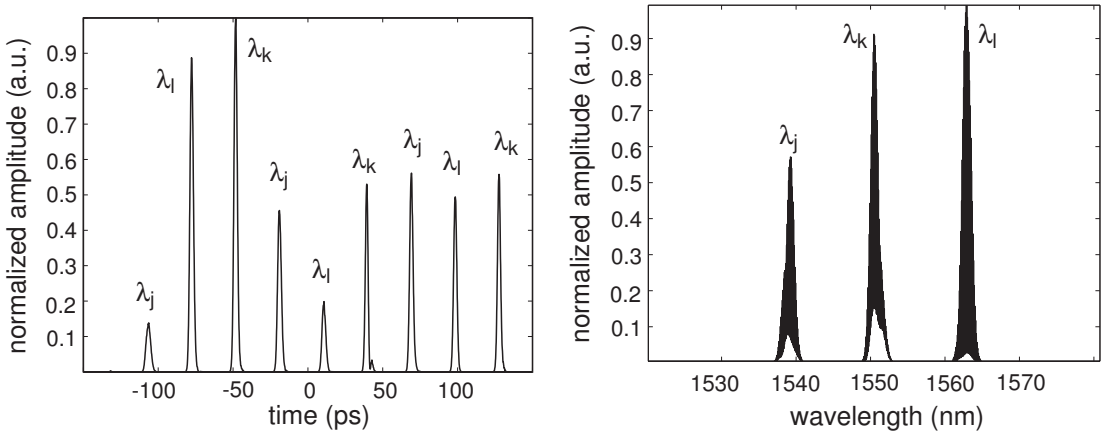

(a) time domain (b) frequency domain

Figure 65: Simulations of laser output with both time and frequency control.

To prove that the laser output is effectively anchored on a time-wavelength grid, Figure 66 gives the spectrogram of the emission. We thus observe that λ_j and λ_k are separated by $2*\Delta_{FSR}$ in the Fourier domain and by $1/f_{pm}$ in the time domain, as well as λ_k and λ_l. As a consequence, no shift in time and wavelength spacings can be observed. The time and spectrum locations of the laser output are thus controlled.

The FWHM pulsewidth is about 2.8 ps in the temporal domain and 163 GHz in the spectral domain, yielding a TBP of 0.46.

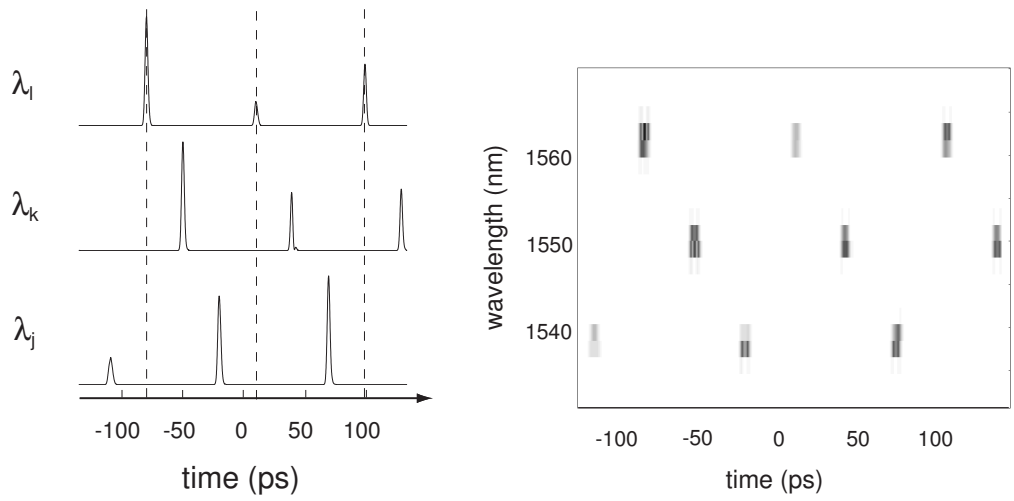

(a) trains separation (b) spectrogram

Figure 66: Optical wavelength identification for each pulse train.

5.1.3.3 Experimental results

In this experiment, a fiber Mach-Zehnder (FMZ), with a free spectral range $\Delta\lambda_{\mathrm{FMZ}}$=5.8 nm, is inserted to act as an intracavity filter. Figure 67 shows the experimental results when the modulation frequency of the PM, f_{pm} = 9.4 GHz, is seven times the modulation frequency of the UMZI, f_m = 1.34 GHz. The experimental parameters are τ_0=1.33 10^{-13} s, $\Delta\tau$=1.2 10^{-15} s, and λ_0=1550 nm.

Once again, three pulse trains at three different wavelengths are obtained. The emitted wavelengths are λ_4 = 1536.9 nm, λ_5 = 1542.7 nm, and λ_6 = 1560.1 nm. The pulsewidths are 39, 44, and 48 ps, yielding a time-bandwidth product of 0.48, 1.1, and 2.23, respectively.

To verify the time and wavelength controls of our setup, we are looking at the spectrogram of the laser output. In Figure 68, many comments can be made. First, the PM being driven at a harmonic of the modulation frequency of the UMZI, a temporal grid is imposed to the laser. It is represented by the vertical lines on the spectrogram.

In the same way, the intracavity filter formed by the FMZ fixes the wavelengths that can be emitted by the source. This spectral grid is represented by the horizontal lines on the spectrogram.

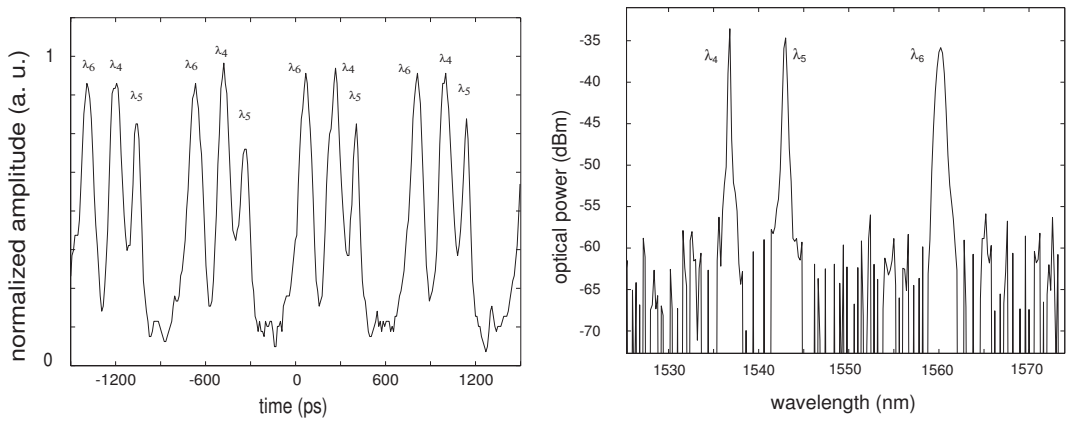

(a) temporal domain (b) spectral domain

Figure 67: Laser output with time-frequency control.

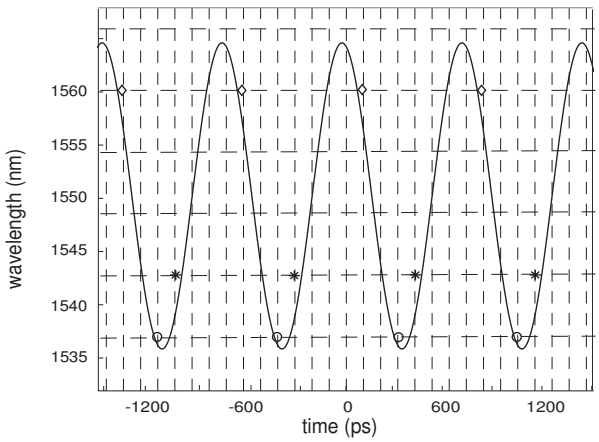

Figure 68: Spectrogram of the multiwavelength laser with a periodic filter and a phase modulator.

Finally, the last constraint is the theoretical temporal variation of the maximum of the transfer function of the UMZI and is represented by Equation 60. It corresponds to the sinusoidal function on the spectrogram. In this figure are also indicated the experimental points. We can observe that these points are precisely located on the time-wavelength map formed by the two grids previously described. Thus, the pulses at λ_6 and λ_4 are separated by $4\Delta\lambda_{FMZ}$ in the frequency domain and by $2/f_{pm}$ in the time domain, whereas those at λ_4 and λ_5 are separated by $\Delta\lambda_{FMZ}$ and $1/f_{pm}$. It is interesting to note that these experimental points correspond quite well to the theoretical sine curve. Nevertheless, the grid use is not optimal. The unoccupied grid locations arise from residual filtering in the cavity, which might be eliminated by improved cavity design to yield tailored operation at any wavelength on the grid.

5.2 Stabilization of the pulsed source

Mode-locked lasers emitting picosecond pulses around the 1550 nm region are potential signal sources for future high-speed optical communication systems because they are easy to build and can produce picosecond pulses at high repetition rates. A large number of designs have been examined, attempting to optimize the operation of the laser to suit the particular application [46, 160].

Nevertheless, potential use of such lasers is ultimately limited by their performances in terms of pulse dropout, stability and jitter. Many schemes have been proposed to improve the stability of mode-locked lasers: locking the electrical phase of the output optical pulse with that of the drive source [161], introducing a mechanism of two-photon absorption [162], and using regenerative mode-locking by feedback of the harmonic longitudinal beat signal [163] or additive-pulse mode-locking [164]. By mixing two harmonics of the fundamental cavity frequency and applying this signal onto an intensity modulator, Takara et al. [165] demonstrated an improved stability as well as the generation of shorter pulses. In this case, pulses were emitted at a repetition rate equal to the lowest of the two mixed

frequencies. In our proposed scheme, we use multi-harmonic phase modulation (MHPM) to mode-lock a fiber laser and, in particular, by adjusting the relative amplitudes of the two mixed frequencies, we show that pulses can be emitted at the highest frequency, thus providing a high repetition rate operation while simultaneously stabilizing the laser output in terms of timing jitter and Bit-Error-Rate (BER) performance [166, 167].

5.2.1 Principle

Figure 69 shows the experimental set-up. The laser cavity is based on an erbium-doped fiber amplifier and polarization controllers that are used to vary and optimize the polarization orientation.

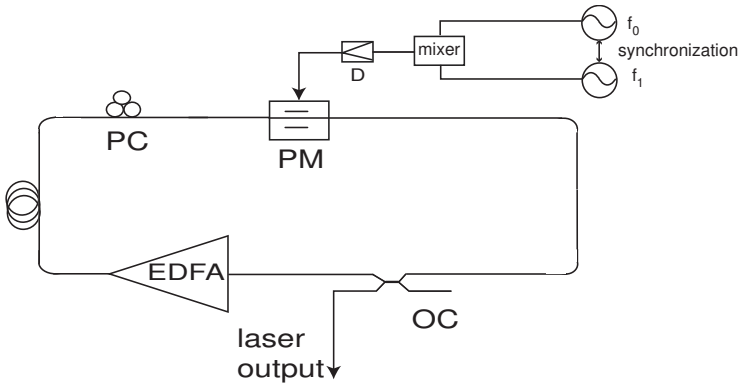

Figure 69: Experimental set-up (PC: polarization controller, EDFA: erbium-doped fiber amplifier, OC: output coupler, PM: phase modulator, D: RF driver).

A fused fiber coupler is used to tap the output signal from the laser. To generate the optical pulses, a phase modulator (PM) is inserted in the cavity to serve as active mode-locker element. The originality of the scheme is to apply to the PM a radio-frequency signal that is the weak mixing of two frequencies. The mode-locking condition is achieved for both frequencies. The first frequency f_0 is the fundamental frequency, equal to the axial mode separation of the cavity, f_{ax}, and the second frequency $f_1 = N f_0$ is a higher harmonic. The two frequency synthesizers are synchronized, in order to optimize the laser behavior. When driving the modulator only at f_1, harmonic active mode-locking is achieved and thus supermodes appear. In an Nth harmonic mode-locked laser, an axial mode is locked to those

that are N axial modes apart on each side. All the modes within the gain bandwidth are thus grouped into N sets, called supermodes. Therefore, if N is the harmonic number of the modulation frequency, N supermodes coexist in the laser cavity. The energy-shifts among these groups and the relative phase-slides among them are the main source of amplitude fluctuations of the emitted pulses. It can lead, in the worst case, to sporadic suppressions of pulses in the train [21, 48, 49]. By combining this frequency with the fundamental frequency in a microwave mixer, the idea is to reduce the supermode competition by coupling them with each other. The cavity axial modes that form one supermode are separated by f_1, i.e. by N other cavity modes. In a conventional mode-locking scheme, as the different supermodes are independent from each other, they suffer diverse losses and fluctuations. This leads to a poor stability of the laser output. As shown in Figure 70, if f_1 is mixed with the fundamental frequency f_0, modulation sidebands are created. As f_0 is equal to the spacing between different successive supermodes, the modulation creates a coupling among supermodes. Thus, all the supermodes will experience and undergo the same variations in the laser cavity, improving the output stability. In this case, not only the mode-locking condition is achieved for each modulation frequency, but also all the cavity modes and supermodes are weakly locked together.

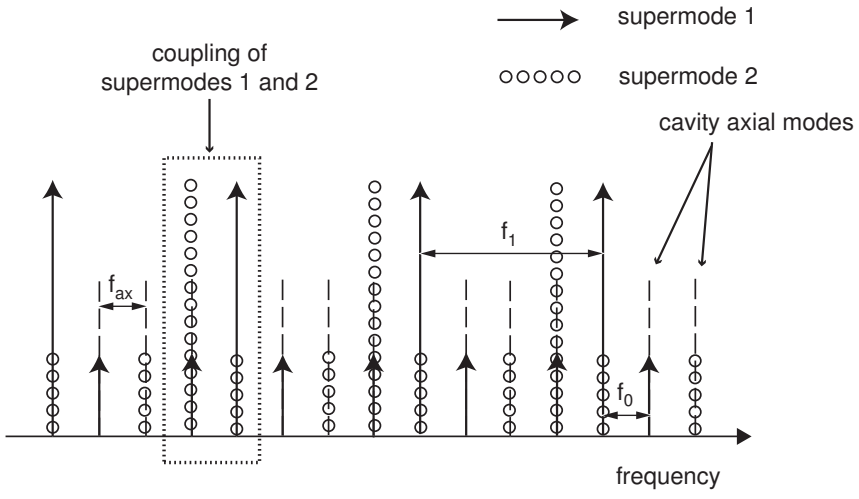

Figure 70: Schematic diagram of the effect of MHPM in the laser in a frequency domain representation.

The voltage applied onto the PM is a mixing of two frequencies; it is time-dependent and equal to:

$$V(t) = V_0 \sin(2\pi f_1 t)[1 + m \sin 2\pi f_0 t + \phi], \tag{133}$$

with V_0 the voltage amplitude, m the modulation depth and ϕ a constant. If the input field in the PM is $E_{\text{in}}(t) = E_0 \cos(\omega t)$, its output is given by [21]:

$$E_{out}(t) = E_0 \cos\left(\omega t + \frac{\pi V(t)}{V_\pi}\right), \tag{134}$$

where ω is the input optical angular frequency and V_π the half-wave voltage. In reference [165], pulses are only emitted when the peak positive voltages of the two sines coincide and so the pulses are emitted at a rate equal to the lowest of the mixed frequencies. In contrast to this option, in our scheme, the repetition rate is determined by the highest frequency of the two mixed signals. In order to allow emission at each local voltage maximum, the relative amplitude of the two mixed frequencies has to be carefully adjusted, and in particular, the modulation index m has to be low, as shown in Figure 71. Indeed, in this case, the energy in the cavity will concentrate under each extremum of the transfer function, their magnitude being similar. Otherwise, the energy will be located only at the global maxima, capturing the impact of the other extrema of weak magnitude.

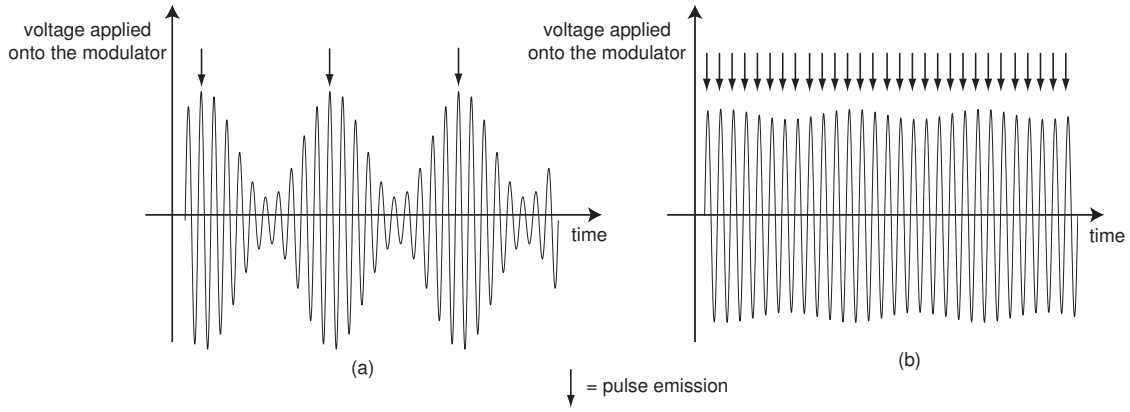

Figure 71: Representation of the voltage applied onto the phase modulator and pulses location when the modulation depth is high (a) and low (b).

5.2.2 Experimental results

Initial characterization of the laser performance involved BER measurements. The fundamental laser frequency is equal to f_{ax}=4.77 MHz, corresponding to a length of the laser cavity of approximately 41.9 m. We set f_1 to 2.52 GHz, corresponding to the 532th harmonic, and f_0 to f_{ax}. Control of the value of *m* leads to emission of pulses at a repetition rate f_1. The characteristics of the laser output are similar to those obtained in the case

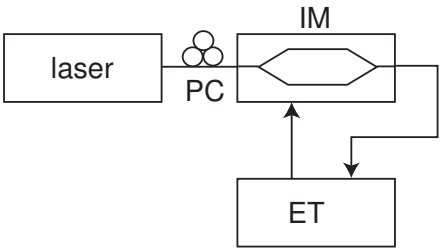

Figure 72: Experimental setup for BER measurement (PC: polarization controller, IM: intensity modulator, ED: error tester).

of conventional mode-locking. Figure 73 shows the time trace and spectrum of the laser output when the modulation depth *m* is equal to 2.5x10^{-2}. One pulse train at a repetition rate f_1=2.52 GHz is observed using a sampling oscilloscope with a 30 GHz photodiode: two successive pulses are separated by $1/f_1 \approx$400 ps. The optical spectrum is obtained via an optical spectrum analyzer with 0.07 nm resolution. The full-widths at half-maximum pulsewidths are recorded to be 20 ps. The output of the laser is externally modulated using a $LiNbO_3$ intensity modulator driven by a pattern generator synchronized with f_1. The length of the pseudo-random sequence is 2^7-1. This signal is fed back to the BER test unit for error detection. Figure 74(a) shows the obtained results with two different modulation depths and these results are compared with those achieved when the mode-locker is only driven at f_1 without mixing. Figure 74(b) and (c) show the radio-frequency spectrum of the signal applied to the PM for two different modulation depths, respectively equal to 1.4x10^{-3} and 2.5x10^{-2}. The BER performance increases with the modulation depth. The sensitivity gain of the MHPM method is 2.94 dB at 10^{-9} BER. This is an indication that the pulse drop out phenomenon is reduced by the MHPM method.

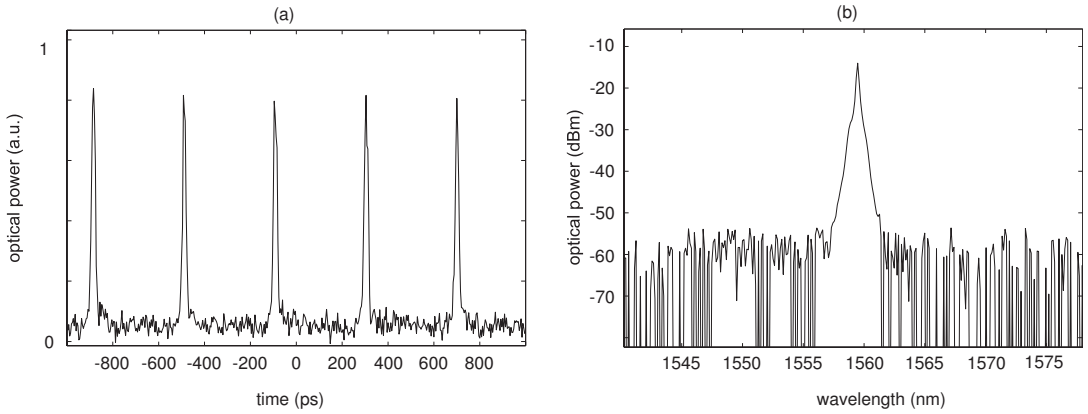

Figure 73: Time trace (a) and optical spectrum (b) of laser output.

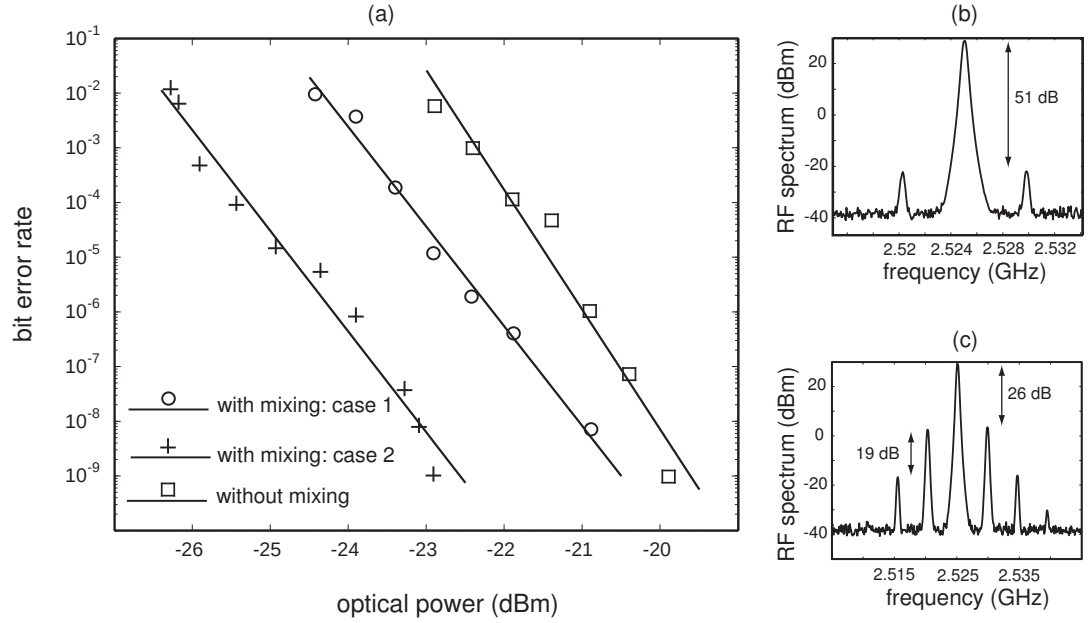

Figure 74: BER performance of the laser output (a) and RF spectrum of the signal applied onto the PM in two cases: case 1 (b) and case 2(c).

The higher the modulation depth, the more efficient the coupling between supermodes, and the more stable the laser output is. However, when the value of the modulation depth is too high, the coupling is too strong and the repetition rate changes from f_1 to f_0, viz., from the highest to the lowest frequency. A compromise has to be found between the modulation depth and the repetition rate in order to generate pulses at the high repetition rate f_1 while introducing a sufficient amount of coupling between supermodes. A modulation depth of $2.5\text{x}10^{-2}$, case 2 in Figure 74, corresponds to this maximum coupling without turning the repetition rate from f_1 to f_0. It is the optimum condition of operation of our experimental set-up.

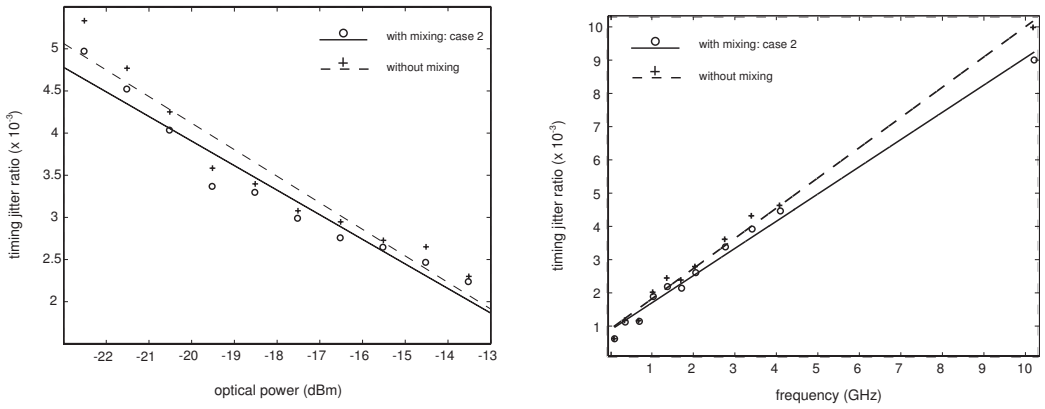

Figure 75: Timing jitter ratio as a function of the optical power with and without mixed frequencies (a) and as a function of the modulation frequency f_1, f_0 being kept equal to f_{ax} (b). Solid lines are linear regression of the experimental data, represented by the points.

To study the improvement of the stability of such a laser, we also measured the timing jitter, σ_T, with and without MHPM. We investigated the timing jitter directly by using the histogram function of a sampling oscilloscope with a 30 GHz photodiode. Figure 75(a) shows the evolution of the timing jitter ratio, defined as $f_1 * \sigma_T$, versus the optical power at a modulation frequency f_1 of 2.52 GHz and compares the performances achieved when two frequencies are combined in the case represented on Figure 74(c) and when no mixing is made. Figure 75(b) shows the evolution of the timing jitter ratio versus the modulation

frequency f_1 with and without mixing between f_1 and f_0. In both cases, mixing of frequencies when driving the PM reduces moderately the timing jitter ratio, leading to a slightly improved stability of the fiber laser output. The principle of operation has been described in the case of phase modulation. We expect that the same technique could be applied in the context of amplitude modulation, since sidebands are also generated in this case.

5.3 Possible investigations

We have presented and synthesized a new and original way of generating alternate multiwavelength pulse trains via a fiber laser. The results to date demonstrate two or three pulse trains at two or three wavelengths. We have also introduced ways of controlling and stabilizing the source. To be practically used, other problems have to be studied to improve the design of this laser.

5.3.1 Increase of number of wavelengths and pulse trains

As the UMZI is the key element in the laser setup, a change of its characteristics will change the output generation. The first idea consists of changing the optical path length difference between the two arms of the modulator. By increasing this path length difference, the free spectral range of the filter will decrease, and that would allow many maxima of the filter to be under the EDFA gain curve. The functionality of the fiber ring laser would be upgraded by allowing a simultaneous multiwavelength emission. In this case, a pulse could be at two wavelengths separated form each other by the value of the free spectral range of the UMZI.

However, in our situation, we focus on an alternate multiwavelength generation. To do so and to increase the number of emitted wavelengths, a solution could be to improve the selectivity of the filter. By cascading many UMZIs, a Lyot filter configuration is used [168]. It would improve the filter finesse, i.e, its ratio FSR over bandwidth. Finally, a simple solution would also be to use an extra intracavity comb filter with a small FSR, in order to increase the density of the wavelength grid. Similarly, in the time domain, the

density of the temporal mapping can be increased by driving the additional modulator at higher harmonics of the modulation frequency of the UMZI.

In the previous experiments, we presented results for an erbium-doped fiber ring laser. However, many experiments have also been conducted with semiconductor optical amplifiers (SOA). The SOA-based lasers can be shorter and more compact than the EDFA lasers, yet have internal fiber coupling loss not present in erbium and often require strong isolation in the cavity. To compare the influence of the gain medium, we obtained a dual-wavelength operation in the same conditions, but with a change of the amplifier.

5.3.2 Influence of gain medium

In a first experiment, a gain-flattened EDFA is inserted in the ring laser. The modulator is driven at 1.6 GHz. Figure 76(a) shows the time trace and spectrum of the laser output. Two pulse trains at two different wavelengths (λ_{12}=1543.8 nm and λ_{13}=1562.6.9 nm) are observed. The pulse widths are recorded to be 25 ps and 44 ps, respectively. The TBP of each pulse is 1.25 and 0.55. The chirp is due to the variation of the center wavelength of the filter with time. Figure 76 shows the theoretical evolution of the maximum of the transfer function of the UMZI as a function of time (with $\tau_0 = 1.33\ 10^{-13}$ s, $\omega_0 = 1.216\ 10^{15}$ rad/s, $\Omega = 9.17\ 10^{9}$ rad/s and $\Delta\tau = 1.18\ 10^{-15}$ s as experimental parameters) and the corresponding experimental data points. The emitted pulses are in agreement with the constraint given by Equation 59.

Figure 77(a) shows the experimental results when the active gain medium is a SOA. The modulation frequency is kept equal to 1.6 GHz. Two other pulse trains at two different wavelengths (λ_{14}=1537.1 nm and λ_{15}=1588.3 nm) can be observed. In this case, the pulse widths are 50 ps and 59 ps, yielding chirped pulses with a TBP of 3.7 and 2.7, respectively. Figure 77(b) shows the temporal theoretical evolution of the two maxima of the UMZI covering the SOA gain curve. In this case, the experimental parameters are $\tau_0 = 1.33\ 10^{-13}$ s, $\Omega = 9.17\ 10^{9}$ rad/s and $\Delta\tau = 2.2\ 10^{-15}$ s, with $\omega_0 = 1.216\ 10^{15}$ rad/s for the below sinusoidal curve and $\omega_0 = 1.17\ 10^{15}$ rad/s for the above one.

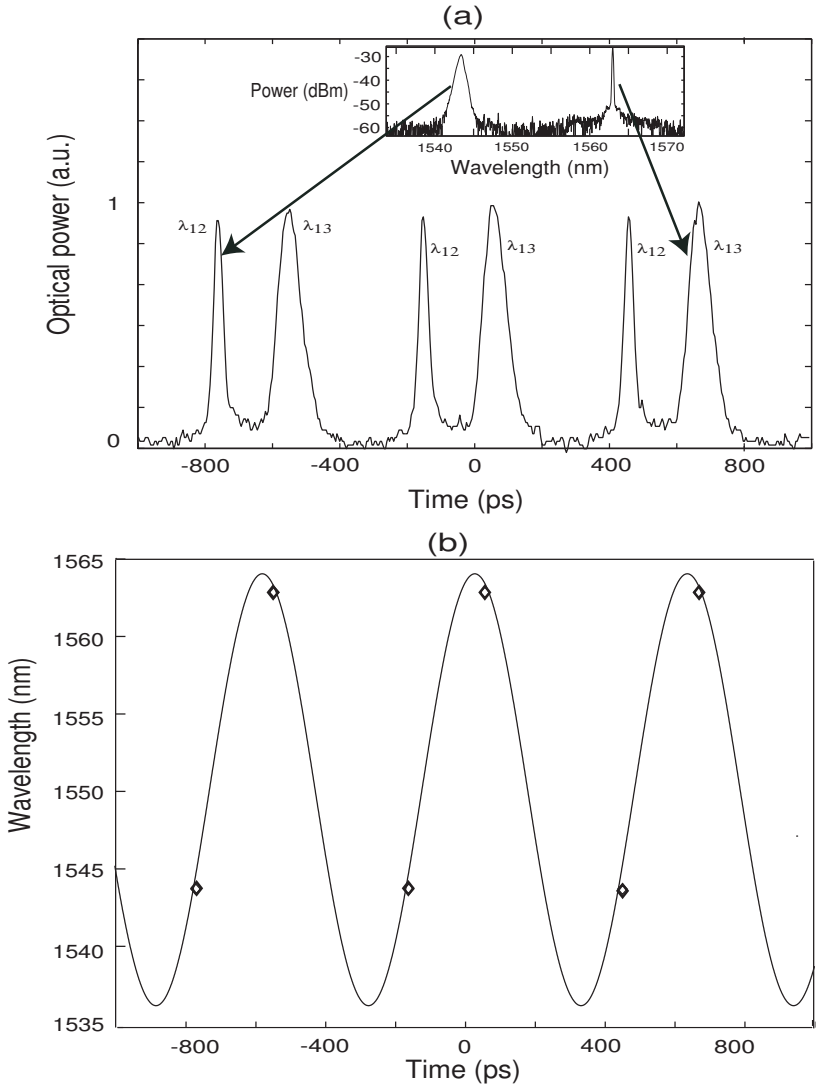

Figure 76: Time trace and spectrum (a) of the laser output in the presence of an EDFA and the corresponding spectrogram (b), with theoretical evolution of the maximum of the transfer function of the UMZI as a function of time (solid line) and experimental data (points).

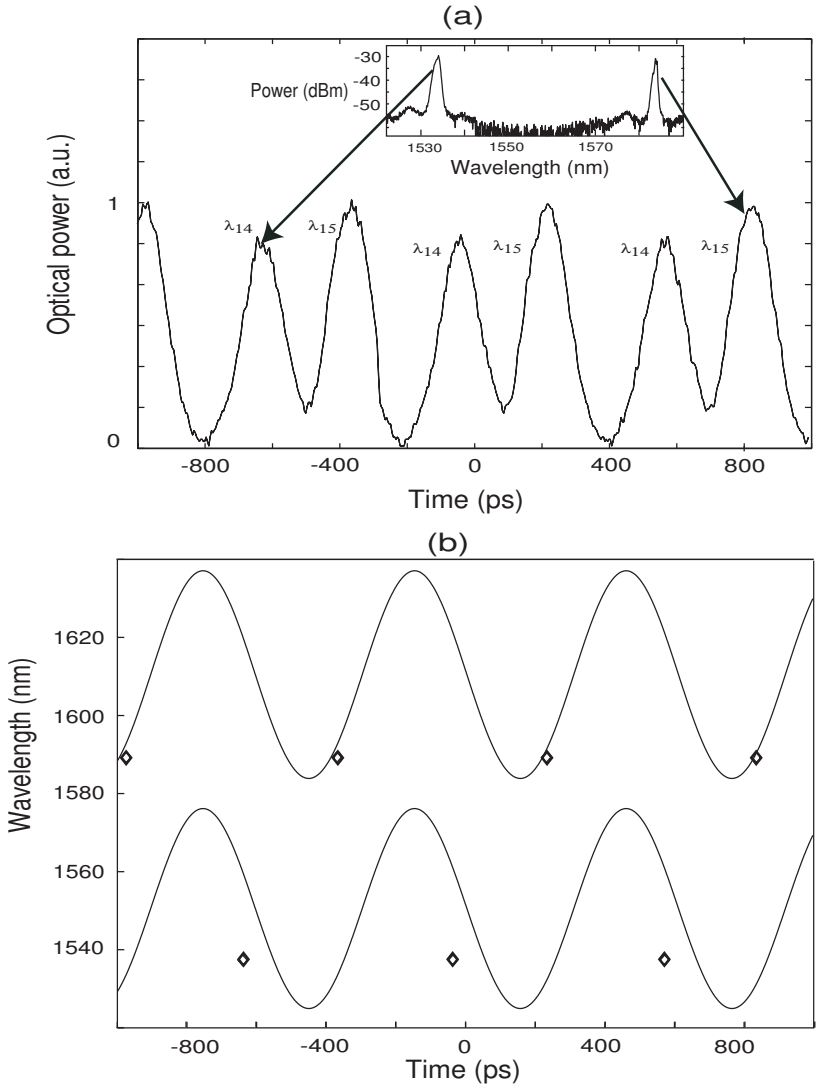

Figure 77: Time trace and spectrum (a) of the laser output in the presence of an SOA and the corresponding spectrogram (b), with theoretical evolution of the maximum of the transfer function of the UMZI as a function of time (solid line) and experimental data (points).

The corresponding experimental data points are also plotted on the figure. We notice that the two wavelengths are selected by two distinct lobes of the tunable filter. The experimental behaviour of λ_{15} is in good agreement with the expected theoretical behavior. However, λ_{14} is not accounted for by the filter transfer function. This might indicate that, for this filter position, the overall frequency selection is dominated by the SOA transfer function.

When comparing the results in both cases, we remark that the same behavior can be obtained. The use of a SOA in the ring cavity allows more lobes of the filter selecting the wavelengths over a wider bandwidth than with an EDFA. Nevertheless, due to the faster dynamics of the SOA, the pulses are wider than when inserting an EDFA. Consequently, it seems difficult to increase the number of trains when using a SOA.

5.3.3 Reduction of chirp or pulse duration

The generated pulses exposed in the previous paragraphs were chirped. To be practically used, these lasers need to produce transform-limited pulses. To do so, we need in particular to reduce the spectral line-width of the different emitted wavelengths. For instance, we can investigate the influence of the filter bandwidth on the produced channel.

Ultra-short pulse with a pulsewidth smaller than 1ps is necessary for over 160 Gbit/s optical signal transmission. We could investigate how to generate this kind of pulse directly from the fiber ring laser. For pulses shorter than 1ps, we can use optical compression technique to realize this function. For pulse compression, there are mainly two methods that are widely used and could be investigated in our scheme to produce ultra-short pulses: compression by higher-order soliton effect and compression using dispersion. In this case, many components can be employed, including for instance chirped mirrors, fiber Bragg gratings or dispersion decreasing fiber (DDF). With these methods, compression factors greater than 10 can be obtained.

5.4 Conclusions

In this chapter, we presented some improvements and some possible investigations that can be made about the alternate multiwavelength laser source. It is possible to control the laser in time by incorporating an additional conventional modulator in the cavity. Control in frequency is also feasible by imposing a spectral grid to the laser. To reduce the phenomenon of pulse dropout and to increase the stability of the laser output, a novel technique of multi-harmonic phase modulation was presented and demonstrated. Different possibilities of investigations have also been proposed to improve the functionality of the source.

In the next chapter, we will introduce a different type of multiwavelength fiber laser: it is a continuous wave source, based on semiconductor optical amplifiers as gain media. In particular, we will investigate its potential as a light source for WDM-PONs.

CHAPTER 6

CONTINUOUS-WAVE MULTIWAVELENGTH FIBER LASER

Multiwavelength laser sources have attracted considerable interest because they can be inexpensive and easy to build. Since one such laser can replace many different laser diodes, it implies less cost, less maintenance, and less inventory. These sources also have great potential because of their versatile possible applications, such as optical fiber sensors, optical instrument sensing spectroscopy, or wavelength-division-multiplexed (WDM) systems.

The previous chapters were dedicated to the presentation of an original alternate multiwavelength pulsed erbium-doped fiber ring laser, based on a new type of mode-locking. We were able to demonstrate its principle thanks to numerical simulations and experimental tests. We were also able to improve the design of the source to gain better control over it. However, the number of channels is still limited: up to three for the moment. For this reason, if we want to use this laser in broadband access networks, the number of concerned customers would be small. Therefore, this chapter introduces a different type of multiwavelength source that is more suitable for access networks applications.

In this chapter, we present a continuous-wave multiwavelength fiber laser source. This source is based on semiconductor optical amplifiers (SOA). Compared to erbium-doped fiber amplifiers (EDFA), SOAs have a dominant property of inhomogeneous broadening. Thanks to this characteristic, multiwavelength generation is easier and supports more channels than with EDFAs. As a consequence, more consumers can be reached by a single light source of this kind. We provide an overview of the SOA-based laser and we use it as a source in a WDM passive optical network (WDM-PON) context. We detail its actual performances and also possible future investigations to improve them.

6.1 Presentation of the source

The source we are using in this part is a continuous-wave laser. The setup of the new laser is simple and easy to build, as shown in Figure 78. An SOA serves as gain medium because its inhomogeneous broadening allows a lot of closely spaced channels to be emitted simultaneously. As no optical pulse is generated, no active mode-locker is included in the ring cavity. To precisely select the desired wavelengths, an interleaver is added to the cavity. This interleaver fixes the spacing between the emitted wavelengths. Thus, by choosing a 25/50 GHz interleaver, two successive generated wavelengths are separated by 50 GHz. To obtain a cost-effective light source for WDM-PON, the multiwavelength SOA-based fiber ring laser should be able to produce as many wavelengths as possible to accommodate a maximum number of customers at the premises.

In our experiment, when the SOA bias current is set to 200 mA and the operating tem-

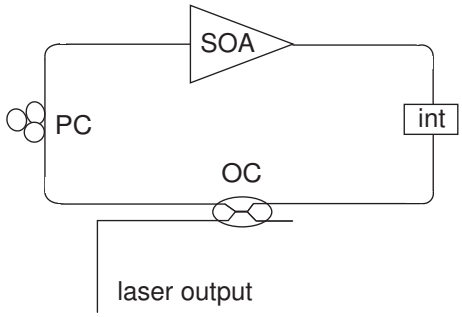

Figure 78: Continuous-wave multiwavelength SOA-based fiber ring laser (PC: polarization controller, Int: interleaver, SOA: semiconductor optical amplifier, OC: output coupler).

perature is 20.5 °C, the center wavelength of the amplified spontaneous emission for the SOA is located at 1455 nm with a 3-dB bandwidth of 60 nm, a small-signal gain of 22 dB, a saturation output power of 12.7 dBm, a polarization dependent gain of 0.3 dB, and a noise figure of 5.6 dB at 1528 nm for an input signal power of -25 dBm. Using this layout, more than 40 simultaneous wavelength lasing oscillations with a frequency separation of 50 GHz are observed, as shown in Figure 79 (a) and (b). The spacing of 50 GHz between two successive wavelengths is imposed by the interleaver.

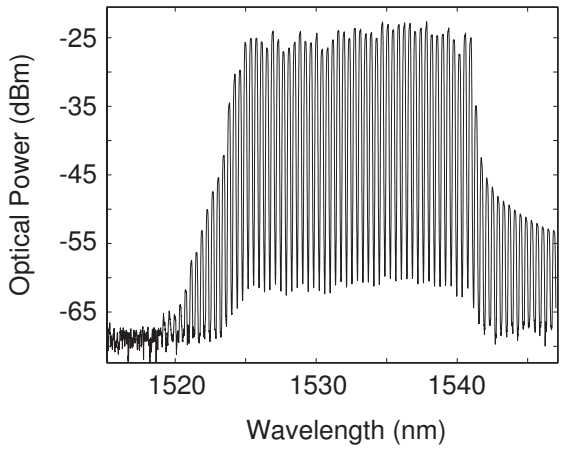

(a)

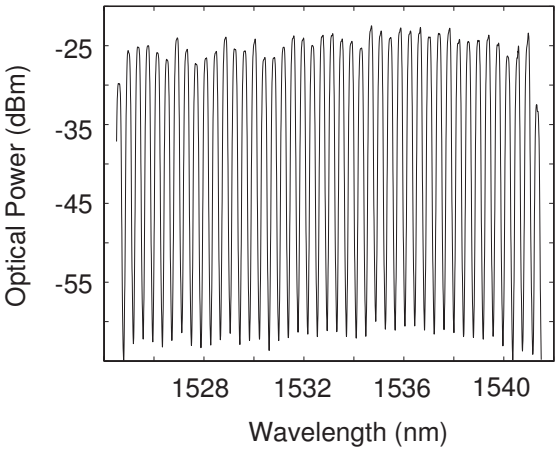

(b)

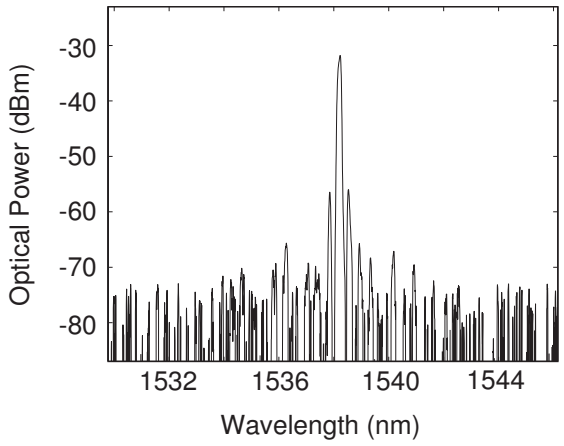

(c)

Figure 79: (a) Laser output spectrum measured after the WDM filter (spectral resolution of 0.01 nm). (b) Expanded laser spectrum of (a) showing over 40 simultaneous wavelength lasing oscillations. (c) Selected wavelength.

With the optical spectrum analyzer resolution of 0.01 nm, the optical signal-to-noise ratio is measured to be greater than 35 dB for all the different channels. The linewidth of the generated oscillations is 0.12 nm. Because of this large value, the transmission will suffer from chromatic dispersion. The state of polarization of light in the laser cavity has to be carefully adjusted to obtain a flat laser spectrum and also to optimize the number of emitted wavelengths. In our experiment, the multiwavelength laser output powers have good flatness even though we can observe a small power variation across the 42 wavelengths. A WDM filter is also used at the laser output to obtain a flat spectrum around the C band. The total output powers before and after the WDM filter are 3.4 dBm and -2.2 dBm, respectively. The laser output remains very stable for several hours in laboratory conditions, as do the different multiwavelength laser output powers. We can notice that a wider spectrum can be observed for a higher bias current. However, with small current changes around 200 mA, the performance of the source does not depend critically on the bias current. Figure 79(c) represents one selected wavelength from the 42 other ones.

6.2 Downstream transmission for WDM-PON

The growth of the Internet is exponential worldwide. The type of transmitted information has changed from voice to multimedia, and the amount of information is always increasing. The end users are attracted by the numerous and versatile emerging applications, such as high-definition videoconferencing, video-on-demand, high-definition television, e-learning, or high-quality audio transmission. To deliver these integrated services effectively and at affordable prices, providers strive to implement new technologies.

The use of WDM techniques in PONs appears to be a promising candidate to solve the bottleneck problem of broadband access for business and residential customers. WDM-PON is an attractive method to deliver high bandwidth services to the premises. This technology has the potential for large capacity, easy management, protocol transparency, and upgradeability [60, 117]. However, for practical implementation, the deployment costs

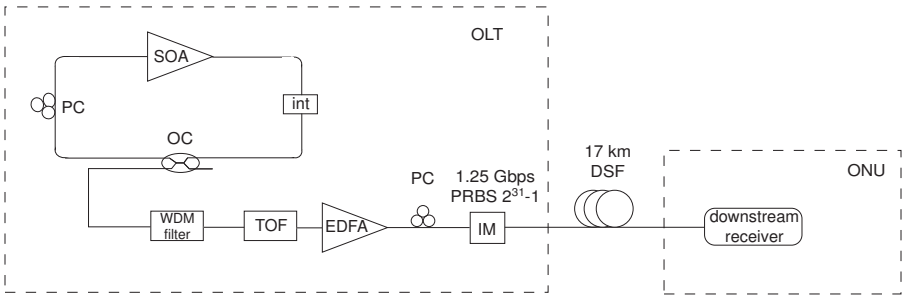

Figure 80: Experimental setup (PC: polarization controller, SOA: semiconductor optical amplifier, Int: interleaver, TOF: tunable optical filter, EDFA: erbium-doped fiber amplifier, IM: intensity modulator, OC: output coupler, DSF: dispersion-shifted fiber).

of such systems have to be reduced. To overcome these economical considerations, several WDM-PON architectures have been proposed, particularly focusing on the development of cost-effective WDM sources. To offer services economically, the optical line terminal (OLT) installed in the central office needs to be able to accommodate as many subscribers as possible and as efficiently as is feasible.

A straightforward solution consists of using an array of distributed feedback (DFB) lasers. However, this method is very expensive, especially when increasing the number of subscribers and wavelengths. To reduce these costs, the use of an optical carrier suppression and separation technique has been proposed [121]. Even if the number of DFB lasers is divided by two with this technique, problems of maintenance and inventory still remain when the number of customers increases. Recently, different techniques have attracted a lot of attention: spectrum-slicing using a broadband incoherent light source such as a light-emitting diode (LED) [84, 169] and amplified spontaneous emission (ASE)-injected uncooled Fabry-Perot laser diodes [62, 63]. While the first solution suffers from low power and high packaging costs, the last one still has problems regarding the wavelength locking under thermal drift of its lasing wavelengths over wide temperature ranges.

Figure 80 illustrates the configuration of the WDM access system considered in our experiment. In the OLT, the light source is a multiwavelength fiber ring laser. This WDM

source is composed of an SOA as the gain medium, a 25/50 GHz interleaver, a polarization controller, and a 50/50 output coupler. Compared to erbium-doped fiber amplifiers, SOAs have a dominant property of inhomogeneous broadening, which makes the multi-wavelength generation possible. Because of SOAs broad gain spectrum, a large number of different wavelengths can oscillate simultaneously [101]. The interleaver acts as a comb filter with a periodic spectral transfer function. Its free spectral range determines the oscillating wavelength spacing.

Before downstream transmission, only one wavelength is selected by a tunable optical filter. This wavelength is dedicated to a specific customer. This optical channel is amplified at the output of the bandpass filter before being externally modulated. The polarization is controlled to achieve maximum efficiency. At the output of the OLT, the signal is transmitted through the fiber. In our experiment, we used 17 km of dispersion-shifted fiber (DSF). By using this type of fiber instead of single mode fiber (SMF), we improve the system performance by overcoming the dispersion effect. At the optical network unit (ONU), a PIN receiver is employed.

A tunable optical filter (TOF) with a bandwidth of 0.25 nm selects one wavelength (λ_1=1538.1 nm) to be amplified by an erbium-doped fiber amplifier and externally modulated by a $LiNbO_3$ intensity modulator with a 1.25 Gb/s NRZ pseudorandom binary sequence (PRBS) of length 2^{31}-1. The signal power is -25.6 dBm after the TOF and 12.7 dBm after the EDFA. The measured downstream spectrum is shown in Figure 79(c). The downstream signal is then transmitted to the ONU through 17 km of DSF to counteract the effects of dispersion. The dispersion of this fiber is 1 ps/nm/km at 1538 nm. At the entrance of the feeder fiber, the measured signal power is 2.3 dBm. At the access node, a downstream PIN optical receiver with a 2 GHz bandwidth is used.

Back-to-back and downstream transmission eye diagrams are shown in Figure 81. We present two situations with two different kinds of feeder fiber. Figure 81(a) and (b) show the eye diagrams obtained for a back-to-back configuration and after transmission over 20

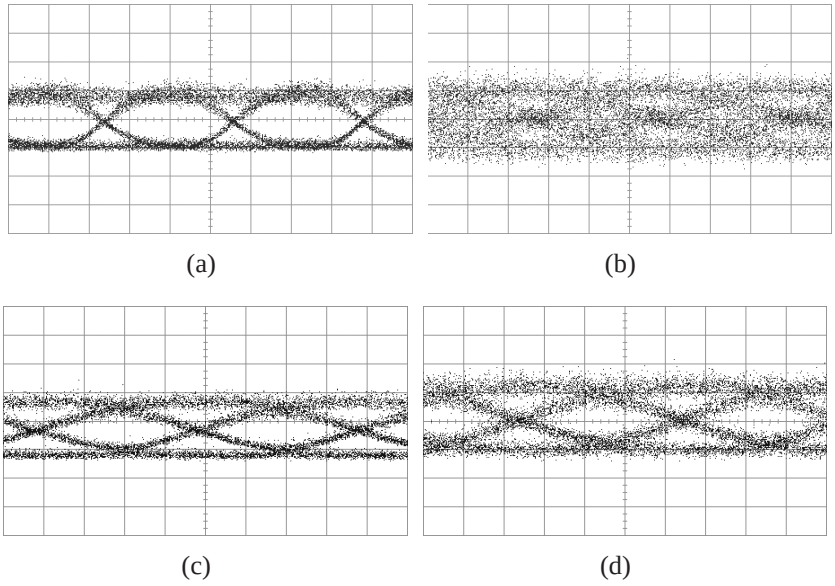

Figure 81: Eye diagrams measured for (a) back-to-back (500 ps/div) and (b) downstream transmission through 20 kms of SMF (500 ps/div) at a bit rate of 622 Mb/s. Eye diagrams for (c) back-to-back (200 ps/div) and (d) downstream transmission through 17 kms of DSF (200 ps/div) at a bit rate of 1.25 Gb/s.

km of conventional SMF-28 at a bit rate of 622 Mb/s. In this case, we can notice that the influence of dispersion is large. Figure 81(c) and (d) also show the eye patterns obtained in a back-to-back configuration and when we use 17 km of DSF at a bit rate of 1.25 Gb/s. We can easily observe the benefits of DSF: it overcomes the dispersion effect and consequently decreases the distortions. To investigate the system dependency on the distribution fiber between the OLT and the ONU in the case of downstream transmission through DSF, we inserted a variable attenuator before the optical receiver. The measured BER curves are presented in Figure 82. The curve obtained after transmission through 17 km of DSF reveals a power penalty of 1.1 dB at a BER of 10^{-9} when compared with the back-to-back case.

6.3 Future investigations

Compared to the PONs architectures employing many laser sources at the OLT, the proposed solution is more cost-effective since it replaces multiple fixed-wavelength lasers by

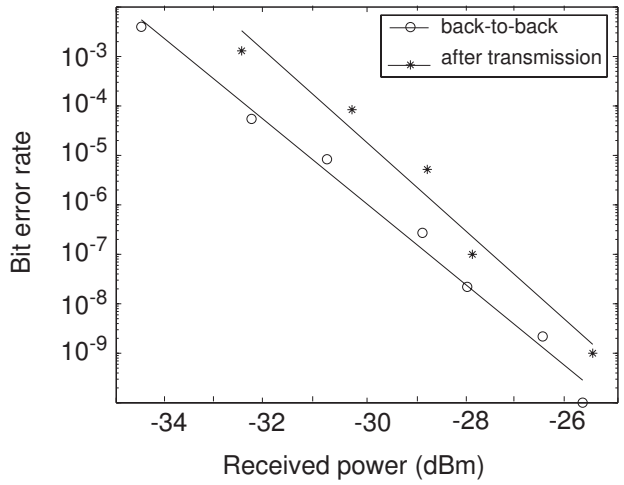

Figure 82: Measured bit-error-rate curves.

a simple multiwavelength fiber ring laser. It also implies less maintenance and less inventory. To the best of our knowledge, the use of an SOA-based multiwavelength fiber ring laser for WDM-PON is shown for the first time. We were able to transmit a 1.25 Gb/s signal per channel. However, to increase the bit rate or the transmission distance, the generated channel linewidth appears as a limitation of our system. Indeed, the transmission suffers from dispersion and so requires the use of DSF in our experiment. Reducing this linewidth would make it possible to transmit the signal through conventional SMF instead of DSF.

To reduce this linewidth, it seems necessary to investigate in more detail the non-linear effects in SOAs. Indeed, these non-linearities (especially gain-saturation, intrachannel FWM, and self-modulation) cause significant distortion and broadening. It has the effect of shifting the peak power toward longer wavelengths when light travels through this optical amplifier: a red shift is obtained [170, 171]. To counteract this fact, the study of the appropriate choice of filter (shape and bandwidth) to be used in the cavity to tailor the output wavelengths has to be conducted.

Our experimental results show that optimizing the cavity losses can result in a broader, more uniform spectrum. To improve the spectral flatness, a gain-equalizing filter can be added in the cavity. To further simplify the setup of the multiwavelength source, a single

uncoated SOA can be used to simultaneously provide both gain medium and comb filtering in the ring cavity [101].

This multiwavelength fiber ring laser could also be used as a centralized light source at the OLT for a low-cost implementation of a bidirectional WDM-PON. In this case, a solution can be to dedicate two specific wavelengths for each ONU. One wavelength will be modulated at the OLT for downstream transmission, whereas the other one will be delivered and modulated at the receiver side to provide upstream transmission [121]. It will thus lessen the wavelength management required at the ONU side.

A possible architecture consists of developing and integrating a new type of multiwavelength source into a WDM-PON to serve as one centralized source at the OLT to provide two kinds of services at the customer side, i.e., at the ONU. In the scheme represented in Figure 83, the future multiwavelength source will have two functionalities. The first one would be to provide basic "always on" downstream services. For each subscriber, a dedicated wavelength would be employed to send a downstream signal at 2.5 Gb/s and to be reused for an upstream signal at 100 Mb/s. A second functionality would be to allocate at anytime an extra dedicated "on-demand" wavelength for a customer requiring large upstream bandwidth on-demand to upgrade his services on the fly. In this situation, using the basic service with the 100 Mb/s upstream signal, a client could inform the OLT at anytime that he needs more upstream bandwidth to transmit more information in a short time. Then, upon receiving the request, the OLT could allocate an additional "on-demand" wavelength to the customer. This wavelength would be sent to the ONU to be used for upstream transmission at 2.5 Gb/s by this customer who has a need to upgrade his services.

The upgradability and scalability of the access networks are thus improved from a customer point of view. It would be a very marketable application of these new multiwavelength sources. The objective is to design, create, and demonstrate a new single and

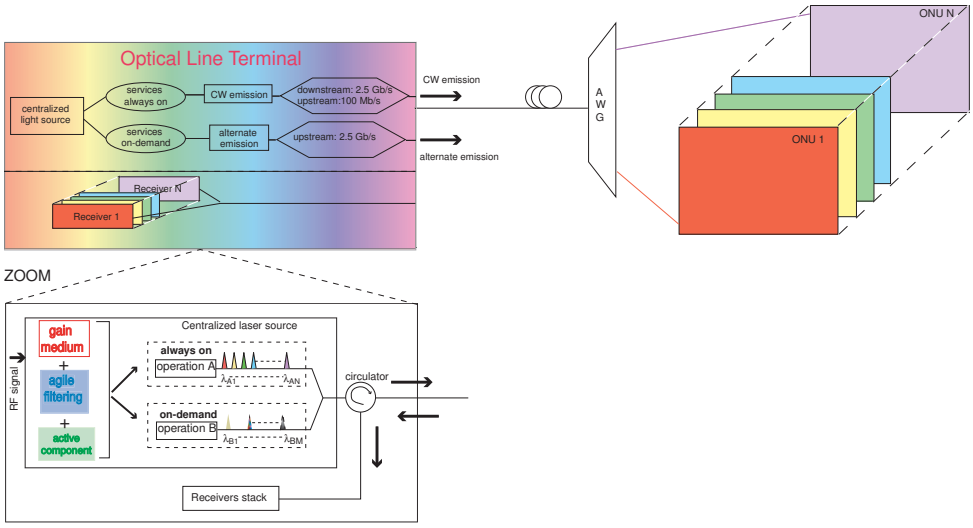

Figure 83: Proposed WDM-PON architecture with a new agile multiwavelength source (AWG: arrayed-waveguide grating).

low-cost source capable of providing this new type of flexible bandwidth service. Furthermore, this would be a new PON design featuring centralized multiwavelength light source generation. It would also dynamically generate alternate wavelengths based on bandwidth on-demand and selective wavelength allocation. This agile WDM-PON architecture leads to a higher level of capacity and resource utilization efficiency. We also focus on the use of one single fiber for both upstream and downstream transmissions to reduce the size and the complexity of the ONU.

6.4 Conclusions

We have proposed and experimentally investigated the use of an SOA-based multiwavelength fiber ring laser as a light source for a WDM-PON. This configuration has generated more than 40 wavelengths with 50-GHz spacing. In the proposed network, we have demonstrated error-free downstream transmission over 17 km of DSF at a bit rate of 1.25 Gb/s per channel and the power penalty at a BER of 10^{-9} is 1.1 dB. The high simplicity and cost-efficiency of this type of source make it suitable for applications in access networks. However, to increase the bit rate of transmission, the linewidth of the generated wavelengths has to be reduced.

CHAPTER 7

CONCLUSION

In the telecommunications market, companies and research groups always try to find and develop new cost-effective solutions to offer high-speed, reliable, secure, and scalable networks. Optical communication traffic for Internet services is expected to double every 9 months, the volume to reach petabit/sec throughput, and the access bandwidth for each user to grow from 100 Mb/s to 2.5 gigabit/sec in the near future. To unlock the available fiber capacity and to increase performances of actual networks, wavelength division multiplexing techniques have been investigated. There has been an intense dedication to the creation of new laser sources for such applications. In this context, multiwavelength fiber ring lasers present many advantages: simple structure, low-cost, and multiwavelength operation. Instead of using many different laser diodes, one simple and agile laser could replace them all. It implies more functions, less cost, less maintenance, and less inventory.

In this work, we focused on two different types of multiwavelength sources: an alternate multiwavelength picosecond pulsed EDFA-based laser and a continuous SOA-based source. In both cases, the chosen architecture was a fiber ring cavity.

In that framework, the first study focused on the conception and the design of a fiber laser emitting alternate multiwavelength pulse trains. The objective was to produce picosecond pulses in the 1550 nm region at GHz repetition rates. For such a source, two basic operations had to be implemented. First and foremost, pulses had to be generated: active mode-locking was used. Then, different wavelengths needed to be selected: tunable filtering was the chosen method. The originality of the source was to use only one key single device to implement both operations. It is an unbalanced Mach-Zehnder interferometer, inserted in an erbium-doped fiber laser. This laser could find a wide range of applications: for instance optical fiber sensors, optical instrument testing, spectroscopy, bi-dimensional optical CDMA codes, or photonic analog-to-digital conversion.

A theoretical study was made by using a circulating Gaussian pulse analysis. It was possible to predict the temporal and spectral pulsewidths of the generated laser output. We were also able to theoretically predict the evolution of the possible emitted wavelength as a function of time. This theoretical study was backed by numerical simulations, based on the split-step Fourier method. Light propagation through all the components of the ring cavity were modeled. The simulations qualitatively validated the functionality of the laser and provided guidelines to order the customized modulator.

Experimental results finally demonstrated the feasibility of this light source. Three 20 ps pulse trains were produced at three different wavelengths. The main problems of this source are its lack of control, handiness, and stability. For all these reasons, we also focused on the different improvements that can be made to this light source. By inserting a periodic filter and a conventional modulator in the cavity, a time-wavelength mapping is imposed on the laser output. We therefore control the wavelength and time spacings of the emitted pulses. To improve the stability of the laser, we developed a novel multi-harmonic phase modulation technique: it consists of mixing two harmonics of the fundamental frequency and driving a modulator with this signal. We also proposed many ways to improve the performances of this laser: increase of the number of wavelengths and pulse trains and reduction of the chirp or of the pulse duration.

The second source we studied is a continuous wave SOA-based fiber laser. We were able to produce over 40 wavelengths with 50-GHz spacing. The spacing was imposed by the periodic filter inserted in the cavity. This laser was investigated as a possible source for WDM passive optical network. In the architecture we proposed, we have demonstrated error-free downstream transmission over 17 km of DSF at a bit rate of 1.25 Gb/s per channel. The power penalty at a BER of 10^{-9} was 1.1 dB. This source presents two main advantages for applications in access networks: high simplicity and cost-efficiency. Moreover, when we lock one wavelength of the laser, all the other wavelengths are locked, contrary to a laser array where all individual sources have to be controlled separately.

The linewidth of the generated wavelengths was large, around 0.12 nm. To increase the bit rate or the transmission distance, this linewidth has to be decreased to reduce the effects of dispersion. To do so, it seems interesting to investigate the non-linear effects of the SOA in the ring cavity. By limiting the impact of dispersion in the fiber, SOA-based multiwavelength laser sources seems promising for future optical access networks. In the future, it will also be interesting to use this laser as a centralized light source at the central office for a low-cost implementation of a bidirectional WDM-PON. This might be a solution to relax the wavelength management required at the customer side. To further simplify and improve the set-up of the multiwavelength source, a single uncoated SOA can be used to simultaneously provide both gain medium and comb filtering in the ring cavity.

As a final conclusion, the proposed research crosses the boundary of two very large fields, namely, laser theory and optical Internet. There is a clear need to bring laser optics to the broadband access network for the integration of signal generation and networking, which provides a path towards gigabit Internet access systems. The integration of optics and photonics in optical Internet can have a broad impact in a number of areas in advanced science and engineering including petabit data transfer, distributed computing, interactive multi-media, and symmetric data applications. This work is a first step towards the integration of agile multiwavelength laser sources in future optical access networks.

REFERENCES

[1] www.internetworldstats.com, consulted on 01/23/06.

[2] www.point-topic.com, consulted on 01/23/06.

[3] www.mobiledia.com, consulted on 01/23/06.

[4] G. P. Agrawal, *Fiber-optic communication systems*. John Wiley and sons, 2002.

[5] B. Saleh and M. Teich, *Fundamentals of photonics*. John Wiley and sons, 1991.

[6] I. Joindot and M. Joindot, *Les télécommunications par fibres optiques*. Dunod, 1996.

[7] R. Ulrich, S. Rashleigh, and W. Eickhoff, "Bending induced birefringence in single-mode fibers," *Opt. Lett.*, vol. 5, pp. 273–275, 1980.

[8] G. P.Agrawal, *Nonlinear fiber optics*. Academic Press, second ed., 1995.

[9] J. A. Buck, *Fundamentals of optical fibers*. Wiley-Interscience, 1995.

[10] P. M. Gong, J. T. Hsieh, S. L. Lee, and J. Wu, "Theoretical analysis of wavelength conversion based on four-wave mixing in light-holding SOAs," *IEEE J. Quantum Electron.*, vol. 40, no. 1, pp. 31–40, 2004.

[11] C. S. Wong and H. K. Tsang, "Polarization-independant time-division demultiplexing using orthogonal-pumps four-wave mixing," *IEEE Photon. Technol. Lett.*, vol. 15, no. 1, pp. 129–131, 2003.

[12] C. J. Koestner and E. A. Snitzer, "Amplification in a fibre laser," *Applied Optics*, vol. 3, pp. 1182–1187, 1964.

[13] P. Urquhart, "Review on rare earth doped fibre lasers and amplifiers," in *IEE Proceedings*, vol. 135, pp. 385–407, 1988.

[14] E. Desurvire, *Erbium-Doped Fiber Amplifiers, Principles and Applications*. Wiley-Interscience, 2002.

[15] J. Lee, U. C. Ryu, S. J. Ahn, and N. Park, "Enhancement of power conversion efficiency for an L-band EDFA with a secondary pumping effect in the unpumped EDF section," *IEEE Photon. Technol. Lett.*, vol. 11, pp. 42–44, 1999.

[16] M. Tachibana, R. Laming, P. R. Morkel, and D. Payne, "Erbium-doped fiber amplifier with flattened gain spectrum," *IEEE Photon. Technol. Lett.*, vol. 3, pp. 118–120, 1991.

[17] S. Namiki and Y. Emori, "Ultrabroad-band raman amplifiers pumped and gain-equalized by wavelengrh-division-multiplexed high-power laser diodes," *IEEE Journal of Selected Topics in Quantum Electronics*, vol. 7, no. 1, pp. 3–16, 2001.

[18] R. H. Stolen and E. P. Ippen, "Raman gain in glass optical waveguides," *Appl. Phys. Lett.*, vol. 22, pp. 276–278, 1973.

[19] M. Connelly, *Semiconductor optical amplifiers*. Prentice Hall, first ed., 2002.

[20] I. Armstrong, I. Andonovic, and A. Kelly, "Semiconductor optical amplifiers: performance and applications in optical packet switching," *Journal of Optical Networking*, vol. 3, no. 12, pp. 882–897, 2004.

[21] A. E. Siegman, *Lasers*. University science books, 1986.

[22] J. T. Verdeyen, *Laser electronics*. Prentice Hall, third ed., 1995.

[23] A. Schawlow and C. H. Townes, "Infrared and optical masers," *Physical Review*, vol. 112, pp. 1940–1949, 1958.

[24] T. Maiman, "Stimulated optical radiation in ruby," *Nature*, vol. 187, pp. 493–494, 1960.

[25] G. A. Ball and W. W. Morey, "Compressive-tuned single-frequency Bragg fiber laser," *Opt. Lett.*, vol. 19, no. 23, pp. 1979–1981, 1994.

[26] A. Bellemare, M. Karasek, C. Riviere, F. Babin, G. He, V. Roy, and G. W. Schinn, "A broadly tunable erbium-doped fiber ring laser: experimentation and modeling," *IEEE Journal of Selected Topics in Quantum Electronics*, vol. 7, no. 1, pp. 22–29, 2001.

[27] N. H. Seong and D. Y. Kim, "A new figure-eight fiber laser based on a dispersion-imbalanced nonlinear optical loop mirror with lumped dispersive elements," *IEEE Photon. Technol. Lett.*, vol. 14, no. 4, pp. 459–461, 2002.

[28] D. Foursa, P. Emplit, R. Leners, and L. Meuleman, "18 GHz from a σ-cavity Er-fibre laser with dispersion management and rational harmonic active mode-locking," *Electron. Lett.*, vol. 33, no. 6, pp. 486–488, 1997.

[29] L. Zenteno, "High-power double-clad fiber lasers," *Journal of Lightwave Technology*, vol. 11, no. 9, pp. 1435–1446, 1993.

[30] J. Nilsson, S. U. Alam, J. A. Alvarez-Chavez, P. W. Turner, W. A. Clarkson, and A. B. Grudinin, "High-power and tunable operation od erbium-ytterbium co-doped cladding-pumped fiber lasers," *IEEE J. Quantum Electron.*, vol. 39, no. 8, pp. 987–994, 2003.

[31] L. A. Zenteno and D. T. Walton, "Novel fiber lasers and applications," *Optics and* & *Photonics News*, pp. 38–41, 2003.

[32] T. King, "Medical fiber lasers and example application to laser nerve stimulation," *Lasers and Electro-Optics Society Annual Meeting*, vol. 1, p. 307, 2002.

[33] R. J. Bussjager, M. J. Hayduk, S. T. Johns, and E. W. Taylor, "Comparison of radiation-induced pasive and dynamic responses in two erbium-doped fiber lasers," *IEEE Aerospace Conference Proceedings*, vol. 3, pp. 1369–1379, 2002.

[34] M. Suzuki, H. Tanaka, N. Edagawa, K. Utaka, and Y. Matsushima, "Transform-limited optical pulse generation up to 20-GHz repetition rate by a sinusoidally driven InGaAsP electroabsorption modulator ," *Journal of Lightwave Technology*, vol. 11, no. 3, pp. 468–473, 1993.

[35] K. Wakita, K. Sato, I. Kotaka, M. Yamamot, and M. Asobe, "Transform-limited 7-ps optical pulse generation using a sinusoidally driven InGaAsP/InGaAsP strained multiple-quantum-well DFB laser/modulator monolithically integrated light source," *IEEE Photon. Technol. Lett.*, vol. 5, no. 8, pp. 899–901, 1993.

[36] H. Tanaka, M. Suzuki, and Y. Matsushima, "Optical short pulse generation by a DFB laser/EA modulator integrated light source ," *IEEE J. Quantum Electron.*, vol. 29, no. 6, pp. 1708–1713, 1993.

[37] H. F. Liu, S. Oshiba, Y. Ogawa, and Y. Kawai, "Method of generating nearly transform-limited pulses from gain-switched distributed-feedback laser diodes and its application to soliton transmission," *Opt. Lett.*, vol. 17, no. 1, pp. 64–66, 1992.

[38] W. Wang, K. L. Lee, C. Shu, and K. T. Chan, "Multiwavelength self-seeded Fabry-Perot laser with subharmonic pulse-gating for two-dimensional fiber optic-CDMA," *IEEE Photon. Technol. Lett.*, vol. 13, no. 12, pp. 1361–1363, 2001.

[39] A. Yariv, *Optical electronics in modern communications*. Oxford University Press, 1997.

[40] D. J. Kuizenga and A. E. Siegman, "FM and AM mode-locking of the homogeneous laser - part I," *IEEE J. Quantum Electron.*, no. 11, pp. 694–708, 1970.

[41] J. J. O'Neil, J. N. Kutz, and B. Sandstede, "Theory and simulation of the dynamics and stability of actively modelocked lasers," *IEEE J. Quantum Electron.*, vol. 38, pp. 1412–1419, October 2002.

[42] H. A. Haus, "A theory of forced mode locking," *IEEE J. Quantum Electron.*, no. 7, pp. 323–330, 1975.

[43] Y. Silberberg, P. W. Smith, D. J. Eilenberger, D. A. B. Miller, A. C. Gossard, and W. Wiegmann, "Passive modelocking of a semiconductor laser diode," *Opt. Lett.*, vol. 9, pp. 507–509, 1984.

[44] U. Keller, K. J. Weingarten, F. X. Kärtner, D. Kopf, B. Braun, I. D. Jung, R. Fluck, C. Hönninger, N. Matuschek, and J. A. der Au, "Semiconductor saturable absorber mirrors (SESAM's) for femtosecond to nanosecond pulse generation in solid-state

lasers," *IEEE Journal of Selected Topics in Quantum Electronics*, vol. 2, no. 3, pp. 435–453, 1996.

[45] D. E. Spence, P. N. Kean, and W. Sibbett, "60-fsec pulse generation from a mode-locked Ti:sapphire laser," *Opt. Lett.*, vol. 16, pp. 42–44, 1991.

[46] M. Horowitz, C. R. Menyuk, T. F. Carruthers, and I. N. D. III, "Theoretical and experimental study of harmonically modelocked fiber lasers for optical communication systems," *Journal of Lightwave Technology*, vol. 18, no. 11, pp. 1565–1574, 2000.

[47] O. Pottiez, O. Deparis, R. Kiyan, M. Haelterman, P. Emplit, P. Mégret, and M. Blondel, "Supermode noise of harmonically mode-locked erbium fiber lasers with composite cavity," *IEEE J. Quantum Electron.*, vol. 38, no. 3, pp. 252–259, 2002.

[48] G. T. HArvey and L. F. Mollenauer, "Harmonically mode-locked fiber ring laser with an internal Fabry-Perot stabilizer for soliton transmission," *Opt. Lett.*, vol. 18, pp. 107–109, 1994.

[49] T. Yilmaz, C. M. Depriest, A. Braun, J. H. Abeles, and P. J. Delfyett, "Noise in fundamental and harmonic modelocked semiconductor lasers: experiments and simulations," *IEEE J. Quantum Electron.*, vol. 39, pp. 838–849, 2003.

[50] K. K. Gupta, N. Onodera, and M. Hyodo, "Technique to generate equal amplitude, higher-order optical pulses in rational harmonically modelocked fibre ring laser," *Electron. Lett.*, vol. 37, no. 15, pp. 948–950, 2001.

[51] S. Li, C. Lou, and K. T. Chan, "Rational harmonic active and passive modelocking in a figure-of-eight fibre laser," *Electron. Lett.*, vol. 34, no. 4, pp. 375–376, 1998.

[52] Alcatel, "Fiber-to-the-user: the ultimate endgame," tech. rep., White paper, 2005.

[53] Alcatel, "How much bandwidth is enough?," tech. rep., White paper, 2005.

[54] www.ponforum.org, consulted on 07/13/05.

[55] G. Kramer, *Ethernet passive optical networks*. McGraw-Hill Professional, 2005.

[56] www.fsanweb.org/initiative.asp, consulted on 07/15/05.

[57] M. Klimek, "ATM passive optical network," *Alcatel Telecommunications Review*, pp. 258–261, 2000.

[58] G. Kramer and G. Pesavento, "Ethernet passive optical network (EPON): building a next-generation optical access network," *IEEE Communications Magazine*, pp. 66–73, 2002.

[59] X. Z. Qiu, P. Ossieur, J. Bauwelinck, Y. Yi, D. Verhulst, J. Vandewege, B. D. Vos, and P. Solina, "Development of GPON upstream physical-media-dependent prototypes," *Journal of Lightwave Technology*, vol. 22, no. 11, pp. 2498–2508, 2004.

[60] K. Iwatsuki, J. I. Kani, H. Suzuki, and M. Fujiwara, "Access and metro networks based on WDM technologies," *Journal of Lightwave Technology*, vol. 22, no. 11, pp. 2623–2630, 2004.

[61] F. T. An, K. S. Kim, D. Gutierrez, S. Yam, E. Hu, K. Shrikhande, and L. G. Kazovsky, "SUCCESS: a next generation hybrid WDM/TDM optical access network architecture," *Journal of Lightwave Technology*, vol. 22, no. 11, pp. 2557–2569, 2004.

[62] H. Kim, S. Kang, and C. Lee, "A low-cost WDM source with an ASE injected Fabry-Perot semiconductor laser," *IEEE Photon. Technol. Lett.*, vol. 12, no. 8, pp. 1067–1069, 2000.

[63] S. M. Lee, K. M. Choi, S. G. Mun, J. H. Moon, and C. H. Lee, "Dense WDM-PON based on wavelength-locked Fabry-Perot laser diodes," *IEEE Photon. Technol. Lett.*, vol. 17, no. 7, pp. 1579–1581, 2005.

[64] S. Murata, I. Mito, and K. Kobayashi, "Spectral characteristics for a 1.5 μm DBR laser with frequency tuning region," *IEEE J. Quantum Electron.*, vol. 23, no. 6, pp. 836–838, 1987.

[65] Y. Tohmori, Y. Yoshikuni, H. Ishii, F. Kano, T. Tamamura, and Y. Kondo, "Over 100 nm wavelength tuning in superstructure grating (SSG) DBR lasers," *Electron. Lett.*, vol. 29, no. 4, pp. 352–354, 1993.

[66] C. J. Chang-Hasnain, "Tunable VCSEL," *IEEE Journal of Selected Topics in Quantum Electronics*, vol. 6, no. 6, pp. 978–987, 2000.

[67] J. L. Zyskind, J. W. Sulhoff, J. Stone, D. J. Digiovanni, L. W. Stulz, H. B. Presby, A. Piccirilli, and P. E. Pramayon, "Electronically tunable, diode-pumped erbium-doped fibre ring laser with fibre Fabry-Perot etalon," *Electron. Lett.*, vol. 27, no. 21, pp. 1950–1951, 1991.

[68] Y. T. Chieng and R. A. Minasian, "Tunable erbium-doped fiber laser with a reflection Mach-Zehnder interferometer," *IEEE Photon. Technol. Lett.*, vol. 6, no. 2, pp. 153–156, 1994.

[69] D. Smith, M. W. Maeda, J. J. Johnson, J. S. Patel, M. A. Saifi, and A. V. Lehman, "Acoustically tuned erbium-doped fiber ring laser," *Opt. Lett.*, vol. 16, pp. 387–389, 1991.

[70] Y. G. Han, G. Kim, J. H. Le, S. H. Kim, and S. B. Lee, "Lasing wavelength and spacing switchable multiwavelength fiber laser from 1510 to 1620 nm," *IEEE Photon. Technol. Lett.*, vol. 17, pp. 989–991, 2005.

[71] J. Sun, "Multiwavelength ring lasers employing semiconductor optical amplifiers as gain media," *Microwave and Optical Technology Letters*, vol. 43, pp. 301–303, 2004.

[72] K. Vlachos, C. Bintjas, N. Pleros, and H. Avramopoulos, "Ultrafast semiconductor-based fiber laser sources," *IEEE Journal of Selected Topics in Quantum Electronics*, vol. 10, pp. 147–154, 2004.

[73] J. Yao, J. Yao, and Z. Deng, "Multiwavelength actively mode-locked fiber ring laser with suppressed homogeneous line broadening and reduced supermode noise," *IEEE Journal of Selected Topics in Quantum Electronics*, vol. 10, pp. 147–154, 2004.

[74] E. D. Park, T. J. Croeze, P. J. Delfyett, A. Braun, and J. Abeles, "Multiwavelength mode-locked InGaAsP laser operating at 12 ch x 2 GHz and 16 ch x 10 GHz," *IEEE Photon. Technol. Lett.*, vol. 14, no. 6, pp. 837–839, 2002.

[75] J. N. Maran, S. LaRochelle, and P. Besnard, "Erbium-doped fiber laser simultaneously mode locked on more than 24 wavelengths at room temperature," *Opt. Lett.*, vol. 28, no. 21, pp. 2082–2084, 2003.

[76] G. E. Town, L. Chen, and P. W. E. Smith, "Dual wavelength modelocked fiber laser," *IEEE Photon. Technol. Lett.*, vol. 12, no. 11, pp. 1459–1461, 2000.

[77] K. L. Lee, C. Shu, and H. F. Liu, "Subharmonic pulse-gating in self-seeded laser diodes for time- and wavelength-interleaved picosecond generation," *IEEE J. Quantum Electron.*, vol. 40, no. 3, pp. 205–213, 2004.

[78] T.-P. Lee, C. Zah, R. Bhat, W. Young, B. Pathak, F. Favire, P. Lin, N. Andreadakis, C. Caneau, A. W. Rahjel, M. Koza, J. K. Gamelin, L. Curtis, D. D. Mahoney, and A. Lepore, "Multiwavelength DFB laser array transmitters for ONTC reconfigurable optical network testbed," *Journal of Lightwave Technology*, vol. 14, no. 6, pp. 967–976, 1996.

[79] S. L. Lee, I. F. Jang, C. Y. Wang, C. T. Pien, and T. T. Shih, "Monolithically integrated multiwavelength sampled grating DBR lasers for dense WDM applications," *IEEE Journal of Selected Topics in Quantum Electronics*, vol. 6, no. 1, pp. 197–206, 2000.

[80] C. Zah, M. R. Amersfoort, B. N. Pathak, F. J. Favire, P. Lin, N. C. Andreadakis, A. Rajhel, R. Bhat, C. Caneau, M. A. Koza, and J. Gamelin, "Multiwavelength DFB laser arrays with integrated combiner and optical amplifier for WDM optical networks," *IEEE Journal of Selected Topics in Quantum Electronics*, vol. 3, no. 2, pp. 584–597, 1997.

[81] H. Takara, T. Ohara, K. Mori, K. Sato, E. Yamada, Y. Inoue, T. SHibata, M. Abe, t. Morioka, and K.-I. Sato, "More than 1000 channel optical frequency chain generation from single supercontinuun source with 12.5 GHz channel spacing," *Electron. Lett.*, vol. 36, no. 25, p. 2089, 2000.

[82] Y. Nan, C. Lou, J. Wang, L. Huo, and Y. Yang, "Improving the performance of a multiwavelength continuous-wave optical source based on supercontinuum by suppressing degenerate four-wave mixing," *Opt. Commun.*, vol. 256, pp. 428–434, 2005.

[83] T. Morioka, K. Mori, and M. Saruwatari, "More than 100-wavelength-channel picosecond optical pulse generation from single laser source using supercontinuum in optical fibres," *Electron. Lett.*, vol. 29, no. 10, pp. 862–864, 1993.

[84] K. H. Han, E. S. Son, H. Y. Choi, K. W. Lim, and Y. C. Chung, "Bidirectional WDM-PON using light emitting diodes spectrum-sliced with cyclic arrayed-waveguide grating," *IEEE Photon. Technol. Lett.*, vol. 16, pp. 2380–2382, 2004.

[85] M. Mielke, G. A. Alphonse, and P. J. Delfyett, "168 x 6GHz from a multiwavelength mode-locked semi-conductor laser," *IEEE Photon. Technol. Lett.*, vol. 15, no. 4, pp. 501–503, 2003.

[86] F. Tong, W. Jin, D. Wang, and P. Wai, "Multiwavelength fibre laser with wavelength selectable from 1590 to 1645 nm," *Electron. Lett.*, vol. 40, no. 10, pp. 594–595, 2004.

[87] H. Dong, g. Zhu, Q. Wang, H. Sun, N. Dutta, J. Jaques, and A. Piccirilli, "Multi-wavelength fiber ring laser source based on a delayed interferometer," *IEEE Photon. Technol. Lett.*, vol. 17, no. 2, pp. 303–305, 2005.

[88] S.-H. Jeong, S. Matsuo, T. Segawa, H. Okamoto, Y. Kawaguchi, Y. Kondo, and H. Suzuki, "Stable and fast 100 GHz-spaced 30-channel digitally tunable operation in monolithically integrated semiconductor laser employing chirped ladder filter," *Electron. Lett.*, vol. 41, no. 21, pp. 1176–1178, 2005.

[89] A. Bellemare, M. Karásek, M. Rochette, S. LaRochelle, and M. Têtu, "Room temperature multifrequency erbium-doped fiber lasers anchored on the ITU frequency grid," *Journal of Lightwave Technology*, vol. 18, no. 6, pp. 825–830, 2000.

[90] K. I. Kitayama and Y. Awaji, "Optical pulse train generation with use of fiber-optic frequency comb generator and waveguide spectrum synthesizer," *Conference on Lasers and Electro-Optics*, p. 135, 1997.

[91] X. Yang, X. Dong, S. Zhang, F. Lu, X. Zhou, and C. Lu, "Multiwavelength erbium-doped fiber laser with 0.8-nm spacing using sampled Bragg grating and photonic crystal fiber," *IEEE Photon. Technol. Lett.*, vol. 17, no. 12, pp. 2538–2540, 2005.

[92] L. R. Chen, "Tunable multiwavelength fiber ring lasers using a programmable high-birefringence fiber loop mirror," *IEEE Photon. Technol. Lett.*, vol. 16, no. 2, pp. 410–412, 2004.

[93] S. Hu, L. Zhan, Y. J. Song, W. Li, S. Y. Luo, and Y. X. Xia, "Switchable multiwavelength erbium-doped fiber ring laser with a multisection high-birefringence fiber loop mirror," *IEEE Photon. Technol. Lett.*, vol. 17, pp. 1387–1389, 2005.

[94] C. S. Kim, F. N. Farokhrooz, and J. U. Kang, "Electro-optic wavelength-tunable fiber ring laser based on cascaded composite Sagnac filters," *Opt. Lett.*, vol. 29, no. 14, pp. 1677–1679, 2004.

[95] G. Das and J. W. Y. Lit, "Multiwavelength fiber laser using a Sagnac loop filter," *Microwave and Optical Technology Letters*, vol. 36, no. 3, pp. 200–202, 2003.

[96] N. Park and P. F. Wysocki, "24-line multiwavelength operatio of erbium-doped fiber-ring laser," *IEEE Photon. Technol. Lett.*, vol. 8, no. 11, pp. 1459–1461, 1996.

[97] T. Chartier, A. Mihaescu, G. Martel, A. Hideur, and F. Sanchez, "Multiwavelength fiber laser with an intracavity polarizer," *Opt. Commun.*, vol. 253, pp. 352–361, 2005.

[98] M. Karásek and A. Bellemare, "Numerical analysis of multifrequency erbium-doped fibre ring laser employing periodic filter and frequency shifter," *IEE Proc.-Optoelectron.*, vol. 147, no. 2, pp. 115–119, 2000.

[99] S. Yamashita and K. Hatate, "Multiwavelength erbium-doped fibre laser using intracavity etalon and cooled liquid nitrogen," *Electron. Lett.*, vol. 32, no. 14, pp. 1298–1299, 1996.

[100] O. Graydon, W. H. Loh, R. L. Laming, and L. Dong, "Triple-frequency operation of an Er-doped twincore fiber loop laser," *IEEE Photon. Technol. Lett.*, vol. 8, no. 1, pp. 63–65, 1996.

[101] N. Pleros, T. Houbavlis, G. Theophilopoulos, K. Vlachos, C. Bintjas, and H. Avramopoulos, "SOA-based multiwavelength laser sources," *Fiber and Integrated Optics*, vol. 23, pp. 263–274, 2004.

[102] D. N. Wang, F. W. Tong, X. Fang, W. Jin, P. K. A. Wai, and J. M. Gong, "Multiwavelength erbium-doped fiber ring laser source with a hybrid gain medium," *Opt. Commun.*, vol. 228, pp. 295–301, 2003.

[103] P.-C. Peng, K.-M. Feng, C.-C. Chang, H.-Y. Chiou, J.-H. Chen, M.-F. Huang, H.-C. Chien, and S. Chi, "Multiwavelength fiber laser using S-band erbium-doped fiber amplifier and semiconductor optical amplifier," *Opt. Commun.*, vol. 259, pp. 200–203, 2006.

[104] Y.-G. Han, T. V. A. Tran, S.-H. Kim, and S. B. Lee, "Development of a multiwavelength Raman fiber laser based on phase-shifted fiber Bragg gratings for long-distance remote-sensing applications," *Opt. Lett.*, vol. 30, no. 10, pp. 1114–1116, 2005.

[105] J.-M. Kang, H.-C. Kwon, S.-H. Lee, and S.-K. Han, "A single to multi-wavelength converter using Fabry-Perot laser diode with linear optical amplifer and its applications to the wavel;ength division multiplexing-passive optical network system," *Opt. Commun.*, vol. 254, pp. 223–235, 2005.

[106] K. K. Qureshi, H. Y. Tam, W. H. Chung, and P. K. A. Wai, "Multiwavelength laser source using linear optical amplifier," *IEEE Photon. Technol. Lett.*, vol. 17, no. 8, pp. 1611–1613, 2005.

[107] S. Li and K. T. Chan, "Electrical wavelength tunable and multiwavelength actively mode-locked fiber ring laser," *Appl. Phys. Lett.*, vol. 72, no. 16, pp. 1954–1956, 1998.

[108] S. Pan and C. Lou, "Multiwavelength pulse generation using an actively mode-locked erbium-doped fiber ring laser based on distributed dispersion cavity," *IEEE Photon. Technol. Lett.*, vol. 18, no. 4, pp. 592–594, 2006.

[109] K. L. Lee and C. Shu, "Alternate and simultaneous generation of 1-GHz dual-wavelength pulses from an electrically tunable harmonically mode-locked fiber laser," *IEEE Photon. Technol. Lett.*, vol. 12, no. 6, pp. 624–626, 2000.

[110] L. R. Chen, G. E. Town, R.-Y. Cortès, S. LaRochelle, and P. W. E. Smith, "Dual-wavelength, actively mode-locked fibre laser with 0.7 nm wavelength spacing," *Electron. Lett.*, vol. 36, no. 23, pp. 1921–1923, 2000.

[111] H. Okamura and K. Iwatsuki, "Simultaneous oscillation of wavelength-tunable, singlemode lasers using an Er-doped fibre amplifier," *Electron. Lett.*, vol. 28, no. 5, pp. 461–463, 1992.

[112] C. Porzi, L. Poti, and A. Bogoni, "Tunable dual-wavelength mode-locked optical source," *Lasers and Electro-Optics Society Annual Meeting*, vol. 2, pp. 479–480, 2003.

[113] D. N. Wang and C. Shu, "Multiple optical paths in a self-seeding scheme for multiwavelength short pulse generation," *Appl. Phys. Lett.*, vol. 71, no. 10, pp. 1305–1307, 1997.

[114] O. Deparis, R. Kiyan, E. Salik, D. Starodubov, J. Feinberg, O. Pottiez, P. Mégret, and M. Blondel, "Round-trip time and dispersion optimization in a dual-wavelength actively mode-locked Er-doped fiber laser including nonchirped fiber Bragg gratings," *IEEE Photon. Technol. Lett.*, vol. 11, no. 10, pp. 1238–1240, 1999.

[115] J. W. Lou, T. F. Carruthers, and M. Curie, "4x10 GHz mode-locked multiple-wavelength fiber laser," *IEEE Photon. Technol. Lett.*, vol. 16, no. 1, pp. 51–53, 2004.

[116] J. van Howe, J. Hansryd, and C. Xu, "Multiwavelength pulse generator using time-lens compression," *Opt. Lett.*, vol. 29, no. 13, pp. 1470–1472, 2004.

[117] R. D. Feldman, e. E. Harstead, S. jaing, T. H. Wood, and M. Zirngibl, "An evaluation of architectures incorporating wavelength division multiplexing for broad-band fiber access," *Journal of Lightwave Technology*, vol. 16, pp. 1546–1559, 1998.

[118] P. Iannone, N. Frigo, and K. Reichmann, "Enhanced privacy in broadcast passive optical networks through the use of spectral slicing in waveguide grating routers," *IEEE Photon. Technol. Lett.*, vol. 9, no. 7, pp. 1044–1046, 1997.

[119] J. Prat, V. Polo, C. Bock, C. Arellano, and J. V. Olmos, "Full-duplex single fiber transmission using FSK downstream and IM remote upstream modulations for Fiber-to-the-Home," *IEEE Photon. Technol. Lett.*, vol. 17, no. 3, pp. 702–704, 2005.

[120] W. Hung, C.-K. Chan, L.-K. Chen, and F. Tong, "An optical network unit for WDM access networks with downstream DPSK and upstream remodulated OOK data using injection-locked FP laser," *IEEE Photon. Technol. Lett.*, vol. 15, no. 10, pp. 1476–1478, 2003.

[121] O. Akanbi, J. Yu, and G. K. Chang, "A New Scheme for Bidirectional WDM-PON Using Upstream and Downstream Channels Generated by Optical Carrier Suppression and Separation Technique," *IEEE Photon. Technol. Lett.*, vol. 18, no. 2, pp. 340–342, 2006.

[122] P. Healey, P. Townsend, c. Ford, L. Johnston, P. Townley, I. Lealman, L. Rivers, S. Perrin, and R. Moore, "Spectral-slicing WDM-PON using wavelength-seeded reflective SOAa," *Electron. Lett.*, vol. 37, no. 19, pp. 1181–1182, 2001.

[123] H. Shin, J. Lee, I. Yun, S. Kim, H. Kim, H. Shin, S. Hwang, Y. Oh, K. Oh, and C. Shim, "Reflective SOAs optimized for 1.25 Gbit/s WDM-PONs," *Lasers and Electro-Optics Society Annual Meeting*, vol. 1, pp. 308–309, 2004.

[124] J.-M. Kang and S.-K. Han, "A novel hybrid WDM/SCM-PON sharing wavelength for up- and down-link using reflective semiconductor optical amplifier," *IEEE Photon. Technol. Lett.*, vol. 18, no. 3, pp. 502–504, 2006.

[125] J. Prat, C. Arellano, V. Polo, and C. Bock, "Optical network unit based on a bidirectional reflective semiconductor optical amplifier for Fiber-to-the-Home networks," *IEEE Photon. Technol. Lett.*, vol. 17, no. 1, pp. 250–251, 2005.

[126] J. A. Salehi, "Code Division Multiple Access Techniques in Optical Fiber Networks-Part 1: Fundamental Principles," *IEEE Transactions on Communications*, vol. 37, no. 8, pp. 824–833, 1989.

[127] A. Yariv and R. G. M. P. Koumans, "Time interleaved optical sampling for ultrahigh speed A/D conversion," *Electron. Lett.*, vol. 34, no. 21, pp. 2012–2013, 1998.

[128] J. Vasseur, M. Hanna, J. Dudley, J.-P. Goedgebuer, J. Yu, G.-K. Chang, and J. R. Barry, "Alternate multiwavelength picosecond pulse generation by use of an unbalanced Mach-Zehnder interferometer in a modelocked fiber ring laser," *IEEE J. Quantum Electron.*, vol. submitted, 2006.

[129] A. Olsson and C. L. Tang, "Time-wavelength multiplexing of mode-locked external-cavity semiconductor lasers," *IEEE J. Quantum Electron.*, vol. 18, no. 11, pp. 1982–1983, 1982.

[130] S. Yegnanarayanan, A. Bhushan, and B. Jalali, "Fast Wavelength-Hopping Time-spreading Encoding/Decoding for Optical CDMA," *IEEE Photon. Technol. Lett.*, vol. 12, no. 5, pp. 573–575, 2000.

[131] S. S. Min, H. Yoo, and Y. H. Won, "Time-wavelength hybrid optical CDMA system with tunable encoder/decoder using switch and fixed delay-line," *Opt. Commun.*, vol. 216, pp. 335–342, 2003.

[132] K. Yu, J. Shin, and N. Park, "Wavelength-time spreading optical CDMA system using wavelength multiplexers and mirrored fiber delay lines," *IEEE Photon. Technol. Lett.*, vol. 12, no. 9, pp. 1278–1280, 2000.

[133] L. R. Chen, "Flexible fiber Bragg grating encoder/decoder for hybrid wavelength-time optical CDMA," *IEEE Photon. Technol. Lett.*, vol. 13, no. 11, pp. 1233–1235, 2001.

[134] S. Kim, K. Yu, and N. Park, "A new family of space/wavelength/time spread three-dimensional optical code for OCDMA networks," *Journal of Lightwave Technology*, vol. 18, no. 4, pp. 502–511, 2000.

[135] T. Clark, J. Kang, and R. Esman, "Performance of a time and wavelength-interleaved photonic sampler for analog-to-digital conversion," *IEEE Photon. Technol. Lett.*, vol. 11, no. 9, pp. 1168–1170, 1999.

[136] K. L. Lee, C. Shu, and H. F. Liu, "10 Gsample/s photonic analog-to-digital converter constructed using 10-wavelength jitter-suppressed sampling pulses from a self-seeded laser diode," *Conference on Lasers and Electro-Optics*, pp. 67–68, 2001.

[137] M. P. Fok, K. L. Lee, and C. Shu, "4x25 GHz repetitive photonic sampler for high-speed analog-to-digital signal conversion," *IEEE Photon. Technol. Lett.*, vol. 16, no. 3, pp. 876–878, 2004.

[138] Z. G. Lu, F. G. Sun, G. Z. Xiao, and C. P. Grover, "A tunable multiwavelength fiber ring laser for measuring polarization-mode dispersion in optical fibers," *IEEE Photon. Technol. Lett.*, vol. 16, no. 1, pp. 60–62, 2004.

[139] U. Sharma, C. S. Kim, and J. U. Kang, "Highly stable tunable dual-wavelength Q-switched fiber laser for DIAL applications," *IEEE Photon. Technol. Lett.*, vol. 16, no. 5, pp. 1277–1279, 2004.

[140] H. B. Yu, W. Jin, Y. B. Liao, G. Stewart, B. Culshaw, H. L. Ho, and Y. H. Li, "A novel fiber-optic intra-cavity sensing network using a mode-locked fiber ring laser," *Optical Fiber Sensors Conference*, pp. 507–510, 2002.

[141] Y. W. Shi, K. Ito, Y. Matsuura, and M. Miyagi, "Multiwavelength laser light transmission of hollow optical fiber from the visible to the mid-infrared," *Opt. Lett.*, vol. 30, no. 21, pp. 2867–2869, 2005.

[142] J. Vasseur, M. Hanna, J. M. Dudley, and J. R. Barry, "Numerical and theoretical analysis of an alternate multiwavelength mode-locked fiber laser," *IEEE Photon. Technol. Lett.*, vol. 17, no. 11, pp. 2295–2297, 2005.

[143] B. R. Washburn and N. R. Newbury, "Phase, timing, and amplitude noise on supercontinua generated in microstructure fiber," *Optics Express*, vol. 12, no. 10, pp. 2166–2175, 2004.

[144] D. von der Linde, "Characterization of the noise in continuously operating modelocked lasers," *Applied Physics B*, vol. 39, pp. 201–217, 1986.

[145] H. P. Weber, "Method for pulse width measurement for ultrashort light pulses generated by phase locked lasers using nonlinear optics," *Journal of Applied Physics*, vol. 38, pp. 2231–2234, 1967.

[146] R. Trebino, *Frequency-resolved optical gating: the measurement of ultrashort optical pulses*. Kluwer, 2002.

[147] J. Vasseur, M. Hanna, J. Dudley, and J. P. Goedgebuer, "Alternate multiwavelength modelocked fiber laser," *IEEE Photon. Technol. Lett.*, vol. 16, no. 8, pp. 1816–1818, 2004.

[148] B. Hitz, "Mode-locked fiber laser emits simultaneous pulse trains at three wavelengths," *Photonics Spectra*, October 2004.

[149] J. Vasseur, M. Hanna, J. Dudley, J. yu, j. R. Barry, and G. K. Chang, "Numerical and experimental study of an alternate multiwavelength mode-locked fiber ring laser," *Optical Fiber Communication Conference*, vol. accepted, 2006.

[150] G. P. Agrawal, *Nonlinear fiber optics*. Academic Press, 2001.

[151] J. Vasseur, M. Hanna, F. Malassenet, and J. P. Goedgebuer, "Alternate multiwavelength picosecond fiber laser," *Conference on Lasers and Electro-Optics*, p. CWA66, 2004.

[152] J. Chow, G. Town, B. Eggleton, M. Ibsen, K. Sugden, and I. Bennion, "Multiwavelength generation in an erbium-doped fiber laser using in-fiber comb filters," *IEEE Photon. Technol. Lett.*, vol. 8, no. 1, pp. 60–62, 1996.

[153] J. Sun, J. Qiu, and D. Huang, "Multiwavelength erbium-doped fiber laser exploiting polarization hole burning," *Opt. Commun.*, vol. 182, pp. 193–197, 2000.

[154] T. Miyazaki, N. Edagawa, S. Yamamoto, and S. Akiba, "A multiwavelength fiber ring-laser employing a pair of silica-based arrayed-waveguide-gratings," *IEEE Photon. Technol. Lett.*, vol. 9, no. 7, pp. 910–912, 1997.

[155] N. J. C. Libatique and R. K. Jain, "A broadly tunable wavelength-selectablr WDM source using a fiber Sagnac loop filter," *IEEE Photon. Technol. Lett.*, vol. 13, no. 12, pp. 1283–1285, 2001.

[156] J. Vasseur, M. Hanna, J. Dudley, and J. P. Goedgebuer, "Control of time and wavelength pulse interleaving in an actively modelocked fibre laser," *European Conference on Optical Communication*, p. Th1.3.3, 2004.

[157] J. Vasseur, M. Hanna, J. Dudley, and J. P. Goedgebuer, "Generation of interleaved pulses on time-wavelength grid by actively modelocked fibre laser," *Electron. Lett.*, vol. 40, no. 14, pp. 901–903, 2004.

[158] J. Vasseur, M. Hanna, J. Dudley, and J. P. Goedgebuer, "Contrôle en temps et en fréquence des impulsions multi-longueurs d'onde émises par un laser à fibre à verrouillage actif de modes," *Journées Nationales d'Optique Guidée*, p. 28, 2004.

[159] H. Sabert and E. Brinkmeyer, "Pulse generation in fiber lasers with frequency shifted feedback," *Journal of Lightwave Technology*, vol. 12, no. 8, pp. 1360–1368, 1994.

[160] J. M. Roth, K. Dreyer, B. C. Collings, W. H. Knox, and K. Bergman, "Actively Mode-Locked 1.5-μm 10-GHz Picosecond Fiber Laser Using a Monolithic Semiconductor Optical Amplifier/Electroabsorption Modulator," *IEEE Photon. Technol. Lett.*, vol. 14, no. 7, pp. 917–919, 2002.

[161] X. Shan, D. Cleland, and A. Ellis, "Stabilising Er fibre soliton laser with pulse phase locking," *Electron. Lett.*, vol. 28, no. 2, pp. 182–184, 1992.

[162] M. E. Grein, E. R. Thoen, E. M. Koontz, N. A. Haus, L. A. Kolodziejski, and E. P. Ippen, "Stabilization of an active harmonically mode-locked fiber laser using two-photon absoprtion," *Conference on Lasers and Electro-Optics*, pp. 24–25, 2000.

[163] M. Nakazawa, E. Yoshida, and Y. Kimura, "Ultrastable harmonically and regeneratively modelocked polarisation-maintaining erbium fibre ring laser," *Electron. Lett.*, vol. 30, no. 19, pp. 1603–1605, 1994.

[164] H. A. Haus, E. P. Ippen, and K. Tamura, "Additive-pulse modelocking in fiber lasers," *IEEE J. Quantum Electron.*, vol. 30, no. 1, pp. 200–208, 1994.

[165] H. Takara, S. Kawanishi, and M. Saruwatari, "Multiple-frequency modulation of an actively modelocked laser used to control optical pulse width and repetition frequency," *Electron. Lett.*, vol. 30, no. 14, pp. 1143–1144, 1994.

[166] J. Vasseur, M. Hanna, and J. M. Dudley, "Stabilization of an actively modelocked fibre laser by multi-harmonic phase modulation," *Opt. Commun.*, vol. 256, pp. 394–399, 2005.

[167] J. Vasseur, M. Hanna, J. Dudley, J. yu, j. R. Barry, and G. K. Chang, "Stabilization of an actively mode-locked erbium-doped fiber ring laser by multi-harmonic phase modulation," *Optical Fiber Communication Conference*, vol. accepted, 2006.

[168] S. Calvez, X. Rejeaunier, P. Mollier, J.-P. Goedgebuer, and W. Rhodes, "Erbium-doped fiber laser tuning using two cascaded unbalanced Mach-Zender interferometers as intracavity filter: numerical analysis and experimental confirmation," *Journal of Lightwave Technology*, vol. 19, no. 6, pp. 893–898, 2001.

[169] D. K. Jung, H. Kim, K. H. Han, and Y. C. Chung, "Spectrum-sliced bidirectional passive optical network for simultaneous transmission of WDM and digital broadcast video signals," *Electron. Lett.*, vol. 37, pp. 308–309, 2001.

[170] G. Agrawal and N. A. Olsson, "Self-phase modulation and spectral broadening of optical pulses in semiconductor laser amplifiers," *IEEE J. Quantum Electron.*, vol. 25, no. 11, pp. 2297–2306, 1989.

[171] A. D. McCoy, P. Horak, B. C. Thomsen, M. Ibsen, and D. J. Richardson, "Noise suppression of incoherent light using a gain-saturated SOA: implications for spectrum-sliced WDM systems," *Journal of Lightwave Technology*, vol. 23, no. 8, pp. 2399–2409, 2005.

VITA

Jérôme Vasseur was born in France in 1978. He received the Diplôme d'Ingénieur degree from Supélec, France in 2001 and the Master of Science degree in electrical and computer engineering from the Georgia Institute of Technology, Atlanta, USA in 2002. He is currently working toward the Ph.D. degree with Georgia Tech and the University of Franche-Comté, Besançon, France. He is affiliated with the GTL-CNRS Telecom Laboratory and the optical networking research group of the ECE department of Georgia Tech. His current research interests include pulsed and continuous wave multiwavelength laser sources and broadband optical access networks.